

Det här verket har digitaliserats vid Göteborgs universitetsbibliotek. Alla tryckta texter är OCR-tolkade till maskinläsbar text. Det betyder att du kan söka och kopiera texten från dokumentet. Vissa äldre dokument med dåligt tryck kan vara svåra att OCR-tolka korrekt vilket medför att den OCR-tolkade texten kan innehålla fel och därför bör man visuellt jämföra med verkets bilder för att avgöra vad som är riktigt.

This work has been digitized at Gothenburg University Library. All printed texts have been OCR-processed and converted to machine readable text. This means that you can search and copy text from the document. Some early printed books are hard to OCR-process correctly and the text may contain errors, so one should always visually compare it with the images to determine what is correct.



CHALMERS TEKNISKA HÖGSKOLA



CHALMERS UNIVERSITY OF TECHNOLOGY
GÖTEBORG
SWEDEN

BETA-DELAYED PROTON EMISSION FROM ISOTOPES OF MERCURY, CESIUM, XENON AND KRYPTON

BJÖRN JONSON



DEPARTMENT OF PHYSICS

1972

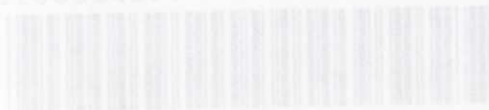
BETA-DELAYED PROTON EMISSION
FROM ISOTOPES OF
MERCURY, CESIUM, XENON AND KRYPTON

BY

BJÖRN JONSON

AKADEMISK AVHANDLING
SOM MED TILLSTÅND AV SEKTIONEN FÖR TEKNISK FYSIK
VID CHALMERS TEKNISKA HÖGSKOLA
FRAMLÄGGES TILL OFFENTLIG GRANSKNING
FÖR TEKNOLOGIE DOKTORSGRADS VINNANDE FREDAGEN
DEN 2 FEBRUARI 1973 KL. 9 FM
Å SAL 6306, FYSISKA INSTITUTIONEN
CHALMERS TEKNISKA HÖGSKOLA .

1200614977



BETA-DELAYED PROTON EMISSION
FROM ISOTOPES OF
MERCURY, CESIUM, XENON AND KRYPTON

by

Björn Jonson

DEPARTMENT OF PHYSICS
CHALMERS UNIVERSITY OF TECHNOLOGY
GOTHENBURG, SWEDEN

1972

PREFACE

The present thesis describes experimental studies on beta-delayed proton emission, performed at the ISOLDE facility at CERN. The main findings presented here have been reported in the articles given below. They will in the following be referred to by capital letters. References to literature quoted, referred to by numbers, are listed at the end of each chapter.

- [A] P. Hornshøj, K. Wilsky, P.G. Hansen, B. Jonson, M. Alpsten, G. Andersson, Å. Appelqvist, B. Bengtsson, and O.B. Nielsen, Beta-delayed proton emission from $^{115,117}\text{Xe}$, and $^{179,181,183}\text{Hg}$, Phys. Letters 34 B, 591 (1971).
- [B] P. Hornshøj, K. Wilsky, P.G. Hansen, B. Jonson and O.B. Nielsen, Beta-delayed proton emission from heavy nuclei (I): The observation of coincidences between protons and gamma rays, Nuclear Phys. A 187, 599 (1972).
- [C] P. Hornshøj, K. Wilsky, P.G. Hansen, B. Jonson and O.B. Nielsen, Beta-delayed proton emission from heavy nuclei (II): The calculation of spectral shapes and intensities in a compound-nucleus model, Nuclear Phys. A 187, 609 (1972).
- [D] P. Hornshøj, K. Wilsky, P.G. Hansen and B. Jonson, Beta-delayed proton emitter ^{73}Kr , Nuclear Phys. A 187, 637 (1972).
- [E] P.G. Hansen, B. Jonson, B.G.G. Jørgensen, E. Kugler, T. Mowinkel and E. Hagberg, Beta-delayed proton emitter ^{113}Xe , to be published in Nuclear Physics.
- [F] P. Hornshøj, P.G. Hansen and B. Jonson, Beta-delayed proton emission from Cs isotopes, to be published.

CONTENTS

	<u>page</u>
<u>CHAPTER I</u> <u>NUCLEI FAR FROM STABILITY AND</u> <u>BETA-DELAYED PARTICLE EMISSION</u>	1
1. INTRODUCTION	1
2. DECAY PROPERTIES OF NUCLEI FAR FROM THE REGION OF BETA STABILITY	2
2.1 Nucleon decay	2
2.2 Two-proton and two-neutron radioactivity	4
2.3 Beta-delayed particle emission	4
3. BETA-DELAYED PROTON EMITTERS	6
3.1 Light elements	6
3.2 Medium- and heavy-weight elements	7
REFERENCES TO CHAPTER I	11
 <u>CHAPTER II</u> <u>MEASUREMENTS OF SINGLES SPECTRA AND</u> <u>PROTON BRANCHING RATIOS</u>	 15
1. PRODUCTION OF THE ACTIVITY	15
2. DETECTOR SYSTEMS	16
3. RESULTS	20
3.1 Mercury isotopes	21
3.2 Cesium isotopes	25
3.3 Xenon isotopes	30
3.4 ^{73}Kr	37
4. SUMMARY	39
REFERENCES TO CHAPTER II	43
 <u>CHAPTER III</u> <u>MEASUREMENTS OF COINCIDENCES BETWEEN</u> <u>DELAYED PROTONS AND GAMMA RAYS</u>	 45
1. INTRODUCTION	45
2. EXPERIMENTAL TECHNIQUES	45
3. RESULTS	48

3.1	^{181}Hg	48
3.2	^{118}Cs	49
3.3	^{117}Xe	55
3.4	^{115}Xe	56
3.5	^{73}Kr	61
4.	THE DETERMINATION OF $Q - B_p$ FROM THE POSITRON COINCIDENCE FRACTIONS	62
5.	SUMMARY	68
	REFERENCES TO CHAPTER III	71
<u>CHAPTER IV</u>	<u>CALCULATIONS OF PROTON BRANCHING RATIOS AND SPECTRAL SHAPES IN A COMPOUND NUCLEUS MODEL</u>	73
1.	INTRODUCTION	73
2.	OUTLINE OF THE CALCULATION	73
2.1	Masses, spins, and parities	76
2.2	The beta strength function and the beta-decay intensity	77
2.3	The partial proton width	80
2.4	The total gamma width	81
2.5	The level density	82
3.	COMPARISON WITH EXPERIMENT	83
4.	CHANGES IN THE PARAMETERS	95
4.1	The spin and parity	95
4.2	Q and B_p	98
4.3	The transmission coefficients	100
4.4	Choice of the level density formula	103
4.5	The beta strength function	105
5.	OTHER MECHANISMS THAT COULD CONTRIBUTE TO THE DELAYED PROTON SPECTRA	109
6.	SUMMARY	109
	REFERENCES TO CHAPTER IV	111
<u>CHAPTER V</u>	<u>FLUCTUATIONS IN DELAYED-PROTON SPECTRA</u>	113
1.	INTRODUCTION	113
2.	GENERAL CONSIDERATIONS	113

3.	THEORETICAL ESTIMATE OF $\text{Var}(I_p / \bar{I}_p)$	116
4.	EXPERIMENTAL RESULTS	119
5.	SUMMARY	120
	REFERENCES TO CHAPTER V	123
<u>APPENDIX</u>	$\text{Var}(I_p / \bar{I}_p)$ FROM THE EXPERIMENTAL DATA	125

CHAPTER I

NUCLEI FAR FROM STABILITY AND BETA-DELAYED PARTICLE EMISSION

1. INTRODUCTION

Nuclei far from the region of beta-stability in many respects exhibit properties that are not found in the immediate neighbourhood of stability. Some obvious, but important, differences are:

- i) the proton-to-neutron ratio,
- ii) the relation between Coulomb and nuclear forces,
- iii) the asymmetry in the binding energy of the nucleons of the two types,
- iv) the large beta decay energy.

It is therefore to be expected that a systematic study of such nuclei will provide new insight into nuclear structure: high-energy beta decay (with the associated process of delayed-particle emission) is one example. In addition, the systematic study of nuclear properties away from stability offers an interesting opportunity to extrapolate and check existing theories of nuclear structure.

During the past decade, a number of specialized techniques have been brought to bear on nuclei far from stability. Experimental difficulties, as, for instance, short half-lives and small formation cross-sections for the products of interest, have been largely overcome. Several facilities, based on the in-beam spectroscopic technique¹⁾ and on-line mass separation²⁾, have successfully been put into operation, and made exotic nuclei in different mass regions available. A thorough comparison of the advantages of the different methods is outside the scope of this work, but it could be worth mentioning that the in-beam technique is most powerful if the formation cross-section for the nuclide of interest is a substantial fraction of the compound nucleus cross-section, while on-line mass separation also gives favourable conditions for observing products formed in low yields.

2. DECAY PROPERTIES OF NUCLEI FAR FROM THE REGION OF BETA-STABILITY

Away from stability the energy available for the beta decay increases, while for neutron-rich/neutron-deficient nuclei the neutron/proton separation energy decreases which may give rise to decay processes involving the emission of nucleons or groups of nucleons. Three new^{*)} decay modes then become possible: nucleon emission from the nuclear ground state (or from an isomeric state), two-nucleon radioactivity, and beta-delayed particle emission.

2.1 Nucleon decay

Very far from stability the least bound nucleon becomes unbound. The chart of the nuclides (Fig. I.1) shows the two curves $B_p \approx 0$ and $B_n \approx 0$ (valid for an odd number of protons and neutrons, respectively), where the separation energy changes sign according to the mass formula by Myers and Swiatecki³⁾. The nuclides outside these curves may decay via nucleon emission which is governed by the strong nuclear force and, consequently, in general much faster than the weak beta-decay process. On the neutron-deficient side, however, the effect of the Coulomb barrier may delay the proton emission to give a measurable half-life. Such a phenomenon is called Coulomb-delayed (or self-delayed) proton emission.

So far only tentative indications of Coulomb-delayed proton emission from the nuclear ground state have been found⁴⁾. With the present experimental possibilities it seems very hard to make proton-radioactive nuclides available for study.

Recently⁵⁾ an isomeric state in ^{53}Co ($I^\pi = 19/2^-$, $T_{1/2} = 247$ ms) has been shown to lie above the proton separation energy. A proton branch (1.5% of the decays) to the ground state of ^{52}Fe has been observed together

*) The well-known process of alpha-decay of the nuclear ground state is deliberately omitted in this discussion.

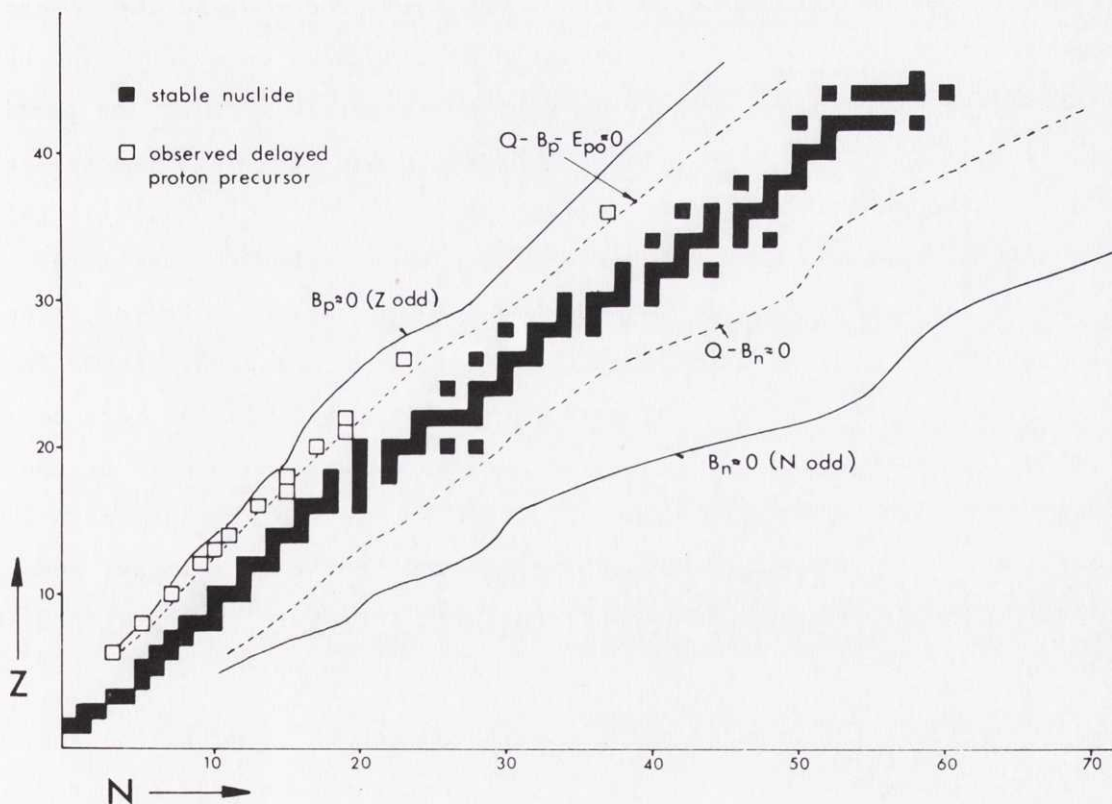
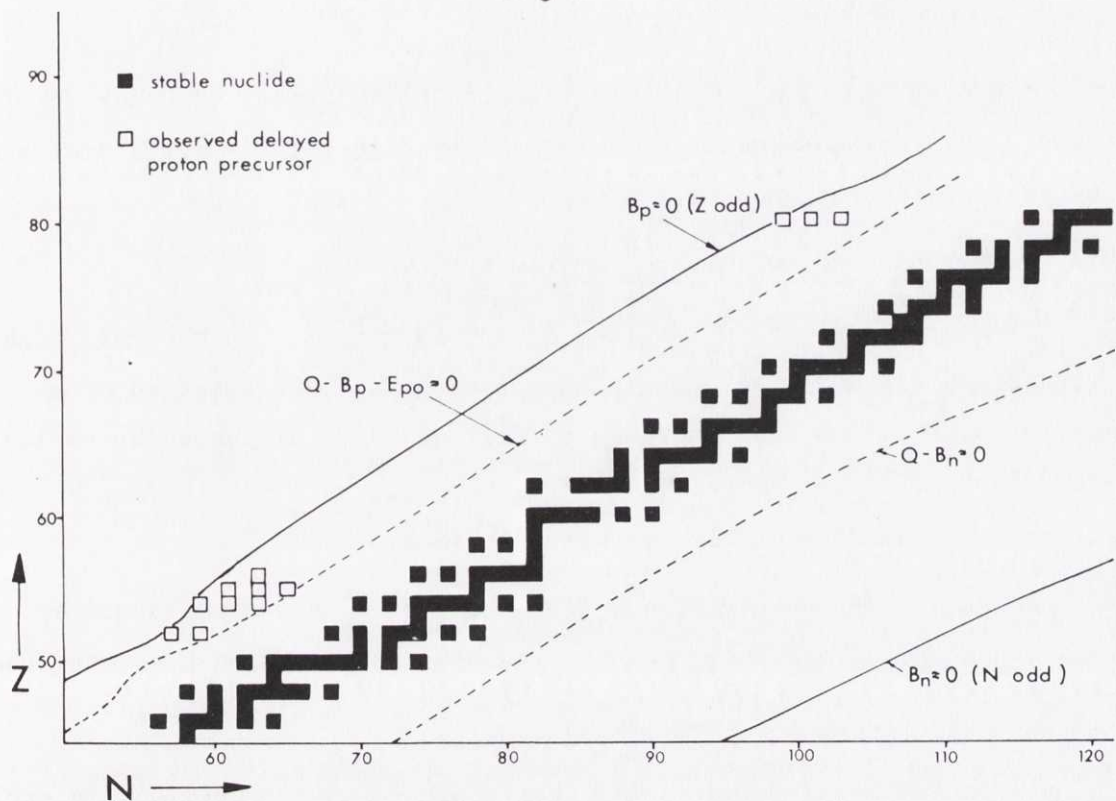


Fig. I.1 Chart of the nuclides. The black squares indicate the nuclides stable against beta decay. The curve $B_p \approx 0$ ($B_n \approx 0$) shows the approximate limit of proton (neutron) stability in nuclides with an odd number of protons (neutrons). The corresponding curve for even Z (N) lies a few mass units further out from stability. The dashed curves indicate the limits of the regions, where one can expect delayed-proton emission ($Q - B_p - E_{po} \approx 0$) and delayed-neutron emission ($Q - B_n \approx 0$).

with the β^+ branch to ^{53}mFe . According to calculations by Peker et al.⁶⁾, there should exist several similar cases of high-spin isomeric states above the nucleon separation energy.

2.2 Two-proton and two-neutron radioactivity

Close to the lines $B_p \approx 0$ and $B_n \approx 0$ in Fig. I.1, a nucleus, stable against nucleon emission, can be unstable against the emission of a nucleon pair. Two-neutron radioactivity has been discussed by Berlovich⁷⁾, and Goldanskii⁸⁾ has suggested that two-proton radioactivity may be found amongst the neutron-deficient even-Z nuclides.

An attempt to observe two-proton decay of ^{16}Ne was performed by Karnaukhov and Si-tin Lu⁹⁾, but no events of the expected kind were observed.

2.3 Beta-delayed particle emission

If the beta-decay energy is high enough, daughter nuclides in excited states above the nucleon separation energy are produced and the de-excitation can proceed either via nucleon emission or via gamma emission. The characteristic life-times for such states are of the order 10^{-14} s. The particle emission will therefore be prompt compared to the beta-decay half-life, and a measurement, based on counting of the emitted nucleons, will reflect the half-life of the mother nuclide (the precursor for the particle emission). This process is called beta-delayed nucleon emission. The maximum energy available for the decay (see the model decay scheme in Fig. I.2) is the difference between the energy available for beta decay (in the following denoted Q) and the nucleon separation energy of the daughter nuclide. A great number of states above the proton separation energy in the intermediate nucleus may be fed in the beta decay, and a typical energy spectrum of the nucleons will therefore show a wide distribution.

Precursors for delayed nucleon emission may be found in the regions outside the dashed curves in Fig. I.1, for which the energy requirement $Q - B_n > 0$ for delayed neutron emission was estimated from the Myers-Swiatecki tables³⁾, while in accordance with Ref. (10) the condition for delayed proton emission was chosen to be $Q - B_p - E_{po} > 0$.

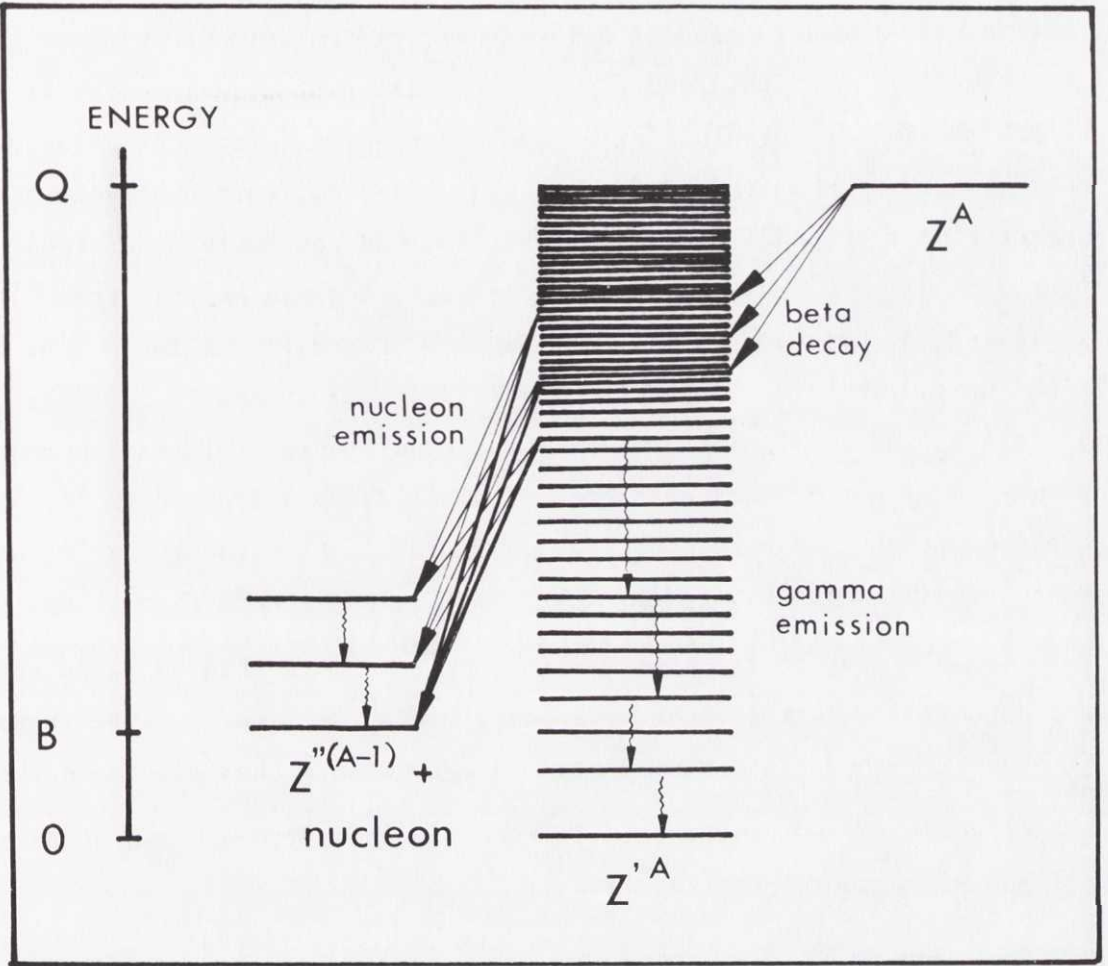


Fig. I.2 Model decay scheme illustrating the process of delayed particle emission. Q is the energy available for beta decay and B the separation energy of the least bound nucleon. For beta delayed-proton emission $Z' = Z-1$ and $Z'' = Z-2$, and for delayed-neutron emission $Z' = Z'' = Z+1$.

The parameter E_{po} is a function of the proton number and is included, since the Coulomb barrier strongly influences the transmission coefficients and makes the proton widths considerably smaller than the gamma widths at lower excitation energies.

Excited states fed in the beta decay may also be unstable against the emission of alpha particles (delayed-alpha emission) and in some cases beta-delayed fission should be a possibility.

The first observation of delayed-particle emission took place already at the beginning of this century. In the decay of the elements belonging to the thorium and uranium series, some particles, with considerably higher energies than the majority of the alpha particles, were observed. Initially the origin of these "long-range" particles was not fully understood, but it could be shown that they were alpha particles and emitted from $^{212,214}\text{Po}$ following the beta decay of $^{212,214}\text{Bi}$ ¹¹⁾. Later it was found that the alpha particles were emitted from excited states in the Po isotopes. An interesting detail is that the first experimental information about gamma-ray life-times was extracted from the delayed-alpha data ¹²⁾. Delayed-alpha emitters have been observed among the light elements ^{13,14)}, and there are indications ¹⁵⁾ of a weak delayed-alpha branch from ^{181}Hg .

Beta-delayed neutrons were first observed more than 30 years ago, and since then several cases have been found [a review is given in Ref. (16)]. Evidence for the occurrence of beta-delayed fission has also been reported ¹⁷⁾.

A short review of the beta-delayed proton emitters known at present will be given in the next section.

3. BETA-DELAYED PROTON EMITTERS

3.1 Light elements

The first attempt to find beta-delayed protons was made by Alvarez ¹³⁾. The experiment was designed in order to search for delayed protons from ^9C , ^{13}O , and ^{17}Ne . No proton events could, however, be observed in that experiment. Goldanskii ⁸⁾ discussed the possibility of delayed-proton emission, and proposed ¹⁸⁾ that, among others, ^{17}Ne could be a precursor for delayed-proton emission. The arguments were based on an analogy with the mirror nuclide of ^{17}Ne , ^{17}N which has been shown to be a delayed-neutron emitter. The first successful experimental results, reported by Barton et al. ¹⁹⁾ and Karnaukhov et al. ^{20,21)}, were obtained for light elements (in all cases nuclides with isospin projection $T_Z = -3/2$). Several delayed-proton precursors with $T_Z = -3/2$, from ^9C ²²⁾ to ^{49}Fe ²³⁾, have been found since then (see Table I.1).

An analysis of the intensity fluctuations in particle spectra, based on different assumptions, will be given in Chapter V.

A summary of the presently known delayed-proton precursors with references is given in Table I.1

Table I.1

Beta-delays proton precursors

Precursor	Half-life (s)	References
^9C	0.127	22
^{13}O	$(8.95 \pm 0.2) \times 10^{-3}$	19,26
^{17}Ne	0.109 ± 0.001	19,24,25,39,40,41,42
^{21}Mg	0.118 ± 0.004	19,40,43
^{23}Al	0.48 ± 0.06	27,44
^{25}Si	0.225 ± 0.006	19,40,43,45
^{29}S	0.195	46
^{32}Cl	0.3	28
^{33}Ar	0.173 ± 0.002	24,25,47,48,49
^{37}Ca	0.170 ± 0.005	47,49,50
^{40}Sc	0.178 ± 0.008	29
^{41}Ti	0.091 ± 0.002	47,49
^{49}Fe	0.075 ± 0.010	23
$^{73}\text{Kr}^{\text{a})}$	34 ± 6	D
^{109}Te	4.2 ± 0.2	31,32,33,51,52,53,54,55
^{111}Te	19.0 ± 0.7	31,34,35,36,38,51,52,53,54
$^{113}\text{Xe}^{\text{a})}$	2.8 ± 0.2	E,56

The study of delayed protons from light elements has been used to determine the half-lives of the precursors, and attempts have been made to construct level schemes of the intermediate (the proton emitting) nuclides. Typically, the spectra show a strong peak due to the collective Fermi beta-transition to the isobaric analogue state together with several other strong peaks believed to reflect the (fractionated) Gamow-Teller strength²⁴⁾. Hardy et al.²⁵⁾ determined absolute ft values for the beta decay branches of ^{17}Ne and ^{33}Ar , and their results indicate isospin impurities in the Fermi branch of $\leq 5\%$ and $\sim 10\%$, respectively. Comparison of the decay rates of the mirror nuclides ^{13}O and ^{13}B has indicated a 15% deviation²⁶⁾ from mirror symmetry.

Three cases of odd Z proton precursors have been observed among the light elements: ^{23}Al ²⁷⁾, ^{32}Cl ²⁸⁾, and ^{40}Sc ²⁹⁾.

3.2 Medium- and heavy-weight elements

The present work mainly describes proton emission from medium- and heavy weight elements -- regions where only a few cases were known.

Flerov et al.³⁰⁾ observed delayed protons from an unidentified nuclide in the neighbourhood of krypton, and suggested that the delayed proton precursor might be ^{70}Br . The half-life determined from proton counting was 23 ± 4 s. It cannot be excluded that the nuclide ^{73}Kr [D] with a half-life of 34 ± 4 s contributes to this result.

Karnaukhov et al.³¹⁾, Siivola³²⁾, and Macfarlane³³⁾ reported on delayed protons from isotopes of tellurium. The mass assignments were initially contradictory, but it was later proved³⁴⁾ that the observed delayed protons had ^{109}Te and ^{111}Te as precursors. This is also expected from the $Q - B_p$ systematics. Bacso et al.³⁵⁾ studied coincidences between delayed protons and positrons. The quantity $Q - B_p$ for ^{111}Te could be determined from their data. A theoretical model for the gross shape of the delayed proton spectrum was suggested by Karnaukhov³⁶⁾. Calculations, under the assumption of a constant beta strength function³⁷⁾, agreed well with the experimental shape. The energy distribution of delayed protons following ^{111}Te shows an unresolved spectrum with fluctuations around the average intensity. Karnaukhov³⁸⁾ made the first steps towards an interpretation of these fluctuations in terms of a statistical model.

Table I.1 continued

Precursor	Half-life (sec)	References
$^{115}\text{Xe}^{\text{a)}}$	18 ± 4	A,B,C,56,57
$^{117}\text{Xe}^{\text{a)}}$	65 ± 6	A,B,C,56,57
$^{116}\text{Cs}^{\text{a,b)}}$	c)	F
$^{118}\text{Cs}^{\text{a)}}$	15 ± 2	F
$^{120}\text{Cs}^{\text{a,b)}}$	58 ± 2	F
^{119}Ba	5.0	58
$^{179}\text{Hg}^{\text{a)}}$	1.09 ± 0.04	A,C,56,57
$^{181}\text{Hg}^{\text{a)}}$	3.6 ± 0.3	A,B,C,56,57
$^{183}\text{Hg}^{\text{a)}}$	11.3 ± 0.5	A,C,56,57

a) This work.

b) Assignment tentative.

c) Not measured.

In the following chapters results on delayed-proton emission with ^{73}Kr , $^{113},^{115},^{117}\text{Xe}$, $^{116},^{118},^{120}\text{Cs}$, $^{179},^{181},^{183}\text{Hg}$ as precursors will be reported.

REFERENCES TO CHAPTER I

- 1) R.M. Diamond, Proc. Int. Conf. on the Properties of Nuclei far from the Region of **Beta-Stability**, Leysin 1970, CERN 70-30 (1970), Vol. I, p. 65.
- 2) W.L. Talbert, Jr., Proc. Int. Conf. on the Properties of Nuclei far from the Region of **Beta-Stability**, Leysin 1970, CERN 70-30 (1970), Vol. I, p. 109.
- 3) W.D. Myers and W.J. Swiatecki, UCRL-11980 (1965).
- 4) V.A. Karnaukhov, D.D. Bogdanov, V.P. Bochinn and L.A. Petrov, Proc. Int. Conf. on Heavy Ion Physics, Dubna 1971, Dubna report D7-5769 (1971), p. 299.
V.A. Karnaukhov, D.D. Bogdanov, V.P. Bochinn and L.A. Petrov, JINR-P6-6313 (1972).
- 5) K.P. Jackson, C.U. Cardinal, H.C. Evans, N.A. Jelley and J. Cerny, Phys. Letters 33B, 281 (1970).
J. Cerny, J.E. Esterl, R.A. Gough and R.G. Sextro, Phys. Letters 33B, 284 (1970).
J. Cerny, R.A. Gough, R.G. Sextro, J.E. Esterl, Nuclear Phys. A188, 666 (1972).
- 6) L.K. Peker, E.I. Volmyansky, V.E. Bunakov and S.G. Ogloblin, Phys. Letters 36B, 547 (1971).
- 7) E.Ye. Berlovich, Proc. Int. Conf. on the Properties of Nuclei far from the Region of **Beta-Stability**, Leysin 1970, CERN 70-30 (1970) Vol. I, p. 497.
- 8) V.I. Goldanskii, Nuclear Phys. 19, 482 (1960).
V.I. Goldanskii, Nuclear Phys. 27, 648 (1961).
J. Jänecke, Nuclear Phys. 61, 326 (1965).
V.I. Goldanskii, Ann. Rev. Nucl. Sci. 16, 1 (1966).
- 9) V.A. Karnaukhov and Si-tin Lu, JINR-P-1679.
- 10) V.A. Karnaukhov and G.M. Ter-Akopyan, Phys. Letters 12, 339 (1964).
- 11) E. Rutherford, J. Chadwick and C.D. Ellis, Radiations from radioactive substances (Cambridge University Press, 1930), p. 94.
- 12) H.A. Bethe, Revs. Modern Phys. 9, 229 (1937).
- 13) L.A. Alvarez, Phys. Rev. 80, 519 (1950).

- 14) R.D. Macfarlane, R.J. Nichels and N.S. Oakey, Proc. Int. Conf. on the Properties of Nuclei far from the Region of Beta Stability, Leysin 1970, (1970) Vol. I, p. 447.
- 15) P. Hornshøj, P.G. Hansen and B. Jonson, to be published.
- 16) L. Tomlinson, AERE-R6993, (1972).
- 17) V.I. Kuznetsov, N.K. Skobelev and G.N. Flerov, Yadernaja Fizika 4, 279 (1966).
N.K. Skobelev, JINR-P7-5584 (1971).
- 18) V.I. Goldanskii, Soviet Physics-Doklady 7, 922 (1963).
- 19) R. Barton, R. McPherson, R.E. Bell, W.R. Frisken, W.T. Link and R.B. Moore, Can. J. Phys. 41, 2007 (1963).
- 20) V.A. Karnaukhov, G.M. Ter-Akopyan and V.G. Subbotin, JINR-P-1072 (1962).
V.A. Karnaukhov, G.M. Ter-Akopyan and V.G. Subbotin, Proc. of the Third Conf. on Reactions between Complex Nuclei (1963) p. 434.
- 21) V.A. Karnaukhov, G.M. Ter-Akopyan, L.A. Petrov and V.G. Subbotin, JINR-P-1388 (1963).
- 22) J.C. Hardy, R.I. Verrall, R. Barton and R.E. Bell, Phys. Rev. Letters 14, 376 (1965).
- 23) J. Cerny, C.U. Cardinal, H.C. Evans, K.P. Jackson and N.A. Jelley, Phys. Rev. Letters 24, 1128 (1970).
- 24) J.C. Hardy, Proc. Int. Conf. on Heavy Ion Physics, Dubna 1971, Dubna report D7-5769 (1971), p. 261.
- 25) J.C. Hardy, J.E. Esterl, R.G. Sextro and J. Cerny, Phys. Rev. C3, 700 (1971).
- 26) J.E. Esterl, J.C. Hardy, R.G. Sextro and J. Cerny, Phys. Letters 33B, 287 (1970).
- 27) R.A. Gough, J. Cerny, R.G. Sextro and J.E. Esterl, UCRL-20436 and Phys. Rev. Letters 28, 510 (1972).
- 28) J.E. Steigerwalt, J.W. Sunier and J.R. Richardsson, Nuclear Phys. A137, 585 (1969).
- 29) R.I. Verrall and R.E. Bell, Nuclear Phys. A127, 635 (1969).
- 30) G.N. Flerov, V.A. Karnaukhov, G.M. Ter-Akopyan, L.A. Petrov and V.G. Subbotin, Nuclear Phys. 60, 129 (1964).

- 31) V.A. Karnaukhov, G.M. Ter-Akopyan, L.A. Petrov and V.G. Subbotin, Soviet. J. Nuclear Phys. 1, 581 (1965).
- 32) A.T. Siivola, Phys. Rev. Letters 14, 142 (1965).
- 33) R.D. Macfarlane, Arkiv för Fysik 36, 431 (1967).
- 34) D.D. Bogdanov, I. Bacso, V.A. Karnaukhov and L.A. Petrov, Soviet J. Nuclear Phys. 6, 807 (1968).
- 35) I. Bacso, D.D. Bogdanov, Sh. Darotsi, V.A. Karnaukhov and L.A. Petrov, Soviet J. Nuclear Phys. 7, 689 (1968).
- 36) D.D. Bogdanov, Sh. Darotsi, V.A. Karnaukhov, L.A. Petrov, G.M. Ter-Akopyan, Soviet J. Nuclear Phys. 6, 650 (1968).
- 37) C.L. Duke, P.G. Hansen, G. Rudstam and O.B. Nielsen, Nuclear Phys. A151, 609 (1970).
- 38) V.A. Karnaukhov, Soviet J. Nuclear Phys. 10, 257 (1970).
- 39) R. McPherson, J.C. Hardy and R.E. Bell, Phys. Letters 11, 65 (1964).
- 40) J.C. Hardy and R.E. Bell, Can. J. Phys. 43, 1671 (1965).
- 41) R.A. Esterlund, R. McPherson, A.M. Poskanzer and P.L. Reeder, Phys. Rev. 156, 1094 (1967).
- 42) J.C. Hardy, J.E. Esterl, R.G. Sextro and J. Cerny, UCRL-18774 (1965).
- 43) R. McPherson and J.C. Hardy, Can. J. Phys. 43, 1 (1965).
- 44) R.A. Gough, J. Cerny, R.G. Sextro and J.E. Esterl, Proc. Int. Conf. on Heavy Ion Physics, Dubna 1971, Dubna report D7-5769 (1971), p. 283.
- 45) P.L. Reeder, A.M. Poskanzer, R.A. Esterlund and R. McPherson, Phys. Rev. 147, 781 (1966).
- 46) J.C. Hardy and R.I. Verrall, Phys. Letters 13, 148 (1964).
- 47) P.L. Reeder, A.M. Poskanzer and R.A. Esterlund, Phys. Rev. Letters 13, 767 (1964).
- 48) J.C. Hardy and R.I. Verrall, Can. J. Phys. 43, 418 (1965).
- 49) A.M. Poskanzer, R. McPherson, R.A. Esterlund and P.L. Reeder, Phys. Rev. 152, 995 (1966).
- 50) J.C. Hardy and R.I. Verrall, Phys. Rev. Letters 14, 764 (1964).

- 51) V.A. Karnaukhov, G.M. Ter-Akopyan, L.S. Vertogradov and L.A. Petrov, Soviet J. Nuclear Phys. 4, 327 (1966).
- 52) V.A. Karnaukhov, G.M. Ter-Akopyan, L.S. Vertogradov and L.A. Petrov, Nuclear Phys. A90, 23 (1967).
- 53) V.A. Karnaukhov and G.M. Ter-Akopyan, Arkiv för Fysik 36, 419 (1966).
- 54) V.A. Karnaukhov, D.D. Bogdanov and L.A. Petrov, Proc. Int. Conf. on the Properties of Nuclei far from the Region of Beta-Stability, Leysin 1970, CERN 70-30 (1970) Vol. I, p. 457.
- 55) D.D. Bogdanov, V.A. Karnaukhov and L.A. Petrov, Dubna report P7-6604 (1972).
- 56) P. Hornshøj, K. Wilsky, P.G. Hansen, B. Jonson and O.B. Nielsen, Int. Conf. on Heavy Ion Physics, Dubna 1971, Dubna report D7-5769 (1971), p. 249.
- 57) P. Hornshøj, K. Wilsky, P.G. Hansen, B. Jonson, E. Kugler, M. Alpsten, Å. Appelqvist, G. Andersson, B. Bengtsson and O.B. Nielsen, Proc. Int. Conf. on the Properties of Nuclei far from the Region of Beta-Stability, Leysin 1970, CERN 70-30 (1970), p. 487.
- 58) V.A. Karnaukhov, private communication.

CHAPTER II

MEASUREMENTS OF SINGLES SPECTRA AND PROTON BRANCHING RATIOS

1. PRODUCTION OF THE ACTIVITY

All the experiments described in this work were performed at the ISOLDE facility¹⁾ at CERN. The activity was produced in spallation reactions with 600 MeV protons from the CERN synchro-cyclotron. The radioactive products were evaporated from the target directly into the ion source of an electromagnetic isotope separator (ISOL = Isotope Separator On Line). Some features of the target systems, used for the production of the nuclides studied here, are summarized in Table II.1

Table II.1

Target systems used for the production of
delayed-proton precursors

Produced activity	Target material	Target temp. °C	Nuclear reaction	Type of ion source	Ref.
Kr	$\text{ZrO}_2(\text{H}_2\text{O})_x$	25-50	$\text{Zr}(p, 5pxn)\text{Kr}$	Plasma	2
Xe	$\text{CeO}_2(\text{H}_2\text{O})_x$	25-50	$\text{Ce}(p, 5pxn)\text{Xe}$	Plasma	2
Cs	La(metal)	1200-1400	$\text{La}(p, 3pxn)\text{Cs}$	Surface ionisation	3
Hg	Pb(metal)	800	$\text{Pb}(p, 3pxn)\text{Hg}$	Plasma	2

The separator, equipped with a fringe-field focusing 55° magnet, has a dispersion of approximately $1500/M_0$ mm (where M_0 is the mass of the central beam) and delivers isotopically pure ion beams within a mass range of $\pm 15\%$ from the central mass⁴⁾. Measuring positions were available both in the

collector chamber of the isotope separator [a detector holder movable in its focal plane^{*)}] and at the end of an ion optical transfer line⁵⁾. To eliminate unnecessary decay losses during transport of the collected activity, the detector system was placed directly behind a thin collector foil which intercepted the ion beam under study. In some of the early measurements, nickel foils, with a thickness of $440 \mu\text{g}/\text{cm}^2$, were used. In most cases, however, the experiments have been performed with $80 \mu\text{g}/\text{cm}^2$ carbon foils as collectors.

2. DETECTOR SYSTEMS

Only a small fraction of the beta decays to states above the proton separation energy of the daughter nucleus leads to the emission of delayed protons. For the heaviest nuclides the proton intensity is further reduced by the competition between alpha and beta decay of the mother nucleus. Therefore, a detector system for measurements of energy spectra of delayed protons must be able to distinguish the protons, in the presence of a strong background from other types of radiation. The conventional technique is to use a counter telescope consisting of a totally depleted surface barrier dE/dx detector in front of a thick E detector of the same type. The different kinds of particles are identified by their typical energy losses in the dE/dx detector, and the energy signal is obtained as the summed output from the two detectors. Some values of the energy loss in Si for protons and alpha particles, with energies typical of these experiments are given in Table II.2.

*) A modified version of the system described in Ref. (1), page 39.

Table II.2

Energy losses^{a)} for protons and alpha particles in Si

	E	Energy loss in Si (MeV)		
	MeV	20 μ	30 μ	40 μ
Protons	2.0	0.58	0.91	1.26
	5.0	0.28	0.42	0.57
	8.0	0.19	0.29	0.39
Alphas	5.5	3.26	5.50	5.50
	6.0	3.10	5.22	6.00
	8.0	2.36	3.82	5.64

a) Ref. (6)

A block diagram of the electronics used is shown in Fig. II.1. The signals from the two detectors were amplified, stretched, and fed into a particle identifier (model ORTEC 423). This unit gives two output pulses: (i) one proportional to the particle energy (sum of the outputs from the two detectors); and (ii) one (the particle identifier signal) formed according to the expression

$$T/\underline{a} = (E + \Delta E)^{1.73} - E^{1.73} \quad (\text{II.1})$$

which gives different and distinct amplitude of the output pulse within a wide range of energies for each particle type^{*)}. E and ΔE represent the signals from the two detectors, T the thickness of the dE/dx detector, and \underline{a} the constant appearing in the empirical relation between the range R of an incident particle and its energy E_t

$$R = \underline{a} E_t^{1.73} \quad (\text{II.2})$$

*) With a 30 μ dE/dx detector Eq. (II.1) gives a value for T/\underline{a} of 2.3 (with E and ΔE in MeV), while the value for alpha particles (above 6 MeV) is about 22.

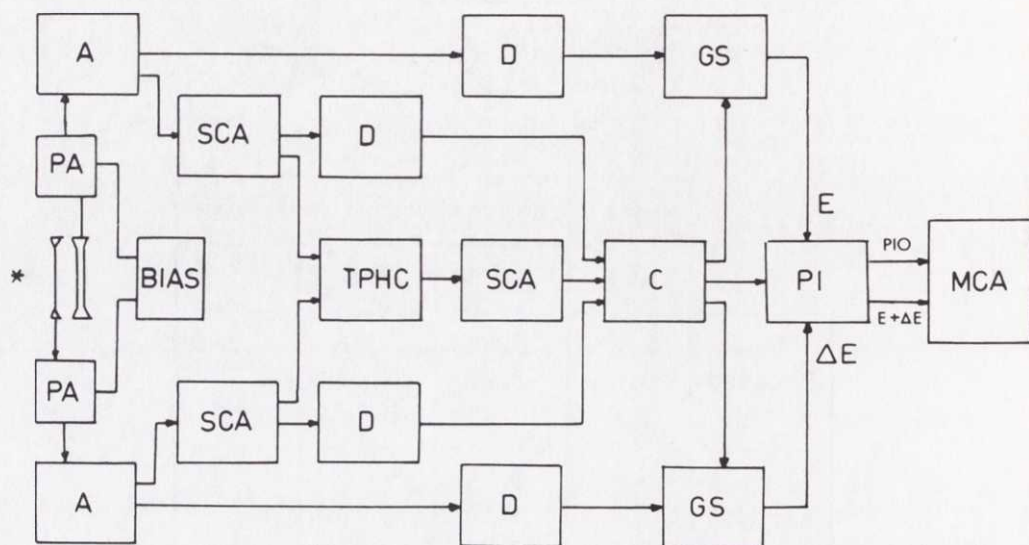


Fig. II.1 Block diagram of electronics used for the measurement of energy spectra of delayed protons (PA: preamplifier; A: amplifier; SCA: single channel analyser; D: delay; TPHC: time to pulse height converter; C: coincidence unit; GS: gate and stretcher; PI: particle identifier; MCA: multichannel analyser).

The output signals from the particle identifier, both gated with requirements as to time (coincident pulses from the two detectors) and energy (proper energy loss in the front detector), are fed into the memory of a multichannel analyser operated in a two-dimensional mode. Such a registering gives a very safe identification of the protons.

Due to the coincidence demand the energy of a proton after having passed the thin detector must be above the threshold in the second detector to give an output pulse. This means that the detecting efficiency for protons drops to zero below a certain energy. The "cut-off" energy depends on the thickness of the dE/dx detector and the threshold energy in the E channel. In the following, the cut-off energy is defined as the energy where the detection efficiency has dropped to 50%. Figure II.2 gives an illustration to the cut-off in delayed-proton spectra from ^{115}Xe .

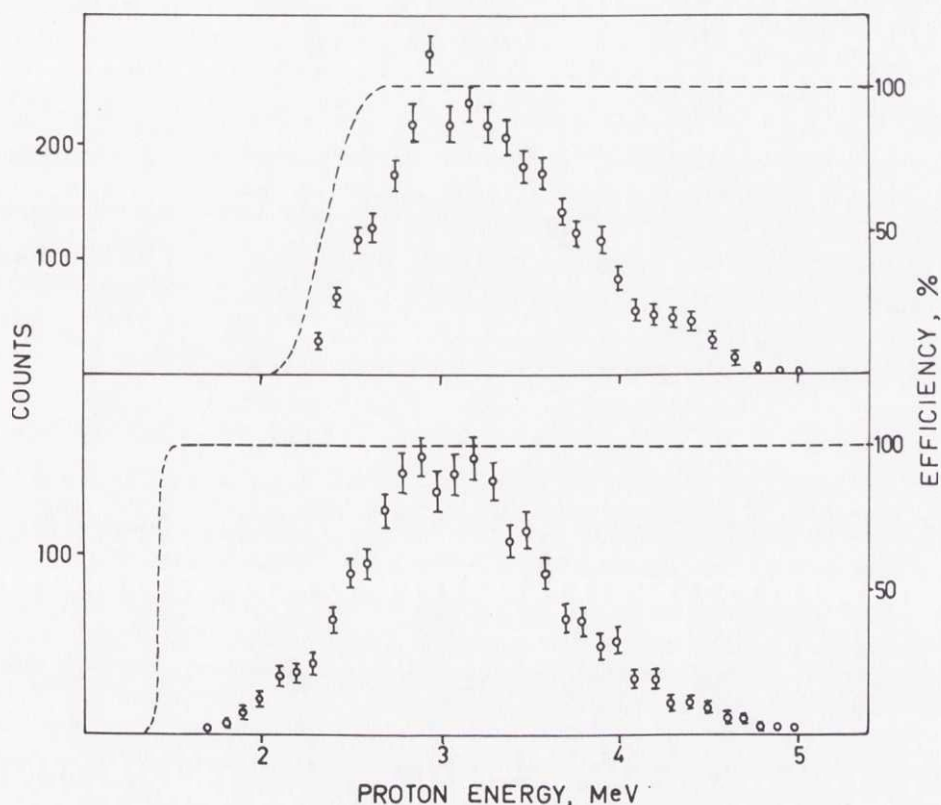


Fig. II.2 Delayed-proton spectra for ^{115}Xe . The spectrum in the upper part of the figure was measured with a $40\ \mu/150\ \text{mm}^2$, $400\ \mu/450\ \text{mm}^2$ telescope detector. The threshold in the E detector was 1 MeV and the solid angle 15% of 4π . The other spectrum was measured with a $20\ \mu/50\ \text{mm}^2$, $700\ \mu/150\ \text{mm}^2$ telescope. The threshold was 600 keV in the E channel and the solid angle 5% of 4π . The dashed curves represent the detector efficiencies calculated from the data given in Ref. (6).

The calculated efficiencies indicate that the spectrum measured with the $20\ \mu$ front detector gives no distortion of the spectral shape at the low energy end. The calibration of the detector telescopes was performed with an alpha source (^{228}Th , $E_\alpha = 5.34\text{--}8.78\ \text{MeV}$) together with a pulse generator. The line width (FWHM) for the alpha particles was typically 50–65 keV. The energy resolution for protons has not been measured, but may be assumed to be somewhat better than for alpha particles, since the line width measured with a pulse generator was about 30 keV. The energy spread for protons, due to different angles of penetration through the

collector foil, is small compared to this line width. With a solid angle of 15% for 3 MeV protons, the spread is about 1.5 keV (for the nickel foil the value is about 15 keV).

In cases where the proton branch is comparatively strong, and where no alpha activities are present, the proton spectrum can be measured with a single detector. A proton line width of 15 keV at best has been obtained in test experiments performed with protons from a Van de Graaff generator.

A fraction of the delayed protons are in prompt coincidence with positrons (Chapter III) which means that there is a chance that a proton and a positron signal will be summed in the detector. The fraction of summed proton-positron events, ξ , can be found from

$$\xi(E_p) = \Omega \cdot \eta(E_p) \quad , \quad (II.3)$$

where Ω is the solid angle for a positron to be detected, and where $\eta(E_p)$ is the positron fraction per proton. The contribution is of importance only at very low proton energies, and in the experiments described here, the distortion of the spectrum from proton-positron summing is negligible.

One experiment has been performed with a nuclear emulsion as the detecting element. The technique, which is most favourable in cases with low counting rates, will be described in section 3.3 (^{113}Xe).

3. RESULTS

Some details from the measurements of singles delayed-proton spectra and proton branching ratios (protons/disintegration) are given in the following. The delayed proton precursor has been assumed to be the first member of the chain. This assumption is supported by energy relations calculated from mass formulas. For the lightest isotopes the energetic requirement for delayed-proton emission ($Q - B_p > 0$) is fulfilled also for some of the daughter products after alpha or beta decay. The decrease in the $Q - B_p$ values indicates, however, that such contributions to the

proton spectra are quite small. For some of the delayed-proton precursors, the assignment was confirmed experimentally by determining a half-life from counting of protons. The observation of coincidences between delayed protons and gamma rays de-exciting known levels in the final nucleus after proton emission also supports the assignments (Chapter III).

3.1 Mercury isotopes

^{183}Hg is so far the heaviest nuclide which has been observed to be a delayed-proton precursor. The measurement of the energy spectrum of the delayed protons, shown in Fig. II.3, was carried out with a $40\ \mu$, $150\ \text{mm}^2$ dE/dx detector and a $400\ \mu$, $450\ \text{mm}^2$ E detector. With a threshold in the E detector at about 1 MeV, the cut-off energy for the telescope was about 2.3 MeV. The proton intensity decreases rapidly below 3 MeV for mercury because of the high Coulomb barrier. The shape of the low energy part of the spectrum was therefore not affected by the detector cut-off in this measurement.

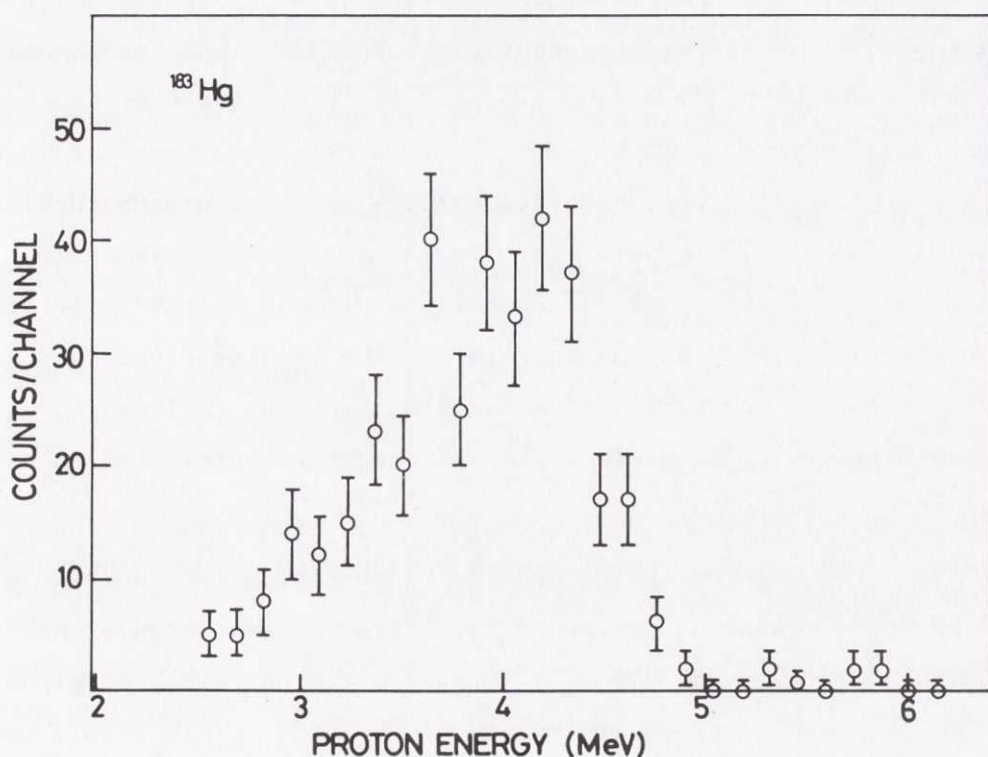


Fig. II.3 Delayed-proton spectrum from ^{183}Hg . Telescope detector; dE/dx: $40\ \mu/150\ \text{mm}^2$; E: $400\ \mu/450\ \text{mm}^2$. Solid angle: 14.5% of 4π . Collector foil $440\ \mu\text{g}/\text{cm}^2$ nickel. Cut-off energy: 2.3 MeV. Line width (for alpha particles): 65 keV.

Since the intensity of the ^{183}Hg alpha branch is known to be 12% ⁷⁾, the intensity of the proton branch can be obtained from simultaneous counting of protons and alpha particles. The alpha particles from ^{183}Hg , with energies 5.905 and 5.830 MeV ⁷⁾, were completely stopped in the front detector (see Table II.2), and a singles alpha spectrum from this detector was registered during the measurement. The number of alpha particles per proton was found to be 63500. The solid angle was 21% of 4π for alpha particles (only the dE/dx detector) and 14.5% of 4π for protons (determined by the back detector) which give $(2.3 \pm 0.3) \times 10^{-5}$ p/alpha and a proton branching ratio of $(2.7 \pm 0.6) \times 10^{-6}$ p/dis.

The assignment of ^{183}Hg as the precursor of the delayed protons is based upon the $Q - B_p$ values taken from the tables by Myers and Swiatecki⁸⁾. Their estimate of this quantity is 4.55 MeV for ^{183}Hg and 1.00 MeV for ^{183}Au . The daughter from alpha decay, ^{179}Pt , has however a $Q - B_p$ value, estimated to be 3.57 MeV, which fulfills the energetic requirement for beta delayed-proton emission. The spectrum can therefore be a superposition of delayed-proton spectra from different precursors. The 12% alpha branch and a $Q - B_p$ value which is almost 1 MeV lower for ^{179}Pt indicate, however, that the contribution to the proton spectrum from this precursor should be comparatively small. The theoretical values of the proton-branching ratios (Chapter IV, Tables IV:2,3) can be used to give an estimate of the contribution to the observed spectra from delayed protons emitted after the decay of the gold and platinum daughters. The results given in Table II.3 indicate that such "contaminations" have no important influence, neither on the experimentally determined proton branching ratios, nor on the gross shapes of the spectra.

^{182}Hg . A brief search for delayed protons from this nuclide was made. During a measuring period of 1.5 hours, three proton events were registered, together with 3.3×10^6 alpha particles. With an alpha branch of 9% for ^{182}Hg ⁷⁾, a proton intensity of the order of 10^{-7} is obtained. This number is considered as an upper limit, since it cannot be excluded that some cross contamination from neighbouring delayed-proton emitters was the source of these events.

Table II.3

Estimated contribution of delayed protons from gold and platinum to the delayed-proton spectra from mercury

Mother nuclide	$Q - B_p$ (MeV)	Alpha branch (%)	Daughter nuclide	$Q - B_p$ (MeV)	Estimated contribution to the Hg delayed-proton spectrum (%)
^{183}Hg	4.55	-	^{183}Au	1.00	~ 0
		12	^{179}Pt	3.57	<1
^{181}Hg	5.99	-	^{181}Au	2.43	~ 0
		36	^{177}Pt	5.03	<5
^{179}Hg	7.44	-	^{179}Au	3.87	~ 0
		53	^{175}Pt	6.52	<10

^{181}Hg . An energy spectrum of delayed protons with ^{181}Hg as the precursor is shown in Fig. II.4. The experimental conditions were the same as for ^{183}Hg . The proton/alpha ratio was found to be $(3.6 \pm 0.6) \times 10^{-4}$. The intensity of the alpha branch was not known for this nuclide, and, therefore, the determination of the proton branch had to be based on absolute counting of gamma rays from long-lived daughter products which had accumulated on the collector foil during the measurement. The best suited daughter activity for such an investigation is ^{181}Re which has a half-life of 18 hours⁹⁾. Figure II.5 shows a part of the gamma spectrum, measured from the activity on the collector foil. The intensities of the two peaks at 360.7 keV and 365.5 keV were used to determine the total number of atoms collected during the measurement. The calculation yielded a proton branch of $(1.25 \pm 0.30) \times 10^{-4}$ and an intensity of the ^{181}Hg alpha branch of $(36 \pm 6)\%$. The strong alpha branch of ^{181}Hg and a $Q - B_p$ value of 5.03 for ^{177}Pt ⁸⁾ indicate that a contribution of delayed protons from this nuclide could be of the order of 5%. Compared to other error sources*) in the determination of the proton branch, such a contribution is negligible.

*) Such as: the uncertainty in the determination of the solid angle, in the intensity of the gamma lines, in the efficiency of the Ge(Li) detector and the uncertainty from the counting statistics.

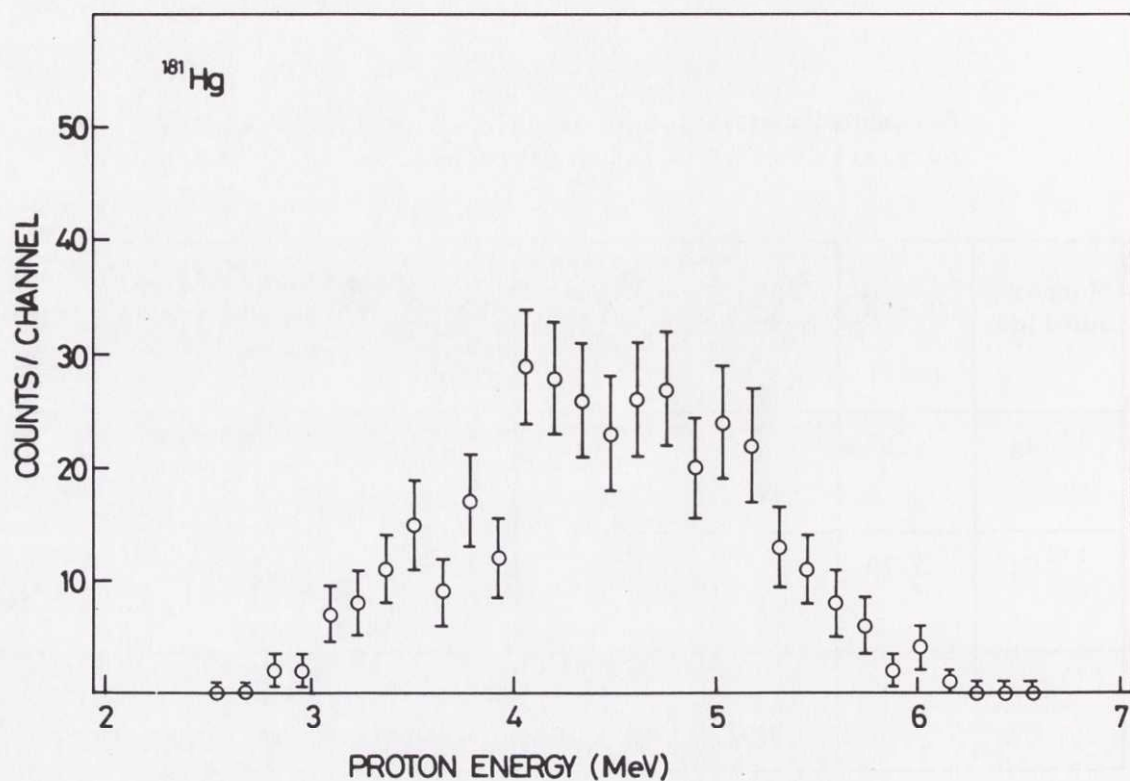


Fig. II.4 Delayed-proton spectrum from ^{181}Hg . The experimental conditions were the same as in the ^{183}Hg case (see Fig. II.3).

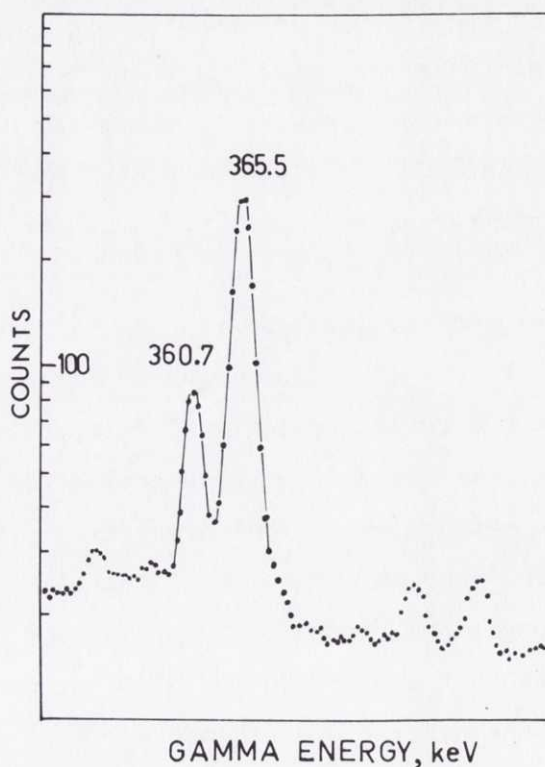


Fig. II.5 Part of a gamma spectrum measured from the collector foil used in a delayed proton experiment on ^{181}Hg . The two lines from ^{181}Re at 365.5 keV and 360.7 keV have the intensities 57% and 12%, respectively. The spectrum was measured with a $25\text{ cm}^3\text{ Ge(Li)}$ detector.

^{179}Hg is the next lightest isotope of mercury that has been found¹⁰⁾. The production yield is of the order of 12 atoms/s with the best running conditions. In a 7.5 hour simultaneous proton- and alpha-counting experiment (with a $20\ \mu/50\ \text{mm}^2$, $400\ \mu/450\ \text{mm}^2$ telescope), 44 proton events were recorded. These were spread in an energy interval ranging from 3 to 7 MeV. The number of alpha particles from ^{179}Hg [6.27 MeV, Refs. (7) and (10)] recorded during the same counting period was 15800. As the solid angle of 5% for this telescope was determined by the front detector, the proton/alpha ratio is $(2.8^{+0.3}_{-0.5}) \times 10^{-3}$. The intensity of the ^{179}Hg alpha branch is not known, but an extrapolation of the beta strength-function systematics¹¹⁾ for the neutron-deficient mercury isotopes yields a partial beta decay half-life of 2.3 s, corresponding to a 53% alpha branch. Consequently, the proton branching ratio is approximately 1.5×10^{-3} . The contribution from the alpha daughter, ^{175}Pt , is estimated to be less than 10% (see Table II.3).

3.2 Cesium isotopes

^{120}Cs . A search for delayed protons from this nuclide was performed with a telescope equipped with a $30\ \mu$, $100\ \text{mm}^2$ dE/dx detector and a $500\ \mu/450\ \text{mm}^2$ E detector. During a counting period of 1.5 hours, 10 proton events were registered. The energies of these were all below 2.5 MeV which is in fairly good agreement with the expected $Q - B_p$ value⁸⁾ which is 3.3 MeV (Table II.4). The total number of atoms collected during the measurement was obtained from absolute counting of gamma rays from the decay of the daughter product ^{120}I . The assumption of an 100% intensity¹²⁾ of the 562 keV line gives a total number of about 1.5×10^9 atoms collected during the measurement. The approximate value of the proton branch is then 5×10^{-8} which is considered as an upper limit.

^{118}Cs . The energy spectrum of delayed protons from ^{118}Cs is shown in Fig. II.6. The detector telescope, with the same detectors as was used for ^{120}Cs , had a solid angle of 13.9% of 4π . The cut-off energy was 1.6 MeV and the line width for alpha particles (^{228}Th) was about 60 keV. The measured energy spectrum has a comparatively smooth shape and only small fluctuations around the average intensity can be observed.

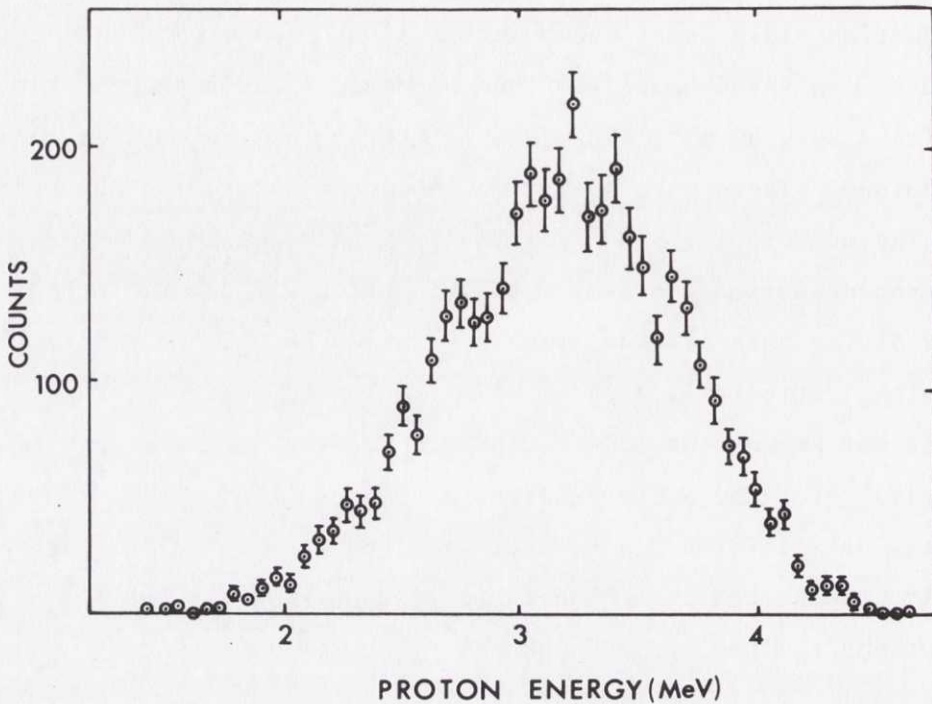


Fig. II.6 Delayed-proton spectrum from ^{118}Cs . Telescope detector, dE/dx : $30 \mu/100 \text{ mm}^2$; E : $500 \mu/450 \text{ mm}^2$. Solid angle: 13.9% of 4π . Collector foil: $80 \mu\text{g}/\text{cm}^2$ carbon. Cut-off energy: 1.6 MeV. Line width (alpha): 60 keV.

As will be shown in Chapter V, the fluctuations in the spectrum are of physical significance. They can be more clearly observed with a detector having higher resolution. As no alpha activities are present for the elements in this region, the most favourable technique would be to measure the delayed-proton spectrum with a high-resolution single detector. The background from beta activities will then give a contribution to the spectrum, but choosing a thin detector limits such a contribution to the low energy part. A measurement with a surface barrier silicon detector, $300 \mu/300 \text{ mm}^2$, gave as a result the spectrum shown in Fig. II.7. The curve in the low energy end of the spectrum shows the shape of a pure beta spectrum measured with the same detector. The fast decline towards higher energies indicates that the contribution to the delayed-proton spectrum from the beta background is completely negligible above 3 MeV. The line width for alpha particles was measured to be 22 keV. The corresponding line width for protons¹³⁾ is then less than 20 keV.

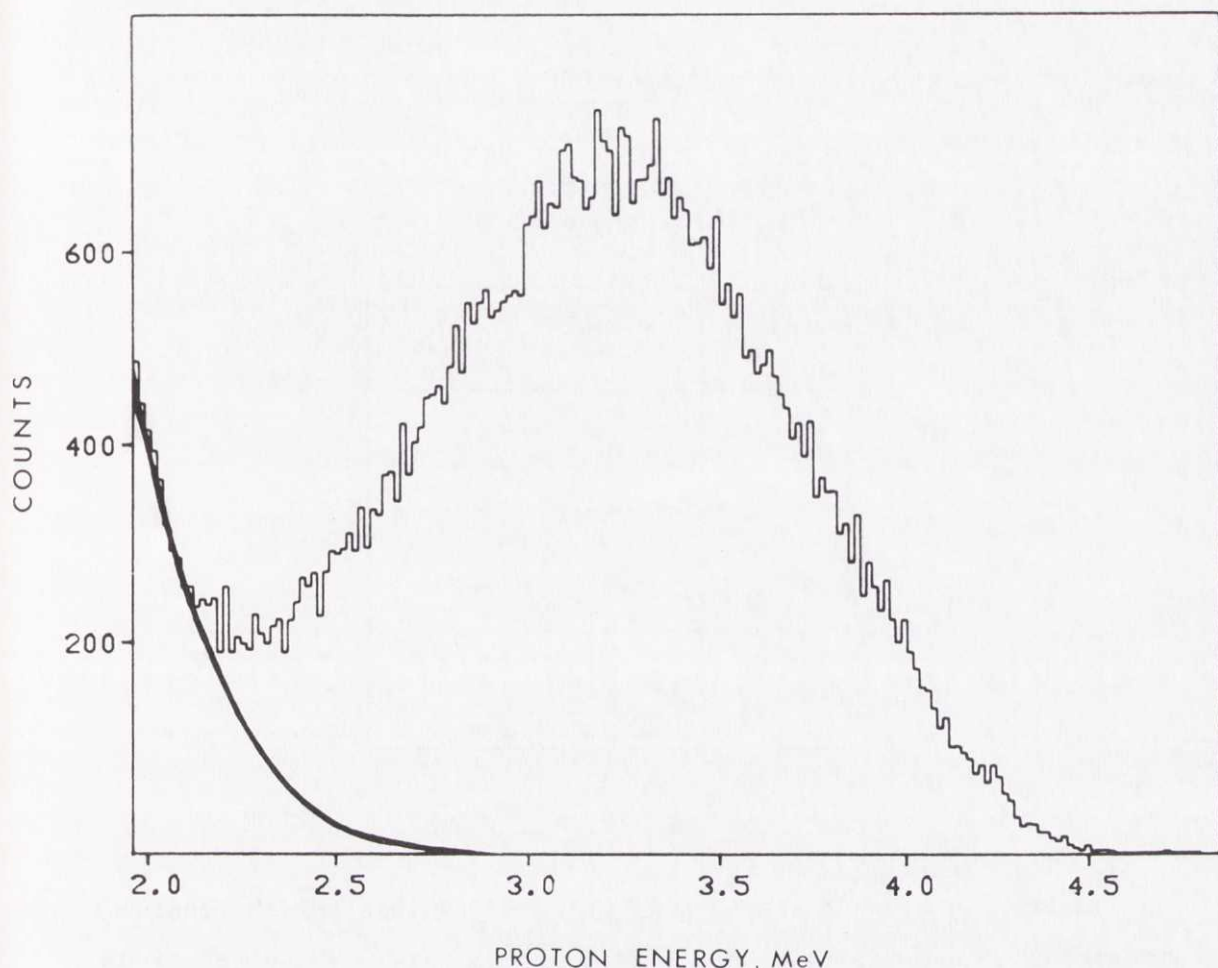


Fig. II.7 Delayed-proton spectrum from ^{118}Cs . Single detector: $300\ \mu/300\ \text{mm}^2$. Solid angle: 25.4% of 4π . Collector foil: $80\ \mu\text{g}/\text{cm}^2$ carbon. Line width: about 20 keV for protons. The curve in the lower part of the spectrum shows a pure beta spectrum measured with the same experimental conditions as during the delayed-proton counting.

The total number of protons in the spectrum shown in Fig. II.7 is about 50000. The determination of the proton branching ratio was based on a measurement of annihilation radiation from positrons in the decay of ^{118}Sb . The counting of the 511 keV gamma rays was performed with a NaI(Tl) crystal in a low background lead container. With a value of 75.5% for the intensity of the positron branch¹⁴⁾, the total number of atoms collected during the measurement was found to be about 5×10^8 . The value of the proton branching ratio is then $(4.2 \pm 0.6) \times 10^{-4}$.

Table II.4

$Q - B_p$ values for cesium
delayed-proton precursors
and their xenon daughters

Isotope	Estimated $Q - B_p$ ^{a)} MeV
^{120}Cs	3.26
^{120}Xe	-1.23
^{118}Cs	5.40
^{118}Xe	0.83
^{116}Cs	7.61
^{116}Xe	3.00

a) From Ref. (8).

Table II.4 gives a summary of the $Q - B_p$ values for the cesium and xenon isotopes of interest for the assignments. These relations strongly support ^{118}Cs as the precursor of the delayed protons.

A direct experimental test of the assignment to ^{118}Cs can be performed by measuring a half-life from counting of delayed protons, which should reflect the half-life of the delayed-proton precursor. The decay curve shown in Fig. II.8 is an example. The experiment was performed in the following way: after collection, the ion-beam was cut off by a screen and the proton events were counted in four successive groups in a multi-scaling mode. The measuring cycle was repeated several times. The half-life, 15 ± 2 s, is in good agreement with the value 16.4 ± 1.2 s ³⁾ obtained from beta counting.

^{116}Cs . An attempt to identify this nuclide from beta counting failed because of a very unfavourable signal-to-background ratio³⁾. An extrapolation of the beta strength function systematics gives an expected beta half-life of 5 s, and the proton branch is estimated to be 2% (Chapter IV).

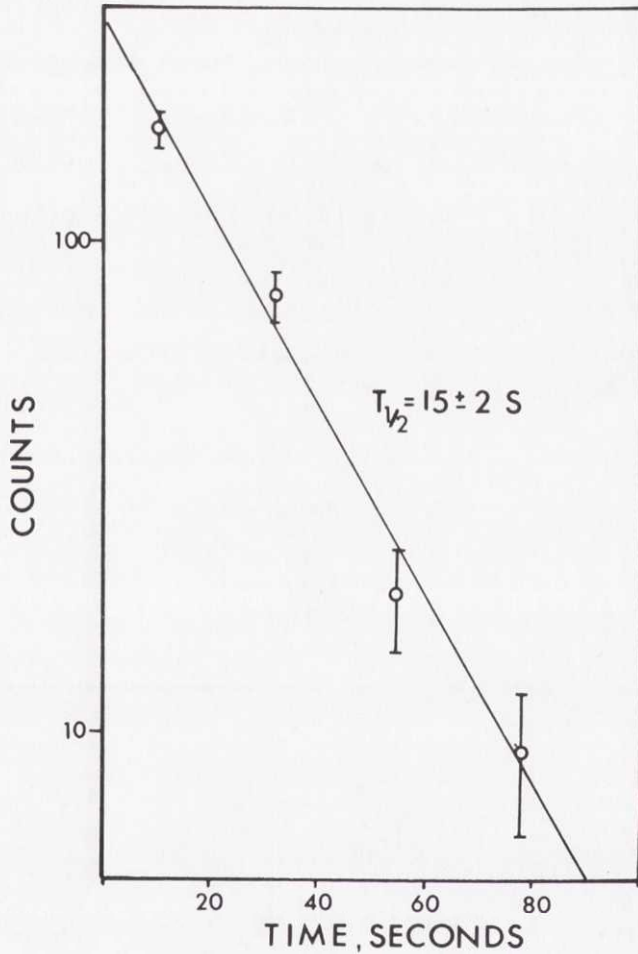


Fig. II.8 Decay curve of ^{118}Cs from counting of delayed protons. The collection time was 20 s and each of the subgroups was counted for 20 s (with 2 s waiting time in between). This gives a half-life of $15 \pm 2 \text{ s}$.

These values indicate that if this nuclide is produced, it should be possible to identify it from counting the protons. In general, delayed protons seem to be the most sensitive way of identifying very neutron-deficient (non alpha-emitting) nuclides, since they can easily be distinguished in a strong background from other types of radiation.

An 1 hour search for delayed protons at the position of mass 116 was performed. During this time, 10 proton events with energies up to 5.5 MeV were recorded. Cross contamination from ^{118}Cs may give some events at the 116 mass position, but measurements¹⁵⁾ for higher mass

numbers indicate that such a contribution should be less than 2 events. With the assumption of a 2% proton branch, these data give an upper limit for the ^{116}Cs yield of 1 atom/s³⁾. For a characterisation of ^{116}Cs , including a half-life determination, a technique, similar to the one used for the identification of ^{113}Xe , could be applied (Section 3.3).

3.3 Xenon isotopes

^{117}Xe . The energy spectrum of delayed protons from ^{117}Xe is shown in Fig. II.9. A 440 $\mu\text{g}/\text{cm}^2$ nickel foil was used as a collector. The determination of the branching ratio was based on absolute counting of the 720 keV gamma rays from the decay product ^{117}Te ($I_\gamma = 100\%$)¹⁴⁾ which yielded the value $(2.9 \pm 0.6) \times 10^{-5}$ p/dis.

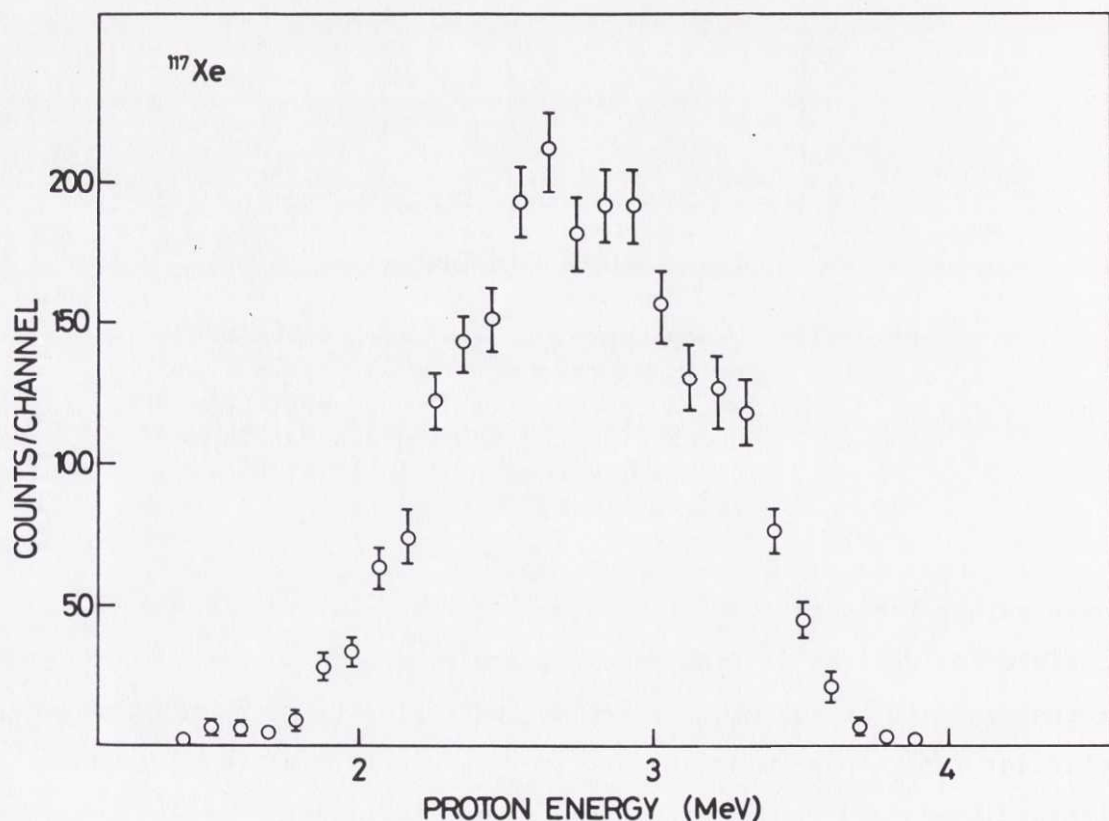


Fig. II.9 Delayed-proton spectrum from ^{117}Xe .
 Detector telescope, dE/dx : 20 $\mu/50 \text{ mm}^2$;
 E : 700 $\mu/150 \text{ mm}^2$. Solid angle: 5% of 4π .
 Collector foil: 440 $\mu\text{g}/\text{cm}^2$ nickel. Cut-off energy: 1.4 MeV. Line width (α): 60 keV.

The $Q - B_p$ systematics⁸⁾ for the xenon and iodine isotopes are given in Table II.5. The assignment of ^{117}Xe as the precursor for the delayed protons is based on these values. Another experiment that supports the assignment to ^{117}Xe will be described in Chapter III: in a delayed-proton gamma ray coincidence experiment it was found that 14% of the delayed protons are in coincidence with the gamma rays from the $2^+ \rightarrow 0^+$ transition in the final nucleus $^{116}\text{Te} \left(^{117}\text{Xe} \xrightarrow{\beta^+, \text{EC}} ^{117}\text{I}^* \xrightarrow{\text{P}} ^{116}\text{Te} \right)$.

^{115}Xe . The singles energy spectrum from this nuclide is shown in Fig. II.2. The spectrum in the lower part of the figure was obtained during a 7 hour counting period. The calculation of the proton branching ratio was based on counting of gamma rays from the daughter products on the collector foil. In this case where the longest lived daughter ^{115}Sb has a half-life of only 31 minutes one has to be especially careful. The correction for variations in the intensity of the ion beam becomes important, and a careful monitoring of the beam intensity had to be performed. The gamma spectrum from the collector foil was measured with a $25 \text{ cm}^3 \text{ Ge(Li)}$ detector. With the assumption of a 99% intensity¹⁴⁾ of the 499 keV transition in ^{115}Sn the proton branch was found to be $(3.4 \pm 0.6) \times 10^{-3}$.

Table II.5

$Q - B_p$ values for the xenon
delayed-proton precursors
and their iodine daughters

Isotope	Estimated $Q - B_p$ ^{a)} MeV
^{117}Xe	3.94
^{117}I	-0.53
^{115}Xe	6.17
^{115}I	1.65
^{113}Xe	8.55
^{113}I	4.01

a) From Ref. (8).

Due to the rather strong proton branch and the high production yield ^{115}Xe is an ideal case for measuring the delayed-proton spectrum with a high resolving single detector. The spectrum shown in Fig. II.10 was measured with a $300\ \mu/300\ \text{mm}^2$ surface barrier detector. The line width obtained with alpha particles was 18 keV which corresponds to a line width for protons of 15 keV according to a test¹³⁾ carried out with 2-8 MeV protons from a Van de Graaf generator.

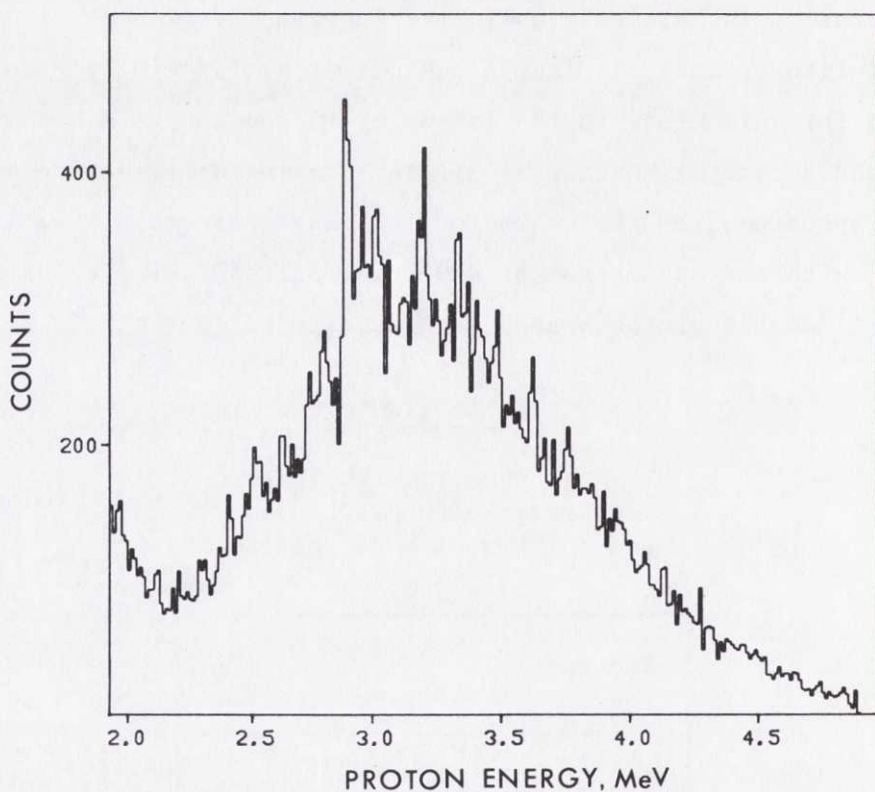


Fig. II.10 Delayed-proton spectrum from ^{115}Xe .
Single detector: $300\ \mu/300\ \text{mm}^2$.
Solid angle: 25% of 4π . Collector
foil: $80\ \mu\text{g}/\text{cm}^2$ carbon. Line width
(protons): 15 keV.

A half-life measurement using the same technique as for ^{118}Cs was also performed. The resulting decay curve is shown in Fig. II.11

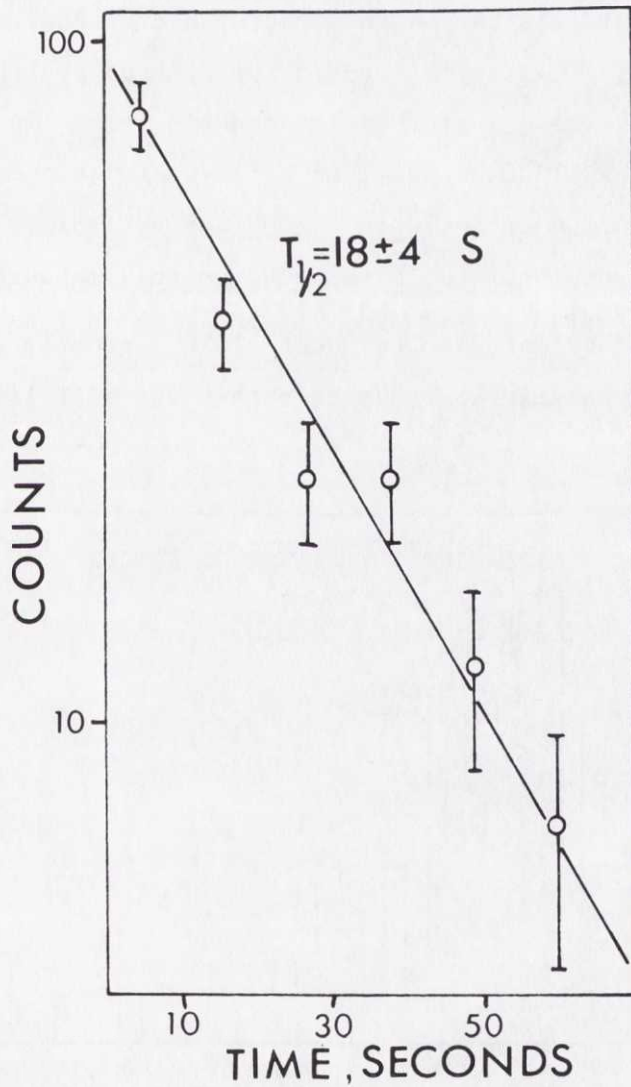


Fig. II.11 Decay curve of ^{115}Xe from counting of delayed protons. The collection time was 20 s and each of the six subgroups was counted for 10 s (with 1 s waiting time in between). This gives a half-life of $18 \pm 4 \text{ s}$.

The corresponding half-life is 18 ± 4 s. This value is in agreement with that obtained from beta counting, which is 19 ± 5 s¹⁶⁾.

^{113}Xe . At the very neutron-deficient wing of the production yield curve, the saturation activity drops by orders of magnitude per mass number. For the target producing xenon the most neutron-deficient nuclide identified by beta and gamma counting is ^{115}Xe . Further out, the possible weak beta activities are completely buried in detector background and contamination from the neighbouring masses. A search for delayed protons was performed with counters at the mass positions 114 and 113. The 114 result was negative, but at the 113 mass position a few proton events were registered. The energy distribution of these is shown in Fig. II.12. No value for the proton branching ratio could be obtained from this measurement.

To obtain further information about ^{113}Xe greatly improved techniques were necessary, especially in order to obtain the half-life of ^{113}Xe .

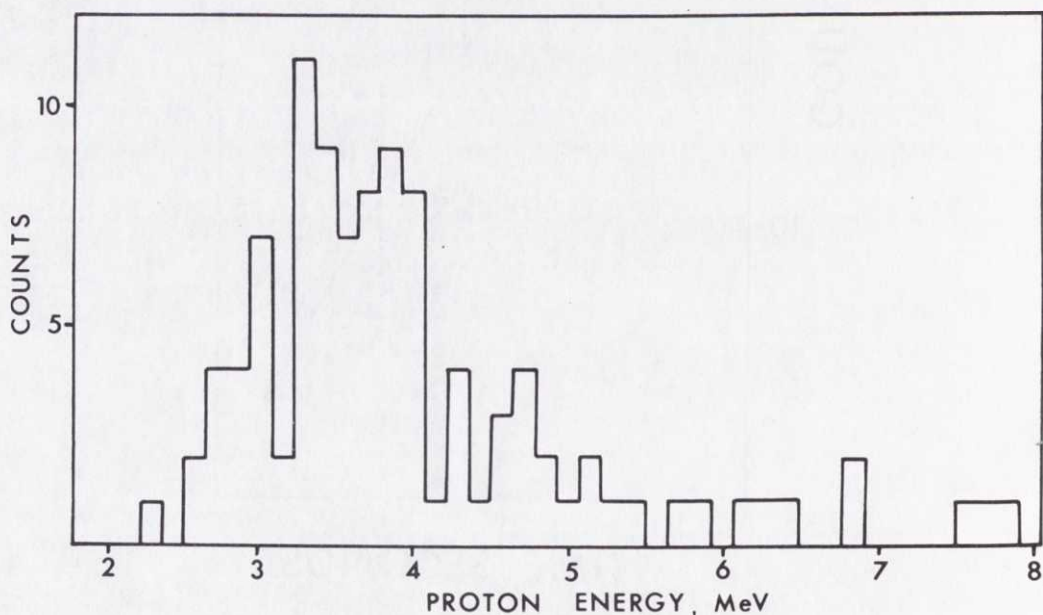


Fig. II.12 Energy distribution of proton events observed at the ^{113}Xe mass position. The experimental conditions were the same as for ^{183}Hg (see Fig. II.3).

As has been pointed out already, the delayed protons are the most easily distinguishable radiation available in this region, and a half-life measurement could best be based on proton detection. The conventional counter technique (see ^{118}Cs and ^{115}Xe) would, however, be far too time-consuming with the actual data rate for ^{113}Xe (about 15 protons/hour).

A much more efficient and sensitive method is to use the apparatus shown in Fig. II.13. The detection is performed with a nuclear emulsion as the detecting device. The set-up, shielded by 2 cm of lead, is placed inside the collector chamber of the isotope separator. Several ion beams can enter the apparatus at the same time through a slit in the lead shield. The activity is collected on a rotating disc which carries it in front of the emulsion.

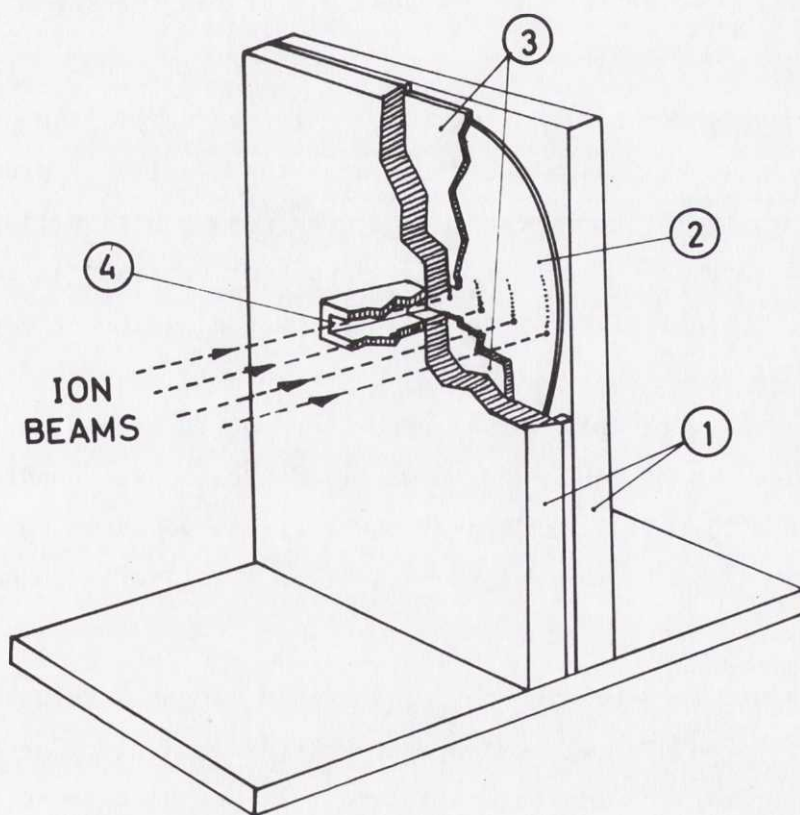


Fig. II.13 Rotating-disc apparatus used when searching for low intensity delayed-proton emitters. The separated isotopes enter the apparatus through a slit (4) and are stopped on a rotating disc (2). Proton events are detected in Ilford K2 nuclear emulsions (3) facing the disc. The set-up is placed inside the collector chamber of the isotope separator and shielded by lead (1).

Tests were performed with different emulsions by first exposing them to protons (4 - 10 MeV) at the Risø tandem, and later placing them inside the ISOLDE collector tank under normal running conditions. From these investigations it was found that the emulsion best suited for the purpose was Ilford K2. For this, the gamma background had only given a very weak fogging of the emulsion, and the entrance part of the proton tracks could clearly be seen. The identification of a proton is easy due to its typical range (50-400 μ) and ionization density.

For xenon the total exposure time was 11 hours and the mass range covered was 115-111. The mapping of the density of proton tracks was performed with a microscope. The field of view was $250 \times 250 \mu^2$. Only proton tracks originating at the surface and stopping in the emulsion were counted. A general background of about 0.5 proton tracks/ mm^2 was found over the whole emulsion plate.

The investigated area (about 6000 mm^2) covered all the masses of interest (111-114). The only region where the density of proton tracks was clearly above the background was at the mass position 113. Since the speed of rotation of the disc had been kept constant during the measurement, the half-life of the delayed-proton precursor could be obtained. The positions of the proton tracks were converted to polar coordinates, and were then sorted according to radius and angle. By summing the number of tracks for 6 mm broad arcs, corresponding to time intervals of 1.15 s ($\pi/12$ radians), the decay curve shown in Fig. II.14 was obtained. From these data the half-life of ^{113}Xe is found to be $2.8 \pm 0.2 \text{ s}$.

In general, the emulsion technique could become a valuable tool for the identification of low yield proton emitters and also for the identification of very weak proton branches. In a strong background of alpha activities a thin absorber could be used to eliminate them. The method should also be applicable to the detection of fission fragments and delayed alpha particles.

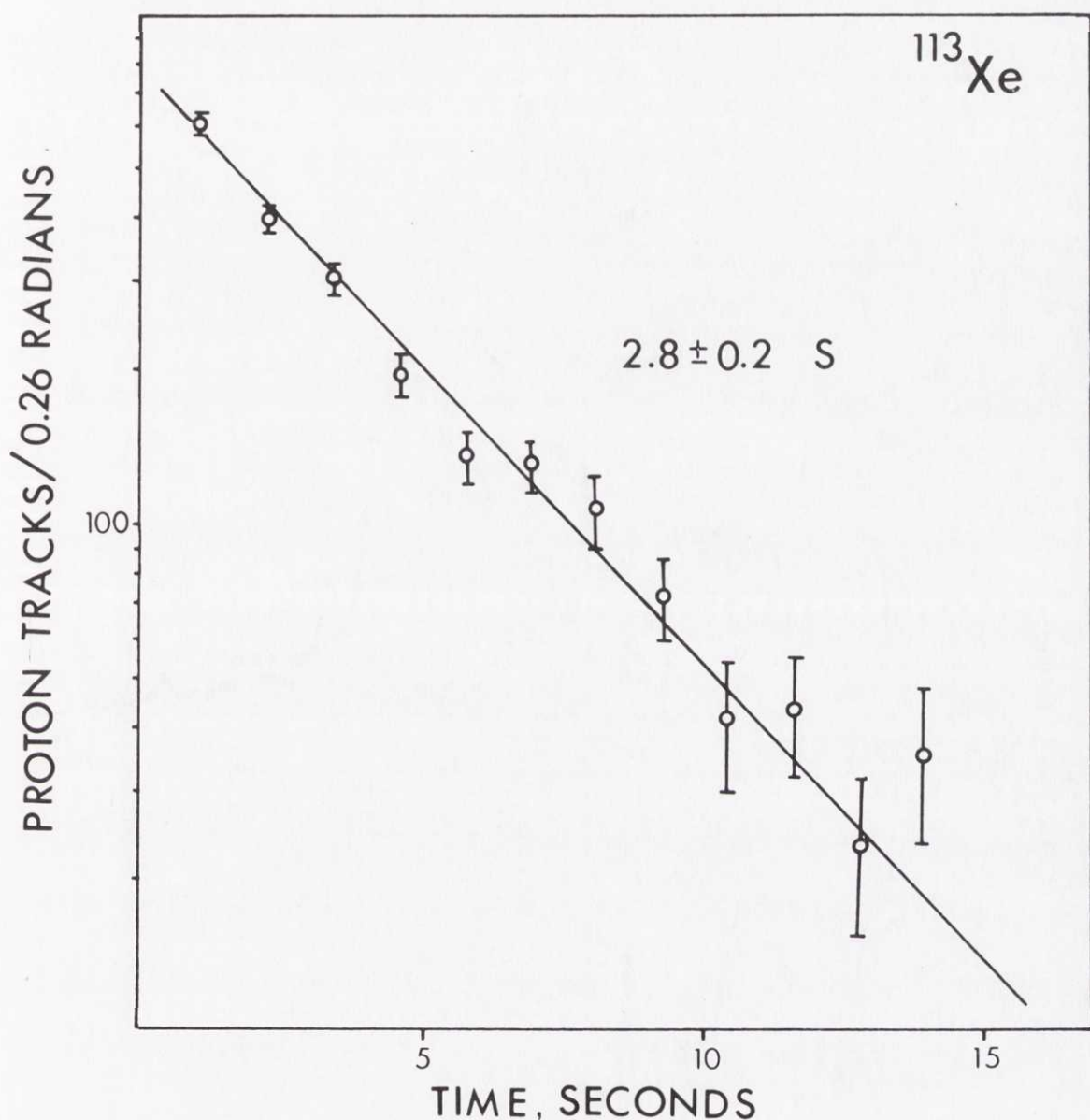


Fig. II.14 Decay curve of ^{113}Xe . The number of protons in the strip corresponding to mass 113 is plotted versus angle (the speed of rotation for the wheel was 27.5 s/r).

3.4 ^{73}Kr

The half-life of this nuclide measured from beta counting is $34 \pm 4 \text{ s}$ ¹⁷. The delayed-proton spectrum shown in Fig. II.15a was measured with a $30 \mu/100 \text{ mm}^2$ dE/dx detector and a $500 \mu/450 \text{ mm}^2$ E detector. The total number of atoms collected during the experiment was found, from counting on the 359 keV gamma ray from the decay of ^{73}Se ($I_\gamma \approx 100\%$)¹⁴, to be 1.5×10^6 . A fraction of the protons was lost in this experiment, because of the detector cut-off at 2 MeV. A correction for the loss was found

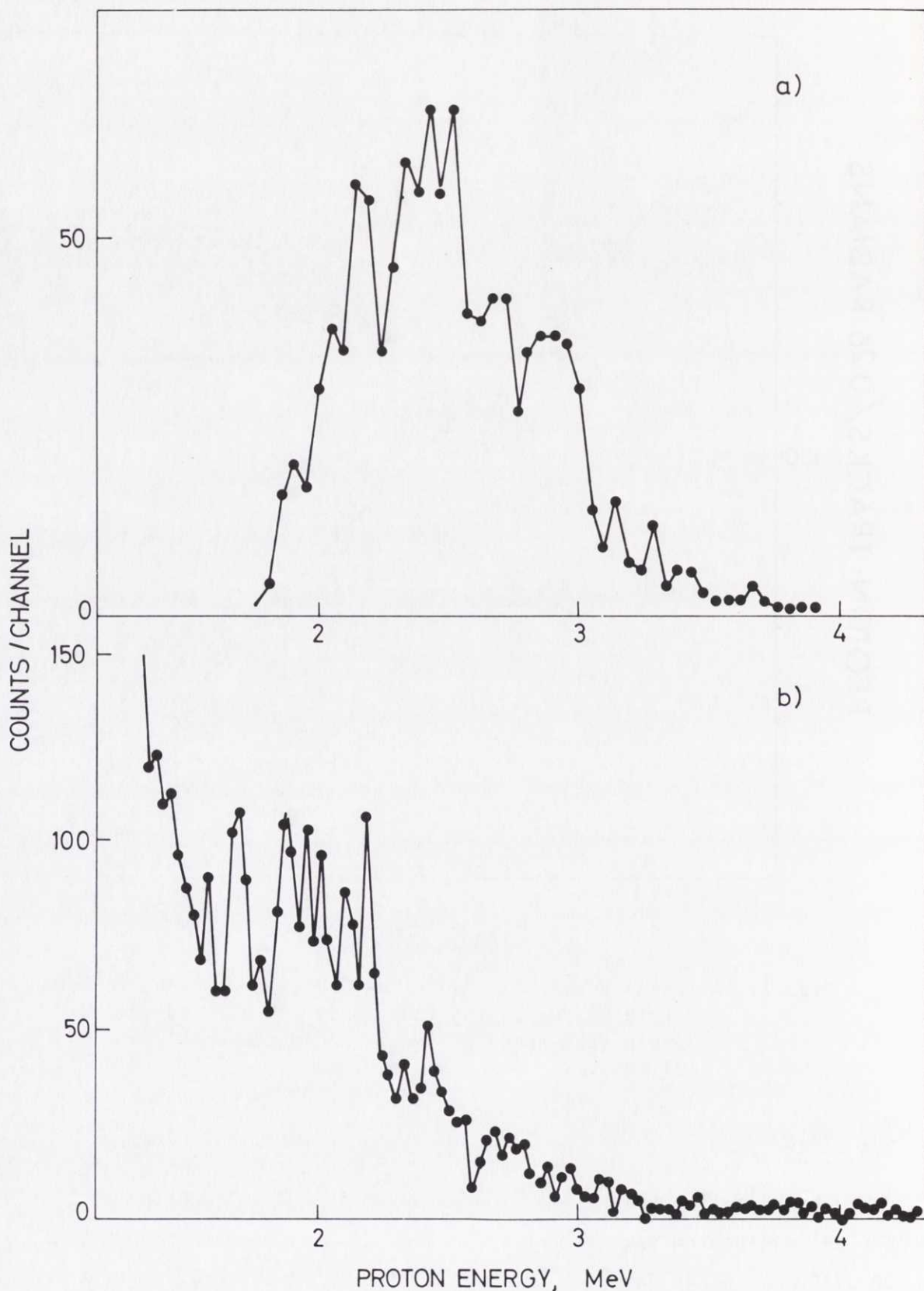


Fig. II.15 a) Delayed-proton spectrum for ^{73}Kr . Telescope detector: dE/dx : $30 \mu/100 \text{ mm}^2$; E : $500 \mu/450 \text{ mm}^2$. Solid angle: 13.9% of 4π . Collector foil: $80 \mu\text{g}/\text{cm}^2$ carbon. Cut-off: 2.0 MeV. Line width (alpha): 60 keV.
b) Delayed-proton spectrum for ^{73}Kr . Single detector: $300 \mu/300 \text{ mm}^2$. Solid angle: 24% of 4π . Collector foil: $80 \mu\text{g}/\text{cm}^2$ carbon. Line width (alpha): 25 keV.

from an experiment, where the delayed-proton spectrum was measured with a single, surface barrier detector (Fig. II.15b). A comparison of the number of protons above 2.5 MeV gave the correction factor and the resulting proton branching ratio was $(7.2 \pm 1.5) \times 10^{-3}$. A determination of the proton branch from the experiment with the single detector gave $(6.4 \pm 1.4) \times 10^{-3}$ p/dis.

According to Ref. (8), the $Q - B_p$ value for ^{73}Kr is 4.75 MeV, and for ^{73}Br delayed-proton emission is energetically forbidden ($Q - B_p = -1.65$ MeV). These relations, and the results reported in Chapter III (a 35% proton branch to the first excited state in ^{72}Se), support the assignment.

4. SUMMARY

The delayed-proton spectra observed in these experiments have all similar shapes: they show a broad bell-shaped hump with no pronounced fine structure. Even in the cases, where the detector line width was 15-20 keV, only relatively small fluctuations around the average intensity could be observed. The explanation to the comparatively smooth shapes of the spectra may be found from the following considerations: the proton-emitting states in the intermediate nucleus are at excitations, where the average level spacing for the medium- and heavy-weight elements is expected to be much smaller than the line width of the detectors used here (see Table V.1). Many levels may therefore contribute within the experimental resolution. Furthermore, all experimental evidence seems to indicate that the configurations giving rise to the beta strength^{11,18)} are distributed over many levels (with the same spin and parity), and over an energy region that is large compared with the detector resolution.

A direct practical application of beta-delayed proton counting has been demonstrated: extremely neutron-deficient nuclides, not detectable from other types of radiations may be identified via beta-delayed protons. (In later sections it will be discussed how delayed-proton emitters contribute to nuclear structure studies.)

A summary of the main results from the measurements of singles proton spectra and proton branching ratios is given in Table II.6.

Table II.6
Branching ratios in beta-delayed proton emission
from mercury, cesium, xenon, and krypton isotopes

Precursor	Half-life s	p/alpha	p/($\alpha + p + EC + \beta^+$)	Comment ^{a)}
^{183}Hg	$8.8 \pm 0.5^{\text{b)}$	$(2.3 \pm 0.3) \times 10^{-5}$	$(2.7 \pm 0.6) \times 10^{-6}$	A, see also Table II.3
^{182}Hg	$11.3 \pm 0.5^{\text{b)}$	$\leq 10^{-6}$	$\leq 10^{-7}$	Assignment tentative, only 3 events observed
^{181}Hg	$3.6 \pm 0.3^{\text{b)}$	$(3.6 \pm 0.6) \times 10^{-4}$	$(1.25 \pm 0.3) \times 10^{-4}$	A, C, see also Table II.3
^{179}Hg	$1.09 \pm 0.04^{\text{c)}$	$(2.8 \pm 0.5) \times 10^{-3}$	$\sim 1.5 \times 10^{-3}$	A, see also Table II.3
^{120}Cs	$58.3 \pm 1.8^{\text{d)}$	-	$\leq 5 \times 10^{-8}$	A, assignment tentative
^{118}Cs	$15 \pm 2^{\text{e)}$	-	$(4.2 \pm 0.6) \times 10^{-4}$	A, B, C
^{116}Cs	Not measured	-	Not measured	A, assignment tentative
^{117}Xe	$65 \pm 6^{\text{f)}$	-	$(2.9 \pm 0.6) \times 10^{-5}$	A, C
^{115}Xe	$18 \pm 4^{\text{g)}$	-	$(3.4 \pm 0.6) \times 10^{-3}$	A, B, C
^{113}Xe	$2.8 \pm 0.2^{\text{h)}$	-	Not measured	A
^{73}Kr	$34 \pm 4^{\text{i)}$	-	$(6.8 \pm 1.2) \times 10^{-3}$	A, C

Table II.6 cont.

- a) The delayed-proton precursor has been assumed to be the first member of the chain. This assignment is based on:
- A: Q - B_p relations from Ref. (8).
- B: Measurements of T_{1/2} on delayed protons.
- C: Observation of coincidences between protons and gamma rays de-exciting known levels in the final nucleus (Chapter III).
- b) Ref. (7).
- c) Ref. (10).
- d) Ref. (3).
- e) Half-life determined by proton counting. The value from beta counting³⁾ is 16.4 ± 1.2 s.
- f) Ref. (16).
- g) Half-life determined by proton counting. The value from beta counting¹⁶⁾ is 19 ± 5 s.
- h) Half-life determined by proton counting. Nuclear emulsion technique.
- i) Ref. (17).

REFERENCES TO CHAPTER II

- 1) The ISOLDE isotope separator on-line facility at CERN (eds. A. Kjelberg and G. Rudstam), CERN 70-3 (1970).
- 2) E. Hagebø, International conference on Electromagnetic Isotope Separators and the Techniques of Their Application, Marburg 1970, BMBW-FB K 70-28 (1970), p. 146.
- 3) H.L. Ravn, S. Sundell and L. Westgaard, Phys. Letters 39B, 337 (1972).
- 4) G. Andersson, H.E. Jørgensen and K.O. Nielsen, CERN 70-3 (1970), p. 19.
- 5) A. Lindahl, O.B. Nielsen and G. Sidenius, CERN 70-3 (1970), p. 55.
- 6) C. Williamson and J.P. Boujot, CEA-2189 (1962).
- 7) P.G. Hansen, H.L. Nielsen, K. Wilsky, M. Alpsten, M. Finger, A. Lindahl, R.A. Naumann and O.B. Nielsen, Nuclear Phys. A148, 249 (1970).
- 8) W.D. Myers and W.J. Swiatecki, UCRL-11980 (1965).
- 9) P.J. Daly, K. Ahlgren, K.J. Hofstetter and R. Hoechel, Nuclear Phys. A161, 177 (1971).
- 10) P.G. Hansen, B. Jonson, J. Żylicz, M. Alpsten, Å. Appelqvist and G. Nyman, Nuclear Phys. A160, 445 (1971).
- 11) C.L. Duke, P.G. Hansen, O.B. Nielsen and G. Rudstam, Nuclear Phys. A151, 609 (1970).
- 12) G. Andersson, G. Rudstam and G. Sörensen, Arkiv för Fysik 28, 37 (1965).
- 13) A. Damkjaer, private communication.
- 14) C.M. Leadrer, J.M. Hollander and I. Perlman, Table of Isotopes, (Wiley, New York, 1969).
- 15) L. Westgaard, private communication.
- 16) The ISOLDE collaboration, Phys. Letters 28B, 415 (1969).
- 17) E. Roeckl et al., to be published.
- 18) P. Hornshøj, B.R. Erdal, P.G. Hansen, B. Jonson, J. Żylicz, K. Johansson and G. Nyman, to be published.

CHAPTER III

MEASUREMENTS OF COINCIDENCES BETWEEN DELAYED PROTONS AND GAMMA RAYS

1. INTRODUCTION

The daughter nucleus, after the emission of a delayed proton, is left in its ground state or in an excited state. Experimental information on the relative feeding of these states can be obtained from counting of coincidences between the protons and the gamma rays de-exciting the final states. Such data provide a direct test of the calculations described in the next chapter, and may give an indication of the spin of the mother nuclide. Besides that, coincidences between protons and annihilation radiation from positrons, feeding the proton-emitting states, can be used to determine the energy available for delayed-proton emission. This energy ($Q - B_p$) is an important parameter for the comparison of theoretical and experimental spectral shapes, and provides also a check of the semi-empirical mass formulas.

2. EXPERIMENTAL TECHNIQUES

The experimental set-up used in the proton-gamma coincidence experiments is shown in Fig. III.1. This arrangement was placed at the end of an ion-optical transfer line¹⁾. The ion beam was intercepted on a $80 \mu/\text{cm}^2$ carbon foil, and the proton and gamma counters were placed directly behind the foil. The whole set-up was shielded with lead. The main background in these experiments was, however, due to daughter activities accumulated on the collector foil.

Four different detector combinations were used:

- A: A surface barrier silicon detector ($400 \mu/450 \text{ mm}^2$) for the protons and a $7.6 \text{ cm} \times 7.6 \text{ cm}$ NaI(Tl) crystal for the gamma rays.

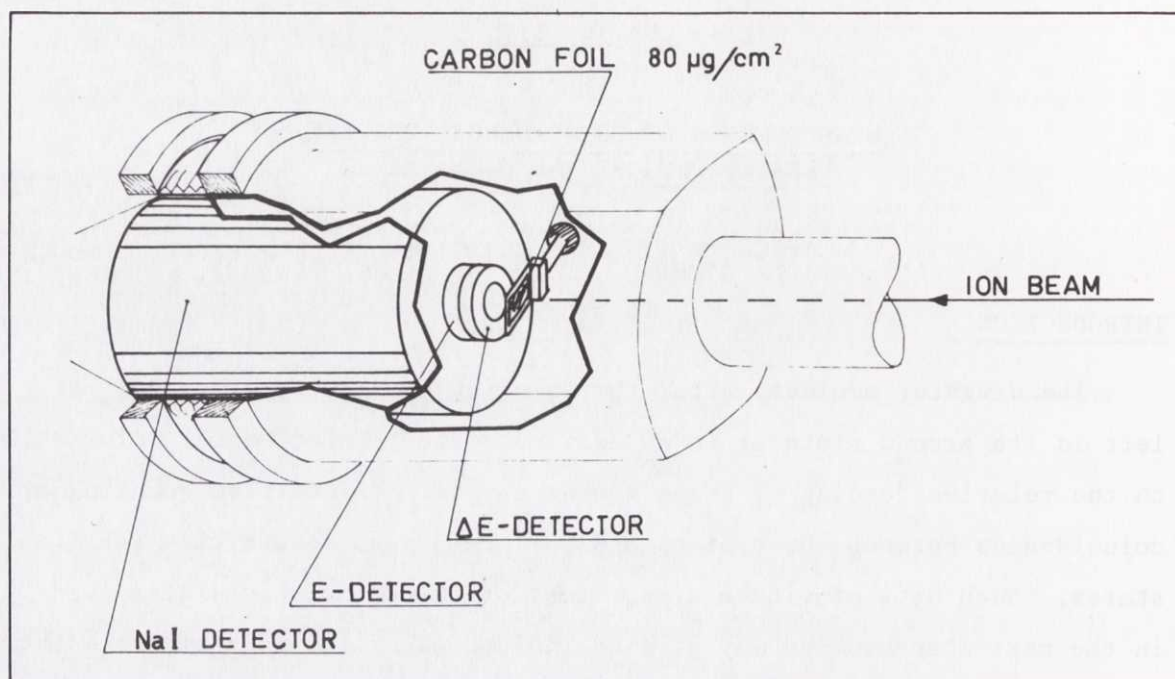


Fig. III.1 Set-up for the determination of proton-gamma coincidences. The ion beam is intercepted by an $80 \mu\text{g}/\text{cm}^2$ carbon foil placed in front of a proton detector. Immediately behind this the gamma detector is placed.

- B: A surface barrier silicon detector ($300 \mu/300 \text{ mm}^2$) for the protons and a $7.6 \text{ cm} \times 7.6 \text{ cm}$ NaI(Tl) crystal for the gamma rays.
- C: A surface barrier silicon detector ($300 \mu/300 \text{ mm}^2$) for the protons and a 25 cm^3 Ge(Li) detector for the gamma rays.
- D: A proton telescope (dE/dx : $40 \mu/150 \text{ mm}^2$; E : $400 \mu/450 \text{ mm}^2$) and a $7.6 \text{ cm} \times 7.6 \text{ cm}$ NaI(Tl) crystal for the gamma rays.

The block diagram in Fig. III.2 shows the main principles of the coupling used in these experiments. The coincidence system was calibrated with a ^{241}Am source (5.486 MeV alpha particles and 59.54 keV gamma rays). The absolute efficiencies of the gamma counters were determined by counting calibrated standard sources placed at the position of the collector foil.

Two kinds of spectra were recorded: (i) singles proton spectra; and (ii) two-dimensional spectra of coincidence events between protons and gamma rays. With such data the proton branch $p(E_f)$, to a level of energy E_f , is calculated from the expression

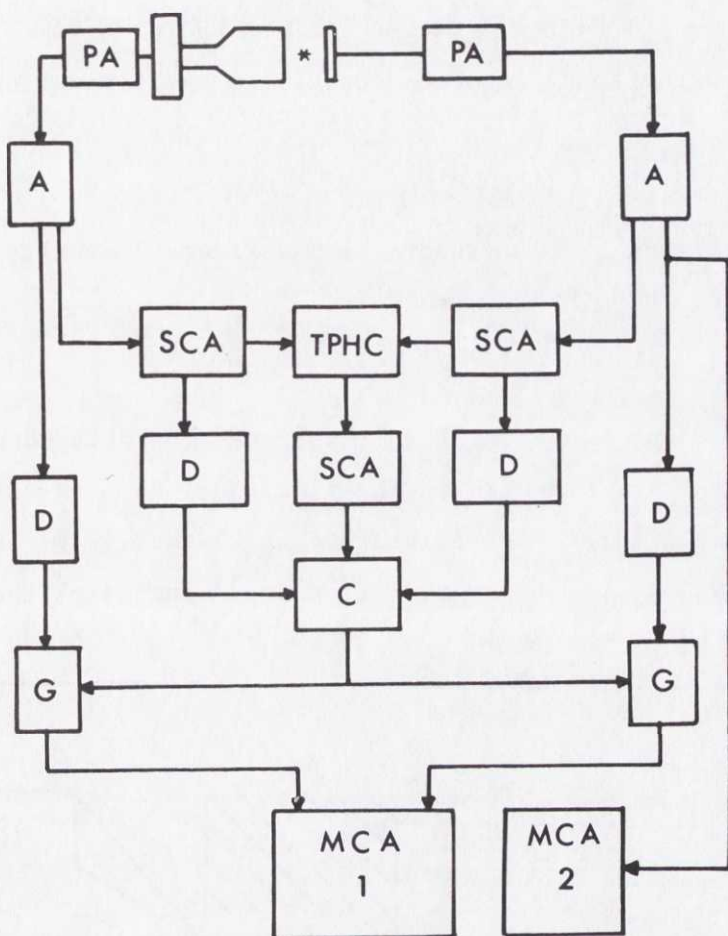


Fig. III.2 Block diagram of the electronics used for counting of proton gamma coincidences. (PA = preamplifier; A = amplifier; SCA = single channel analyzer; TPHC = time-to-pulse height converter; D = delay; C = coincidence unit; G = gate; MCA1 = multi-channel analyzer for registering of the two dimensional spectrum of coincidence events between protons and gamma rays; MCA2 = multi-channel analyzer for registering of the singles proton spectrum).

$$p(E_f) = \frac{N_c (1 + \alpha_T)}{N_T \cdot \epsilon_\gamma(E_f - E_0)} \quad (\text{III.1})$$

where N_c is the number of coincidence events between protons and gamma rays of energy $(E_f - E_0)$, N_T is the total number of protons in the singles

spectrum, $\epsilon_Y(E_f - E_0)$ is the detector efficiency for a gamma ray from E_f to E_0 , and α_T is the total internal conversion coefficient of the transition.

3. RESULTS

In the following a summary of the experimental results for ^{181}Hg , ^{118}Cs , $^{117,115}\text{Xe}$, and ^{73}Kr is given.

3.1 ^{181}Hg

The decay scheme in Fig. III.3 illustrates the delayed-proton emission with ^{181}Hg as the precursor. The final nucleus after proton emission ^{180}Pt , has its first excited state²⁾ at 159 keV (2^+). Furthermore, the level systematics of the even Pt isotopes³⁾ indicates that the

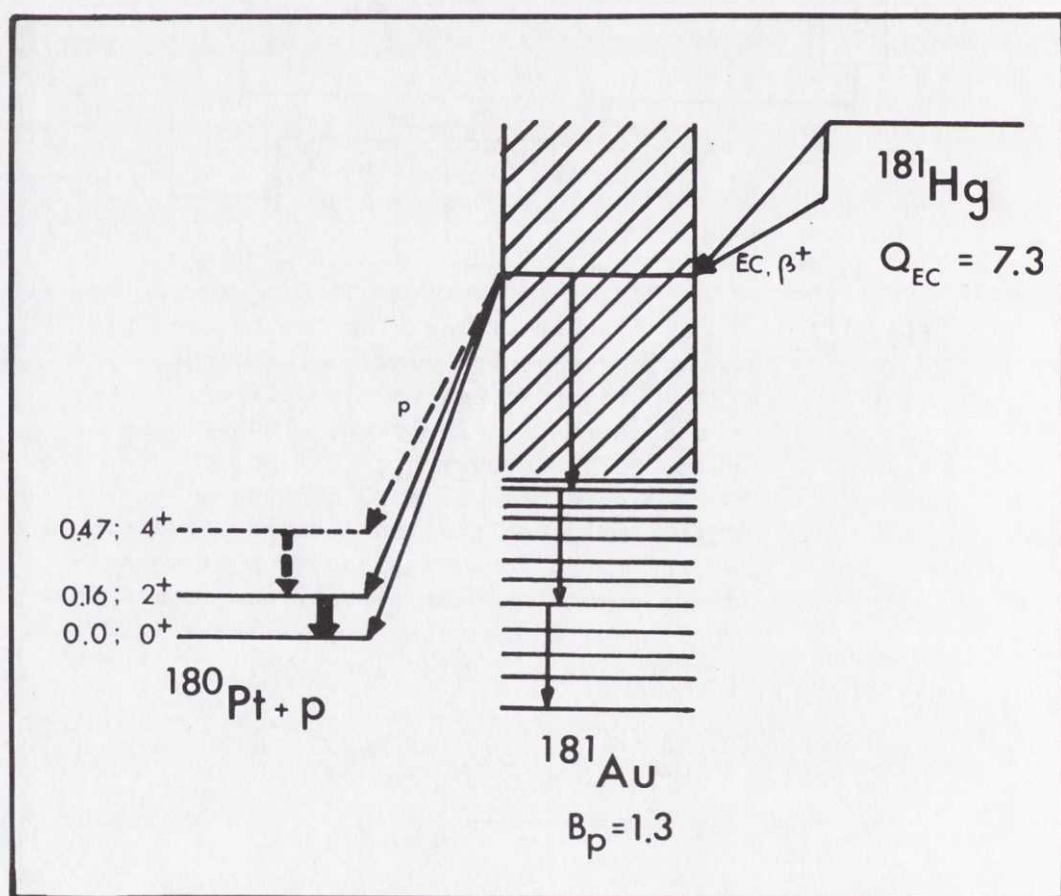


Fig. III.3 Delayed-proton emission in the decay of ^{181}Hg . Q_{EC} and B_p values are taken from Ref. (11). Energies in MeV.

lowest 4^+ -level has an excitation energy of about 470 keV. The beta decay to highly excited states in ^{181}Au is dominated by electron capture, giving rise to proton-K-X coincidences in addition to the same type of coincidences from internal conversion of the transitions in ^{180}Pt (mainly $2^+ \rightarrow 0^+$). The experiment was carried out with a telescope detector (set-up D). The two-dimensional spectrum was recorded in a 4096 channel analyzer, operated in the 32×128 channel mode. The energy range for protons was 2-7 MeV (32 ch), and gamma energies up to 500 keV were covered (128 ch). The total time used in this experiment was 10 hours, and during this time 988 protons were recorded in the singles spectrum. The spectrum of gamma rays, in coincidence with protons recorded during the same counting period, is shown in Fig. III.4. The lines in this spectrum correspond to coincidences with K-X-rays (from ^{180}Pt and ^{181}Au), a line at 150 ± 15 keV ($2^+ \rightarrow 0^+$ in ^{180}Pt), and a line at 235 ± 25 keV (sum peak of $2^+ \rightarrow 0^+$ and K-X-rays from ^{181}Au). The feeding of the 2^+ level is $50 \pm 10\%$. The $4^+ \rightarrow 2^+$ transition in ^{180}Pt is expected to have an energy of approximately 310 keV. In this energy region of the coincidence spectrum only a few events can be seen. The corresponding upper limit to the feeding to the 4^+ level is 6%.

3.2 ^{118}Cs

This nuclide is the only odd-Z delayed-proton emitter for which proton-gamma counting has been performed. The final nucleus after proton emission is ^{117}I . A complete level scheme for ^{117}I is not yet known, but data⁴⁾ from counting of gamma rays from the decay of ^{117}Xe indicate that several low energy levels exist. The energies and intensities of the strongest lines in the gamma spectrum are given in Table III.1.

The proton-gamma experiment was performed with set-up B. The total counting period was 10 hours, and the singles proton spectrum recorded during that time is shown in Fig. II.7. The spectrum of gamma rays, in coincidence with protons registered during the same counting period, is shown in Fig. III.5. As expected, several lines with relatively low energies (42 ± 10 keV, 114 ± 20 keV, 159 ± 20 keV, 218 ± 25 keV, 305 ± 30 keV, and 511 ± 20 keV) are found in the spectrum.

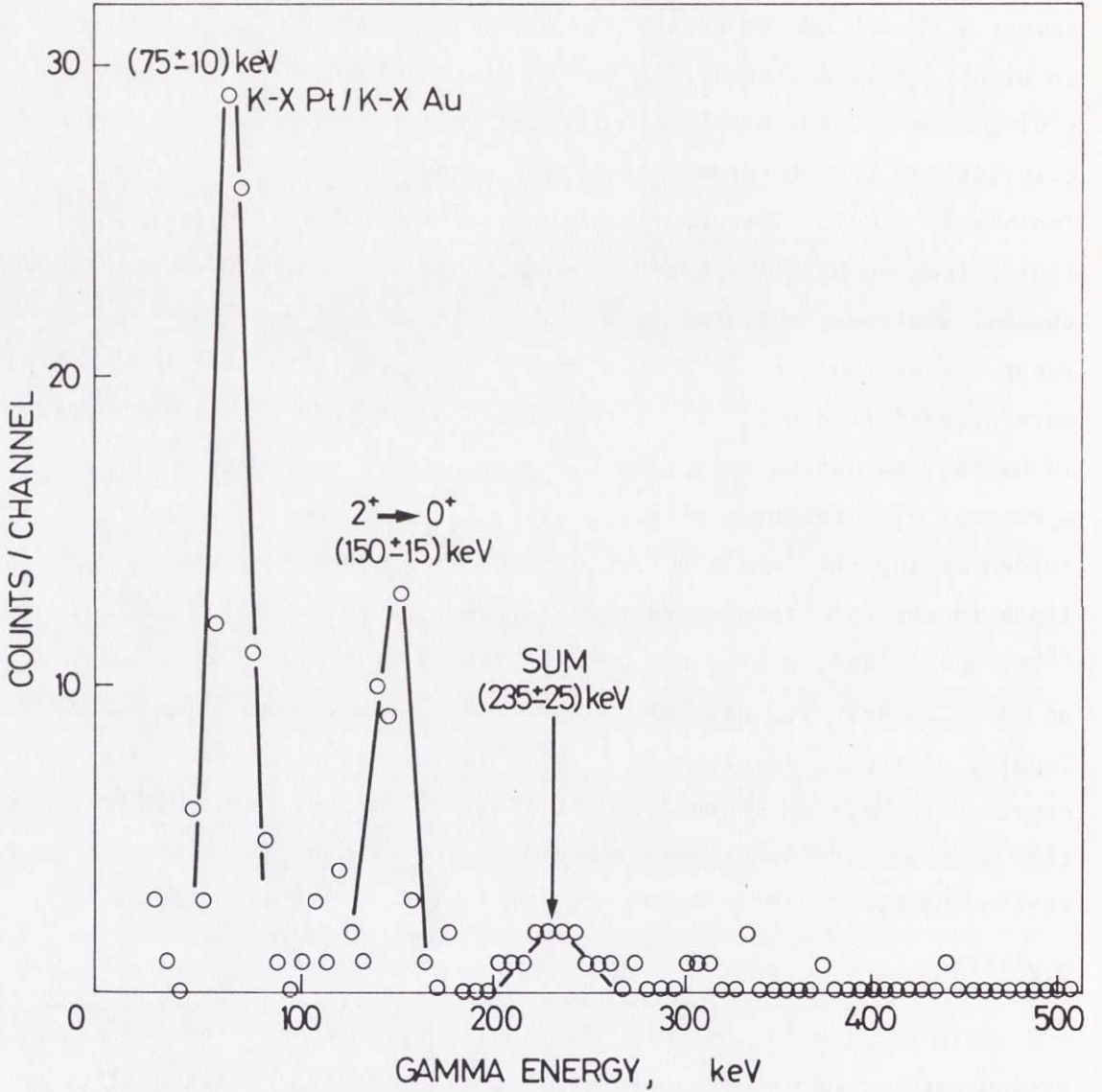


Fig. III.4 Spectrum of gamma rays in coincidence with delayed protons from ^{181}Hg . Coincidences are observed between delayed protons and K-X-rays (from ^{181}Au and ^{180}Pt) and a gamma line at 150 ± 15 keV (corresponding to the $2^+ \rightarrow 0^+$ transition in ^{180}Pt at 159 keV). The sum line consists of K-X-rays from ^{181}Au and gamma rays from the $2^+ \rightarrow 0^+$ transition in ^{180}Pt . No pronounced peak is observed at 310 keV (corresponding to the $4^+ \rightarrow 2^+$ transition in ^{180}Pt).

The corresponding coincidence intensities given in Table III.2 have not been corrected for internal conversion (Eq. III.1). The last column in the table gives the energies of those lines in the ^{117}Xe gamma spectrum which are probably identical with the observed coincidence lines.

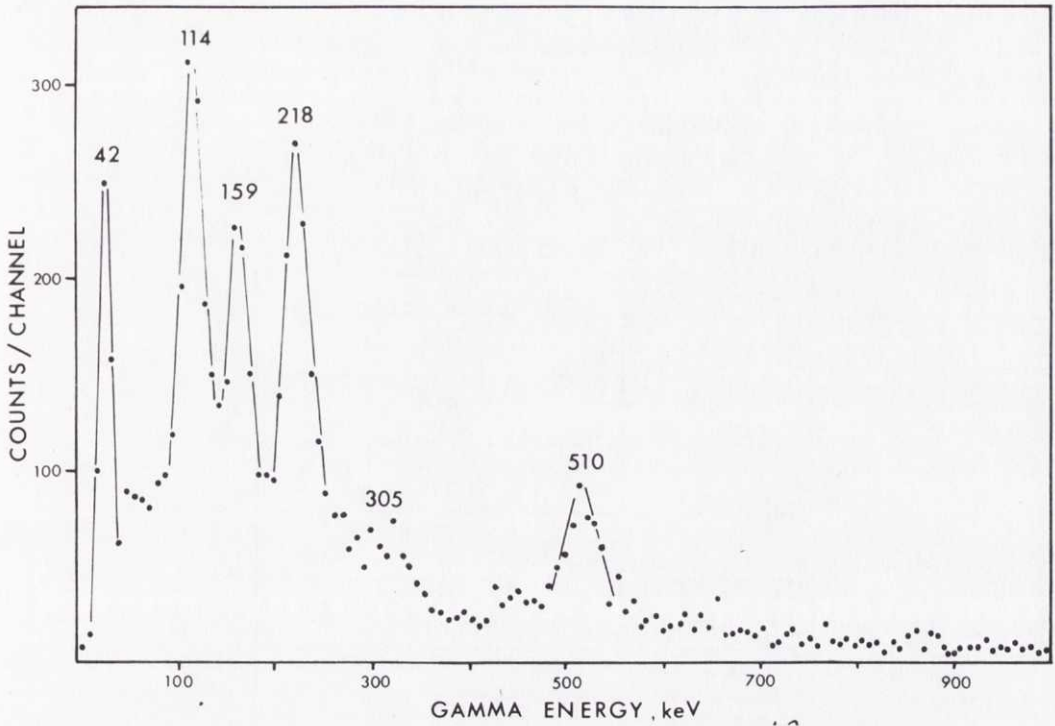


Fig. III.5 Spectrum of gamma rays in coincidence with delayed protons from ^{118}Cs . The four gamma lines at 114, 159, 218, and 305 keV can be identified as the 116, 161 (155), 220, and 295 keV gamma rays from the decay of ^{117}Xe . The line at 42 keV lies just at the cut-off in the spectrum and the energy is therefore uncertain. The line at 510 keV is proton coincidences with annihilation radiation from positrons feeding the excited states in the intermediate nucleus, ^{118}Xe . The additional counts above 510 keV can be explained as chance coincidences between delayed protons and gamma rays from the background.

Table III.1

Energies and intensities^{a)}
of the main gamma lines
in the decay of ^{117}Xe

E (keV)	Relation intensity (%)
28	100
32	40
44	5
57	5
59	9
94	4
116	10
155	4
161	6
221	15
295	10
438	6
518	8

a) Ref. (4).

Table III.2

Results of the delayed proton-gamma coincidence experiment for ^{118}Cs

Energy (keV)	Coincidence intensity (%)	E_{γ} in ^{117}I a) (keV)
$42 \pm 10^{\text{b)}}$	~ 40	44
114 ± 20	14	116
159 ± 20	8	$161^{\text{c)}}$
218 ± 25	13	221
305 ± 30	3	295
511 ± 20	(2.1 ± 0.5)	$511^{\text{d)}}$

- a) Gamma ray energy observed in the decay of ^{117}Xe which is probably identical with the observed line.
- b) The energy is uncertain, since the line lies just at the cut-off of the detector system.
- c) Could as well be the line at 155 keV or both 155 keV and 161 keV.
- d) Annihilation radiation from positrons feeding the proton emitting states.

The proton spectra in coincidence with the gamma rays at 114, 159, 218, and 305 keV are shown in Fig. III.6. The endpoints of these spectra should in principle give information that could be used to determine the excitation energy of the final levels, but the statistics are too low here. The increased intensity at lower energies is mainly due to positron-gamma coincidences from the decay of ^{118}Cs and its daughters.

A background of coincidence events is spread over the whole spectrum, shown in Fig. III.5. An analysis of these events indicates that they have to be explained partly as "chance" proton-gamma coincidences and partly

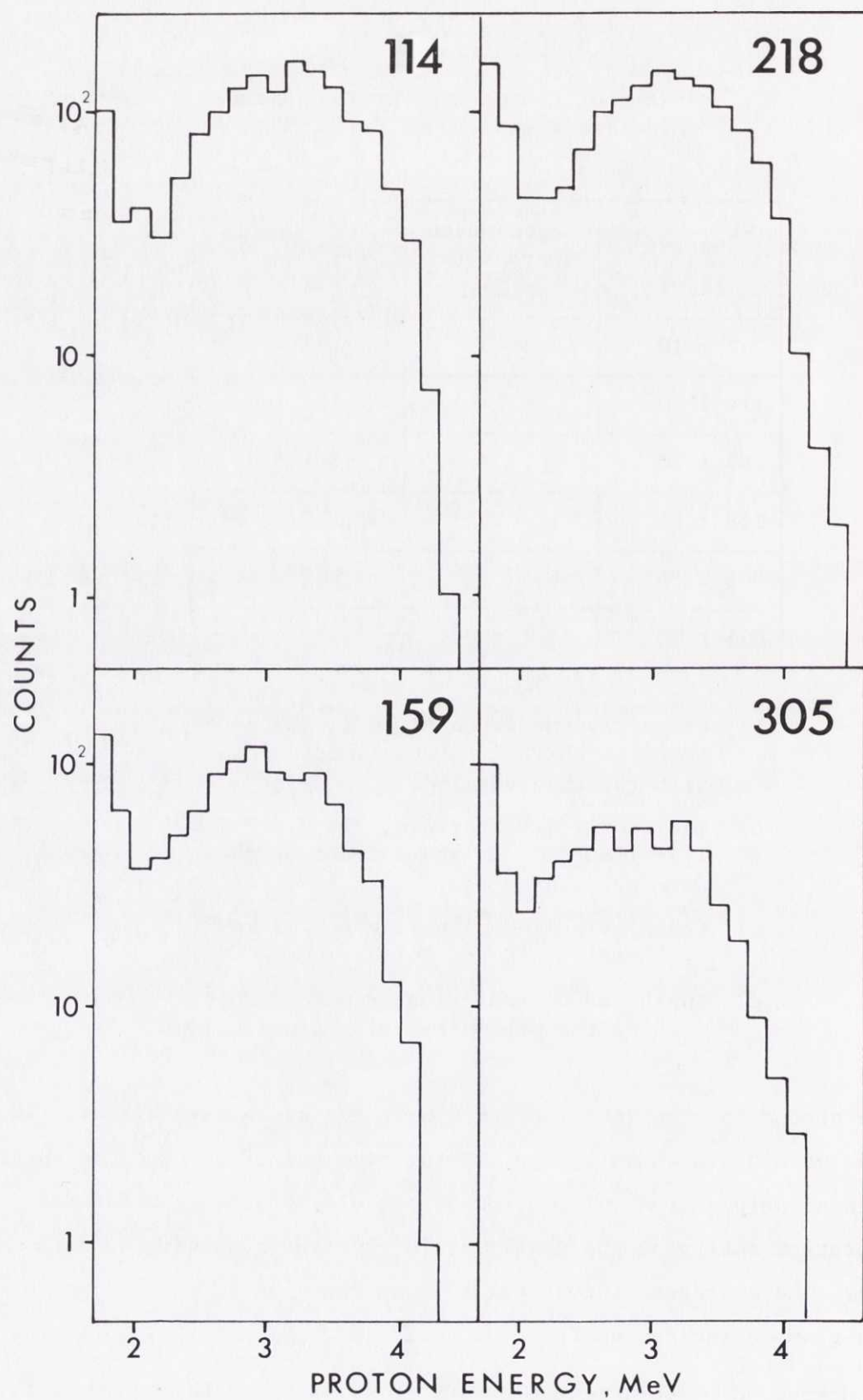


Fig. III.6 Delayed-proton spectra from ^{118}Cs in coincidence with gamma rays at 114, 159, 218, and 305 keV.

as positron-gamma coincidences. The total number of such proton-gamma coincidences is found to be about 1% of the total number of protons registered in the singles spectrum. The gamma background during the experiment was of the order of 25000 counts/s and the window in the time channel was about 350 ns. The expected chance coincidence rate is then about 0.9% which indicates that the additional counts in the spectrum can be explained as chance coincidences.

3.3 ^{117}Xe

The final nucleus after delayed-proton emission from ^{117}Xe , ^{116}Te , has excited levels⁵⁾ at 679 keV (2^+) and at 1359 keV (4^+). The proton branch of ^{117}Xe is relatively weak (Table II.6) which means that the number of non-coincident positrons per proton is high. The proton-gamma coincidence experiment therefore had to be performed with a telescope detector, for the protons to eliminate the high beta background (set-up D).

The spectrum of coincident events between gamma rays and delayed protons collected during a 7 hour counting period is shown in Fig. III.7. During the same time 3300 protons were registered in the singles proton spectrum. The peak in the coincidence spectrum, at about 650 keV, corresponds to the $2^+ \rightarrow 0^+$ transition in ^{116}Te . At 500 keV, corresponding to the expected minimum in the Compton distribution of the 650 keV transition, 10 counts are observed, while the 650 keV contribution should be about 3 counts. The excess seems to be statistically significant, and the peak at about 500 keV is interpreted as annihilation radiation. The solid curve in the spectrum, based on the measured detector response for 511 and 662 keV gamma lines (from ^{22}Na and ^{137}Cs), indicates that the coincidences at lower energies can be explained as caused by the sum of the two Compton distributions from the gamma rays. Based on these data, the feeding of the 2^+ level is $14 \pm 3 \%$, and the percentage of protons preceded by positron decay is $3.0 \pm 1.5 \%$. In order to reduce the gamma background from the accumulated daughter activities, the collector foil was changed several times during the experiment. Still, the mean rate in the gamma detector was of the order of 50000 counts/s. The window in the time channel was 200 ns. The additional counts above the 650 keV peak may therefore be interpreted as chance coincidences.

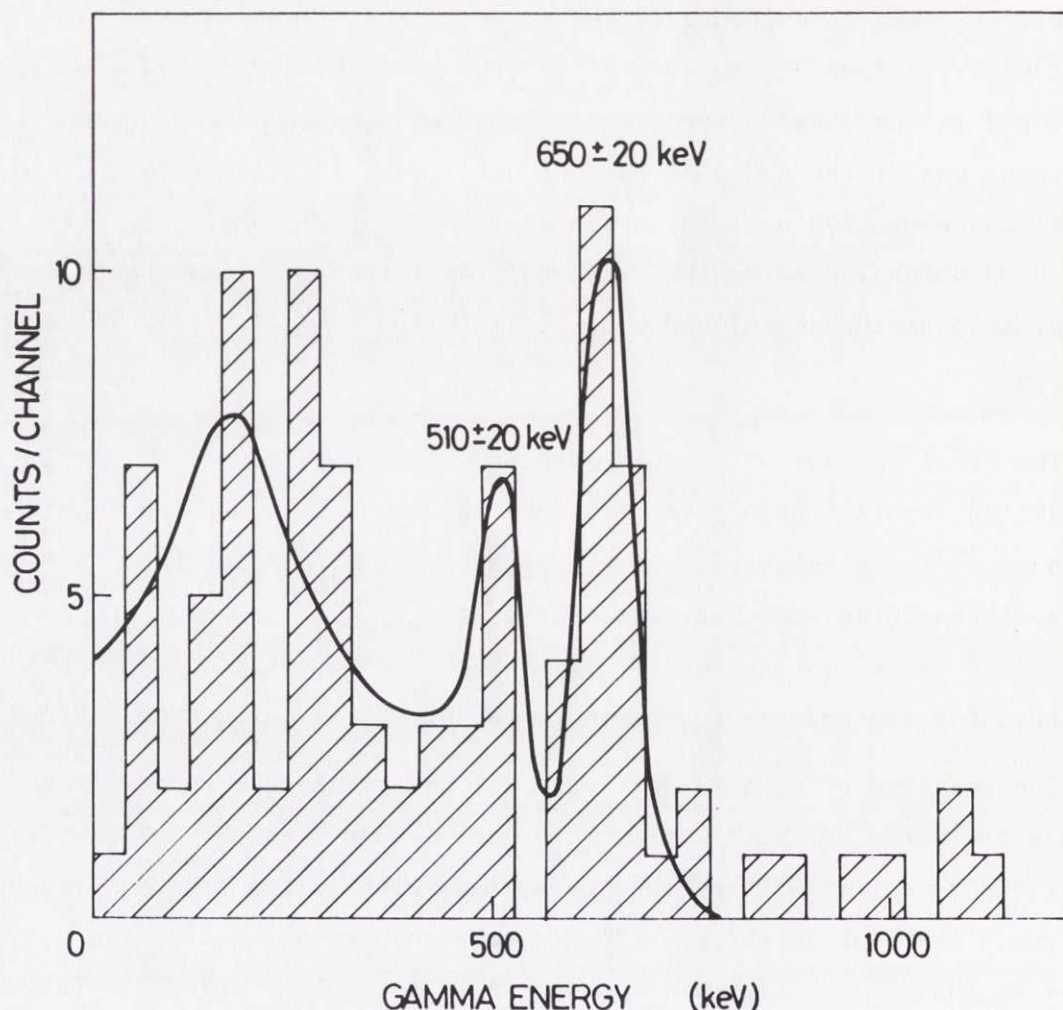


Fig. III.7 Spectrum of gamma rays in coincidence with delayed protons from ^{117}Xe . Coincidences with the $2^+ \rightarrow 0^+$ gamma ray in ^{116}Te are observed (679 keV). The peak at 510 keV is interpreted as proton coincidences with annihilation radiation. The solid curve is based on the measured detector response for 511 and 662 keV gamma rays.

3.4 ^{115}Xe

The final nucleus after delayed-proton emission from ^{115}Xe is ^{114}Te which has excited levels⁵⁾ at 709 keV (2^+) and 1484 keV (4^+). The coincidence experiment was performed with set-up A. During a counting period of 20 hours, a total number of about 70000 protons were registered in the singles spectrum. The corresponding proton-gamma coincidence spectrum is shown in Fig. III.8. The gamma projection of this spectrum has two

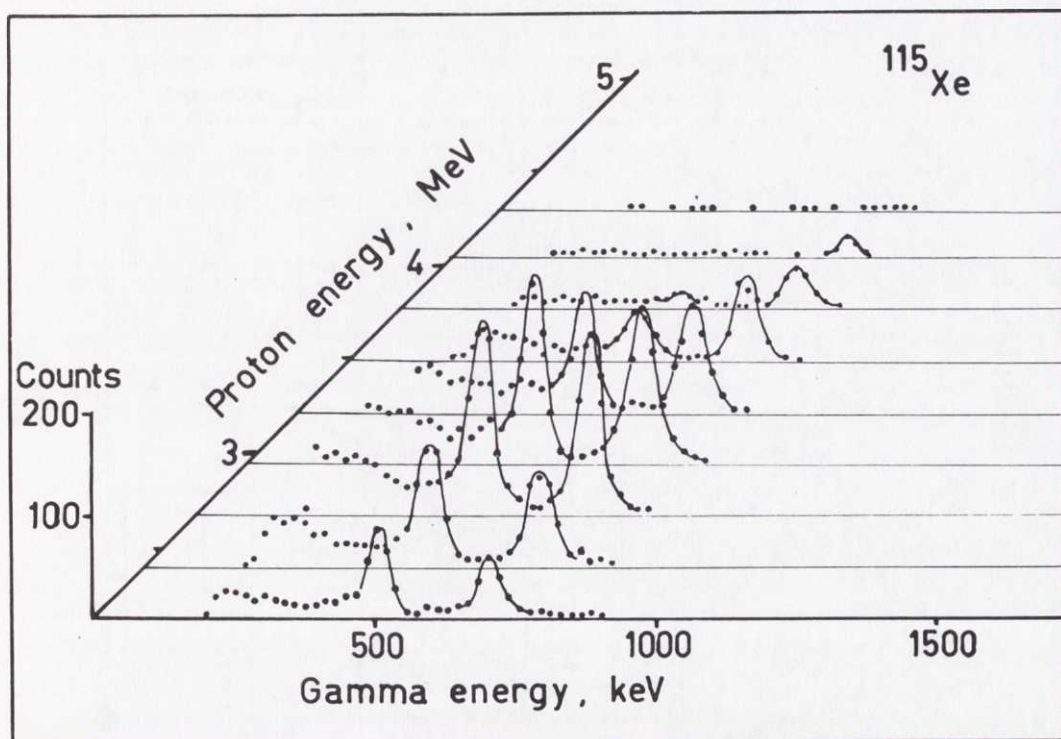


Fig. III.8 The two-dimensional spectrum of coincidence events between delayed protons and gamma rays from ^{115}Xe . The lines at 510 ± 20 keV and 710 ± 20 keV correspond to annihilation radiation from positrons in the beta decay of ^{115}Xe and gamma rays from the $2^+ \rightarrow 0^+$ transition in ^{114}Te (709 keV), respectively.

prominent lines: a 710 ± 20 keV line corresponding to the $2^+ \rightarrow 0^+$ transition in ^{114}Te and a line at 510 ± 20 keV representing coincidences with annihilation radiation from positrons feeding the excited levels in ^{115}I . Gamma energies up to 2 MeV were covered, and a weak tail of counts was observed up to the end of the spectrum. This can be explained as due to chance coincidences (less than 1%), and besides that the large fraction of positrons per proton will cause some 511-709 keV summing. The intensity data are given in Table III.4, and Fig. III.9 shows a comparison between the singles proton spectrum and the spectra in coincidence with 709 keV and 511 keV gamma rays. The coincidence spectra in the figure have been corrected for the efficiency of the NaI(Tl) crystal. The coincidence rate, as a function of the proton energy, is also listed in Table III.3.

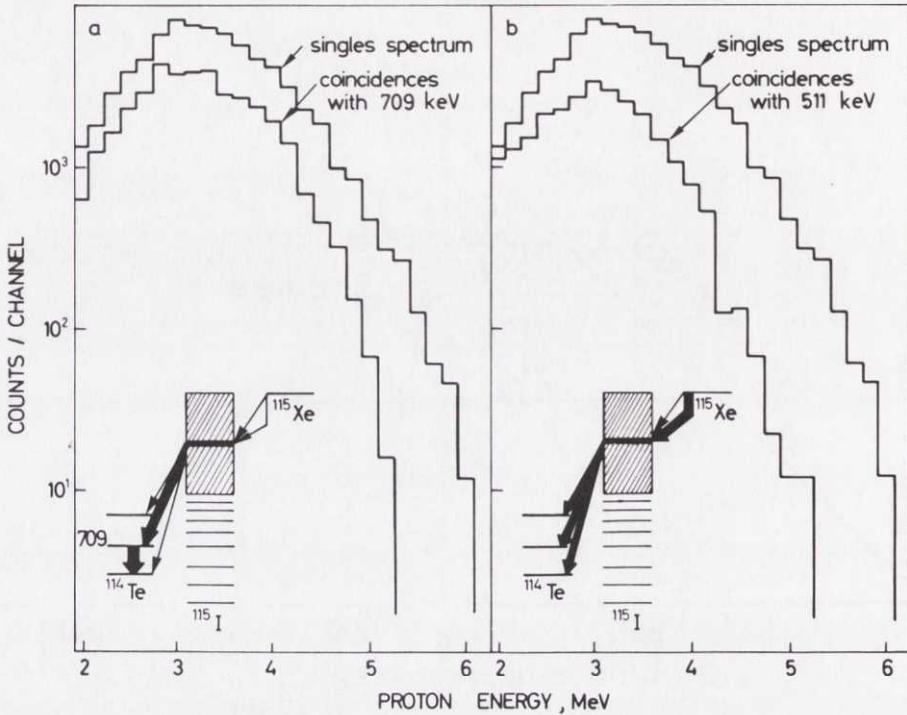


Fig. III.9 a) ^{115}Xe singles proton spectrum and spectrum in coincidence with the 709 keV transition in ^{114}Te . The coincidence spectrum has been corrected for the efficiency of the NaI(Tl) crystal. The decay scheme of the process is also shown. b) ^{115}Xe singles spectrum and spectrum in coincidence with annihilation radiation.

The population of the 4^+ level at 1484 keV in ^{114}Te should be detectable, either via the $4^+ \rightarrow 2^+$ gamma ray (775 keV), or via the 1484 keV sum line in the NaI(Tl) counter. As the proton decay to the 4^+ level is energetically unfavoured, the 775 keV $4^+ \rightarrow 2^+$ transition is expected to have a low intensity compared to that of the 709 keV line, and, therefore, cannot be resolved from this with the NaI(Tl) spectrometer. At the position of the sum peak of 709 keV and 775 keV gamma rays, no significant increase of the coincidence rate could be observed. An upper limit of the 4^+ feed of 4% was obtained.

It was obvious that a more sensitive experiment had to be carried out to get further information on the feed of the 4^+ level. With a $25 \text{ cm}^3 \text{ Ge(Li)}$ counter the two interesting gamma lines (709 keV and 775 keV)

Table III.3

Percentage of coincidences with 511 keV
and 709 keV gamma rays for ^{115}Xe .
Data taken with detector system A.

Proton energy (MeV)	Positrons per proton (%)	709 keV gamma rays per proton (%)
2.35	67 ± 6	84 ± 7
2.65	52 ± 3	73 ± 3
2.95	39 ± 2	63 ± 2
3.30	36 ± 2	63 ± 2
3.60	27 ± 2	51 ± 3
3.90	17 ± 2	52 ± 3
4.20	9 ± 2	43 ± 5
4.55	0	27 ± 5
4.85	0	22 ± 6
5.15	0	3 ± 3

should easily be resolved. An experiment was therefore performed with the detector combination C. The time used for data collection was about 15 hours, and the singles proton spectrum contained about 36000 proton events (Fig. II.10). The resulting spectrum of gamma rays in coincidence with protons is shown in Fig. III.10. The expected coincidences with annihilation radiation and with the 709 keV gamma rays are seen in the spectrum. No coincidences with a 775 keV gamma ray can be found, and an assumed upper limit of two counts corresponds to a limit on the 4^+ feed of 2%. The results from the two coincidence experiments with ^{115}Xe are summarized in Table III.4.

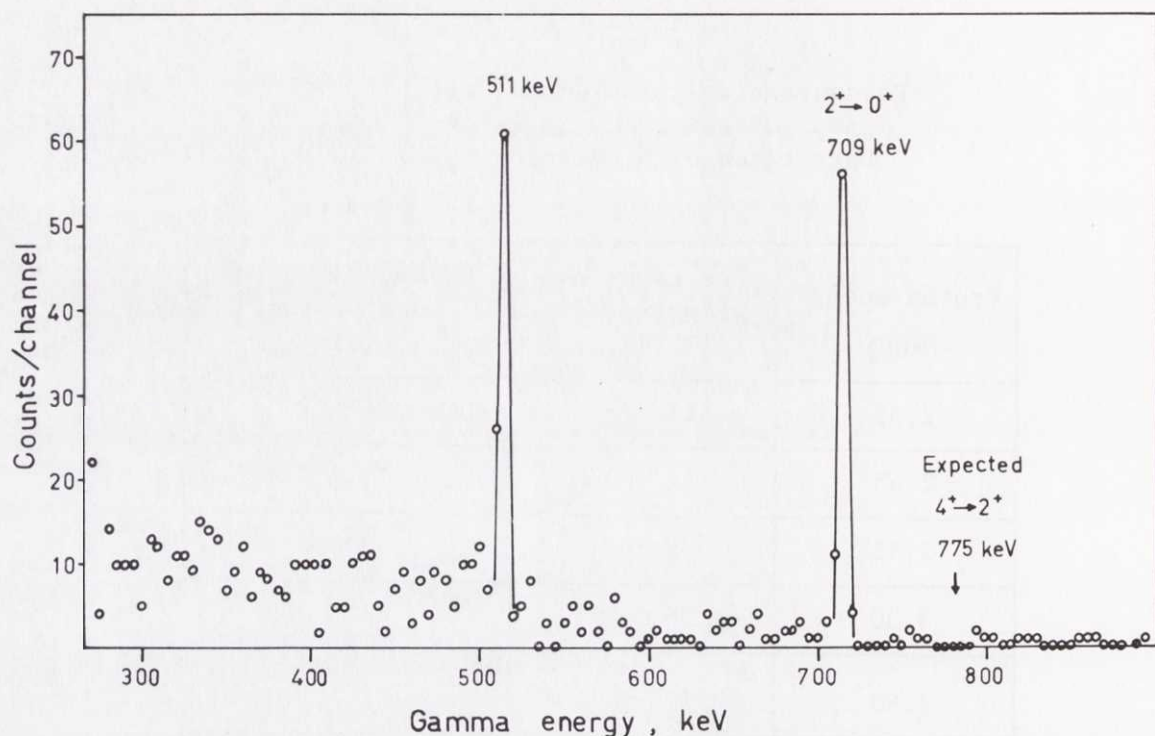


Fig. III.10 Spectrum of gamma rays in coincidence with beta-delayed protons from ^{115}Xe . A $300\ \mu/300\ \text{mm}^2$ surface barrier silicon detector was used as the proton detector and a $25\ \text{cm}^3$ Ge(Li) detector for the gamma rays. Coincidences with annihilation radiation and the $2^+ \rightarrow 0^+$ transition in ^{114}Te are observed. No events coincident with a 775 keV gamma ray (corresponding to the $4^+ \rightarrow 0^+$ transition in ^{114}Te) can be seen.

Table III.4

Results from the delayed proton-gamma coincidence experiment for ^{115}Xe

$2^+ \rightarrow 0^+$ 709 keV (%)	$4^+ \rightarrow 2^+$ 775 keV (%)	Annihilation radiation 511 keV (%)	Detector system
57 ± 10	<4	32 ± 6	A
59 ± 9	<2	25 ± 6	C
58 ± 7	<2	28 ± 4	Best value

3.5 ^{73}Kr

The final nucleus after proton emission in this case, ^{72}Se , has excited levels⁶⁾ at 862 keV (2^+), 1317 keV (2^+), and 1637 keV (4^+). The proton-gamma coincidence experiment was performed with set-up B. The spectrum of gamma rays in coincidence with delayed protons recorded during a 7 hour counting period is shown in Fig. III.11. The strong line at

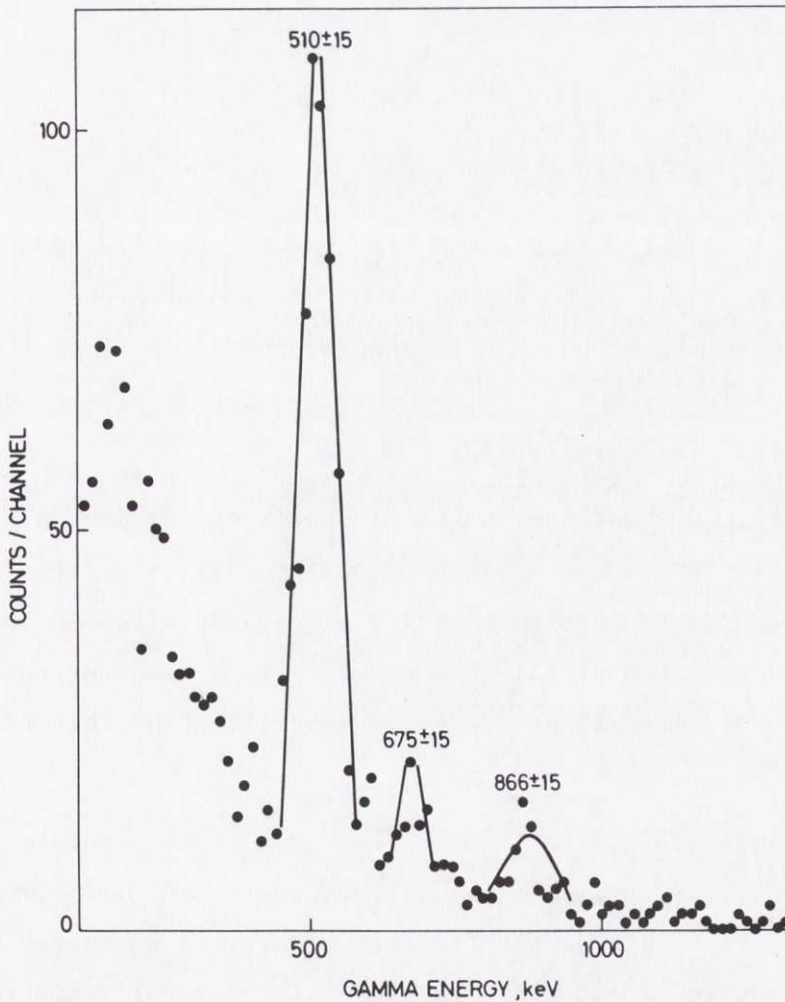


Fig. III.11 Projection of a two-dimensional spectrum from the ^{73}Kr proton-gamma coincidence experiment. The line at 866 ± 15 keV corresponds to coincidences between protons and gamma rays from the $2^+ \rightarrow 0^+$ transition in ^{72}Se . The lines at 510 ± 15 keV and 675 ± 15 keV correspond to proton coincidences with annihilation radiation and with the sum of a 511 keV and backscatter from the other 511 keV gamma ray of the pair.

510 \pm 15 keV is mainly due to coincidences between positrons and their annihilation quanta, and the line at 675 \pm 15 keV due to summing of one 511 keV gamma ray with a back-scatter quantum from the other 511 keV gamma ray of the pair. Coincidences with the gamma rays from the 862 keV $2^+ \rightarrow 0^+$ transition in ^{72}Se are also seen in the spectrum. The feeding of the 2^+ level is found to be $35 \pm 9\%$. An analysis of annihilation radiation in coincidence with protons with $E_p > 1.75$ MeV (Fig. II.15b) yields a value of $45 \pm 10\%$ for the fraction of protons preceded by positron decay.

4. THE DETERMINATION OF $Q - B_p$ FROM THE POSITRON COINCIDENCE FRACTIONS

Bacso et al.⁷⁾ determined the $Q - B_p$ value for ^{111}Te by counting the rate of proton-positron coincidences as a function of proton energy. They made the assumption that the feeding of the 2^+ level of ^{110}Sn could be neglected. This assumption is probably correct in view of the high energy (1213 keV)⁸⁾ of this level.

The information about the number of positrons per proton (in the following referred to as the positron fraction), given in this chapter, can be used for a determination of the $Q - B_p$ value with a method similar to the one used by Bacso et al. The rather strong branches to the first excited states have made it necessary, however, to take this feed into account.

In the general case, protons with energy E_p will populate various final states with excitation energy E_f (see the model decay scheme in Fig. IV.1). If $X_f(E_p)$ is the fraction of protons of energy E_p going to the level denoted f , and $\omega(E_\beta)$ is the positron/total ratio for the beta decay with the (electron capture) energy E_β , one can express the positron fraction $\eta(E_p)$ as

$$\eta(E_p) = \sum_f X_f(E_p) \omega [Q - B_p - E_f - E_p A / (A - 1)] , \quad (\text{III.2})$$

where Q is the total beta-decay energy of the initial nucleus and B_p the proton separation energy of the intermediate nucleus.

In the expression

$$\omega(E_\beta) = f_{\beta+}(Z, E_\beta - 2mc^2) / [f_{\beta+}(Z, E_\beta - 2mc^2) + f_{EC}(Z, E_\beta)] \quad (\text{III.3})$$

the statistical rate function for positron decay was calculated with the use of formulas given in Ref. (9). f_{EC} was calculated from

$$f_{EC}(Z, E_\beta) = \frac{\pi}{2} g_K^2(Z) \left(\frac{Q - E - B_K}{mc^2} \right)^2 + 1.3 \frac{\pi}{2} g_{L_1}^2(Z) \left(\frac{Q - E - B_{L_1}}{mc^2} \right)^2 \quad (\text{III.4})$$

where $(\pi/2)g_K^2(Z)$ and $(\pi/2)g_{L_1}^2(Z)$ are the average values of the K- and L_1 -electron radial wave functions at the mother nucleus¹⁰⁾, and B_K and B_{L_1} are the respective binding energies of the captured electrons (in the daughter nucleus). The factor 1.3 is included to correct for the contribution from higher shells. E is the excitation energy of the intermediate nucleus.

In the case where the experiment gives the average of the positron fraction for protons in the energy interval E_1 to E_2 one has

$$\bar{\eta}(E_1, E_2) = \frac{\int_{E_1}^{E_2} I_p(E_p) \eta(E_p) dE_p}{\int_{E_1}^{E_2} I_p(E_p) dE_p}, \quad (\text{III.5})$$

where $I_p(E_p)$ is the total proton intensity per unit energy.

If $I_p(E_p)$ and the branching $\chi_f(E_p)$ are known from experiment, one may use the expressions (III.2) and (III.5) to calculate $\bar{\eta}$ as a function of $Q - B_p$. Comparison with the experimental value for $\bar{\eta}$ then determines a value for $Q - B_p$.

The results from the NaI(Tl) experiment on ^{115}Xe are shown in Fig. III.12 for several proton energy intervals. The values of $Q - B_p$ are consistent and give an average of 6.3 ± 0.2 MeV, where the experimental error stems mainly from the calibration of the gamma detector.

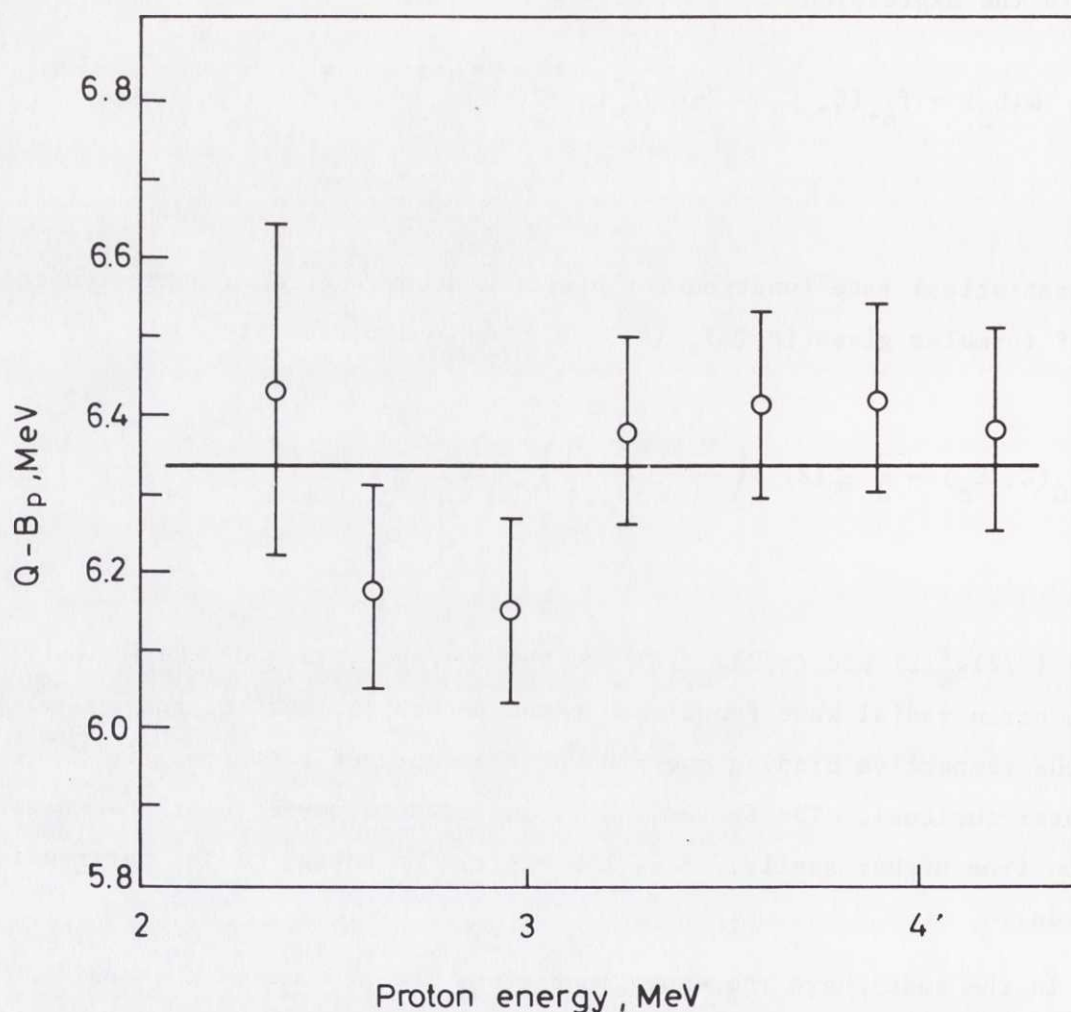


Fig. III.12 $Q - B_p$ value for ^{115}Xe determined from the NaI(Tl) coincidence data (Table III.3). The mean value of $Q - B_p$ is 6.3 ± 0.2 MeV.

For the total spectrum, the proton fraction was found to be $28 \pm 4 \%$ (average over the two experiments performed with set-up A and C, Table III.4). A graphical representation of the function (Eq. III.5) integrated over the whole energy interval of the protons is shown in Fig. III.13. The determination of $Q - B_p$ from this diagram gives 6.20 ± 0.13 MeV.

Similarly, for ^{117}Xe , $Q - B_p$ is found to be 4.1 ± 0.2 MeV and for ^{73}Kr 4.85 ± 0.30 MeV (Figs. III.14 and III.15).

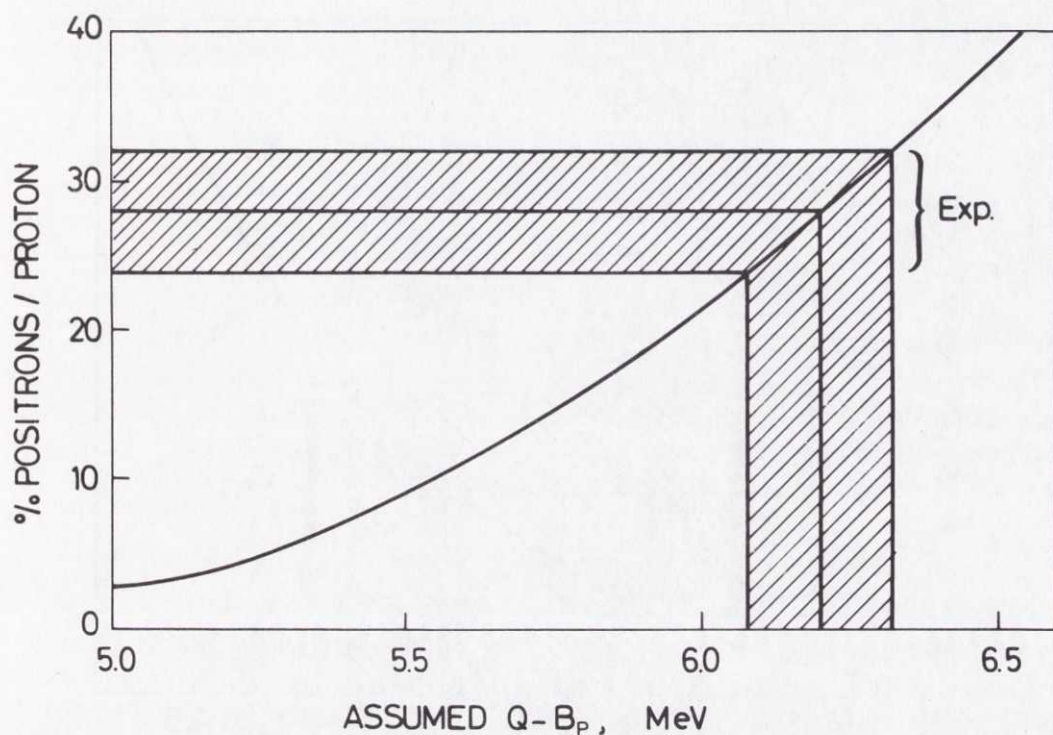


Fig. III.13 $Q - B_p$ value for ^{115}Xe including both NaI(Tl) and Ge(Li)^p data. The solid curve is the number of positrons/proton (in %) as a function of the $Q - B_p$ value calculated by integrating Eq. III.5 from zero to $(Q - B_p)(A - 1)/A$. The adopted best value 28 ± 4 % (Table III.4) yields a $Q - B_p$ value of 6.20 ± 0.13 MeV.

The method for $Q - B_p$ determination given above cannot be used for ^{118}Cs as long as the level scheme of ^{117}I is unknown. A good estimate may, however, be given if a reasonable assumption is made for the excitation energies of the final states. The coincidence data indicate that only a few levels at low excitation energies are fed in the proton decay. Fig. III.16 shows Eq. (III.5) as a function of $Q - B_p$ calculated under the assumption of excited levels at 0.12, 0.16, 0.22 and 0.31 MeV. The result is $Q - B_p = 4.7 \pm 0.1$ MeV. The assumption that all the feed to excited states goes to a level at 0.3 MeV gave the same result.

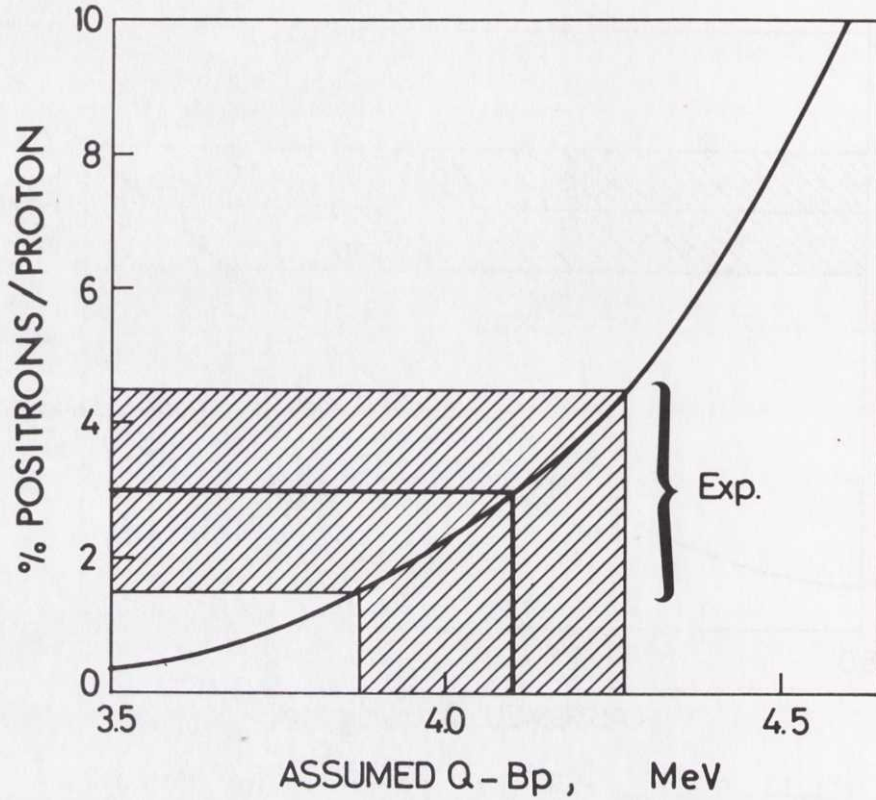


Fig. III.14 $Q - B_p$ value for ^{117}Xe . With the experimental value of $3.0 \pm 1.5\%$ for the positron/proton fraction the value is 4.1 ± 0.2 MeV.

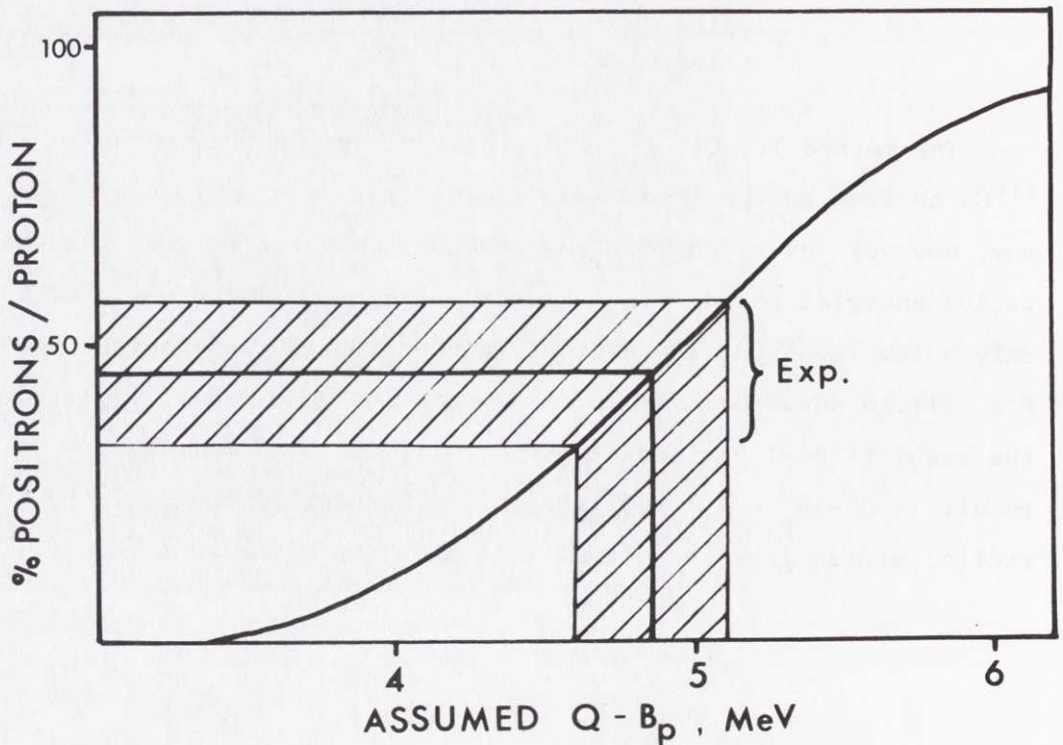


Fig. III.15 $Q - B_p$ value for ^{73}Kr . The experimental value for the positron/proton ratio was $45 \pm 10\%$ which yields a value of 4.85 ± 0.30 MeV.

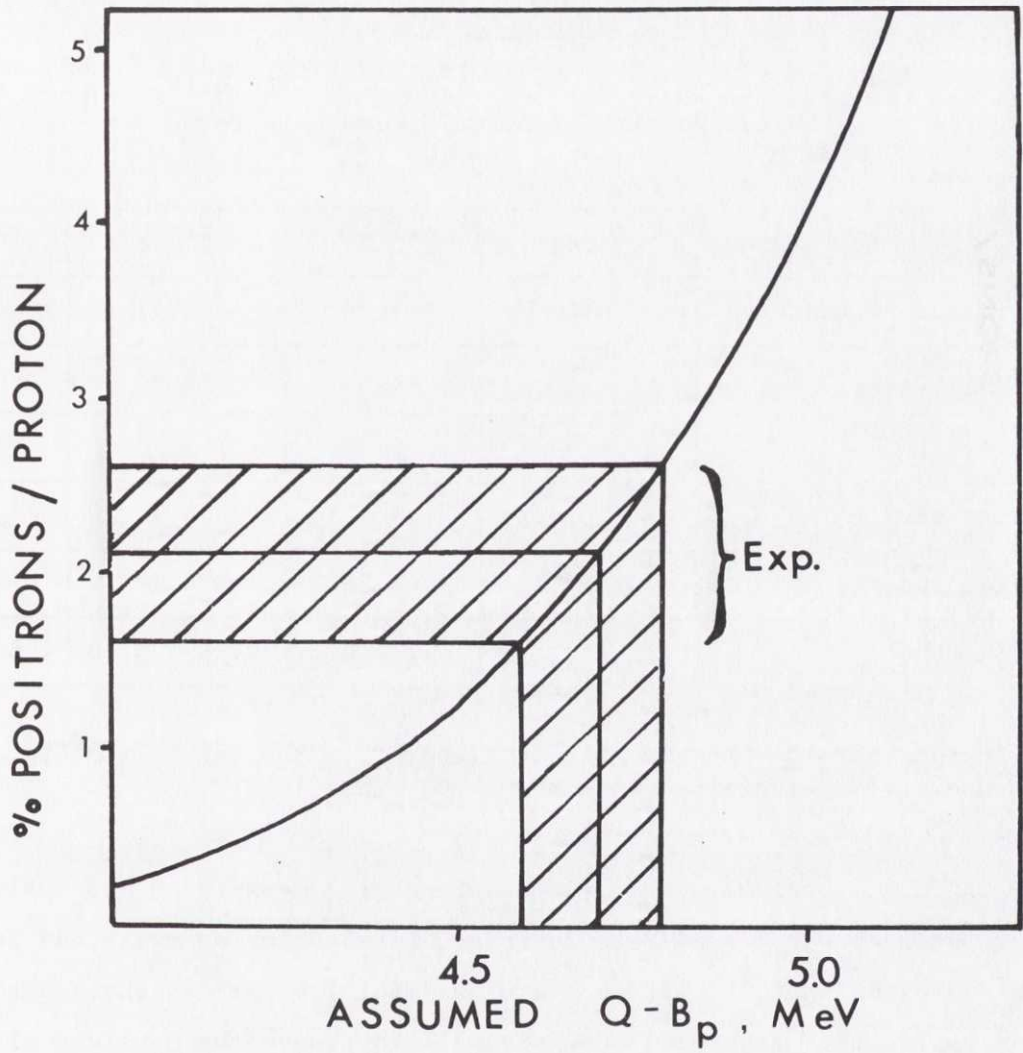


Fig. III.16 $Q - B_p$ value for ^{118}Cs . The curve was calculated from p proton branches to final states at 0.00, 0.12, 0.16, 0.22, and 0.31 MeV. The experimental value for the positron/proton ratio was 2.1 ± 0.5 % which yields a value of 4.7 ± 0.1 MeV.

Table III.5

Comparison of the experimental $Q - B_p$ value
with values taken from different mass formulas

	^{118}Cs	^{117}Xe	^{115}Xe	^{73}Kr
Myers and Swiatecki ¹¹⁾	5.40	3.94	6.17	4.75
Zeldes et al. ¹²⁾	4.65	3.47	5.43	4.08
Garvey et al. ¹³⁾	4.83	3.85	5.70	3.73
Truran et al. ¹⁴⁾	5.78	3.91	5.94	3.27
Seeger and Perisho ¹⁵⁾	4.96	3.86	6.19	3.42
EXPERIMENT	$4.7 \pm 0.3^a)$	4.1 ± 0.2	6.20 ± 0.13	4.85 ± 0.30

a) Error estimated to be somewhat higher than the value from Fig. III.16, due to the assumption made about the final levels.

Table III.5 gives a comparison between the measured $Q - B_p$ values and those taken from some mass formulas. The tables by Myers and Swiatecki¹¹⁾ give estimates that lie within the experimental errors in three cases. These tables have also been shown to well reproduce the Q -values of neutron-deficient nuclides in the mercury region¹⁶⁾. In the following, when estimates of Q or B_p are needed, they will therefore be taken from Ref. (11).

5. SUMMARY

The proton-gamma-ray coincidence experiments demonstrate that only one or a few of the lowest excited states in the final nucleus are populated appreciably in the proton decay. The relative feedings may, as will be shown in the next chapter, be understood from a statistical model calculation. The calculated feedings are strongly dependent on the assumption made about the spins involved, and may therefore, in combination with the experimental results, be used to determine the spin of the initial or the final state (provided that one of them is known). One could even

imagine, in a case where both the initial and final spins are known, that information on the relative beta feedings of the intermediate states (the spin weight factors) could be extracted from the data.

The experimental $Q - B_p$ values obtained from the positron coincidence fractions provide a check of the semi-empirical mass formulas in regions where neither of the two parameters involved can be measured directly with the present techniques. The experimental $Q - B_p$ values are also of importance in the analysis of the spectral shapes given in the next chapter.

REFERENCES TO CHAPTER III

- 1) A. Lindahl, O.B. Nielsen and G. Sidenius, The ISOLDE isotope separator on-line facility at CERN (Eds. A. Kjelberg and G. Rudstam), CERN 70-3 (1970), p. 55.
- 2) P.G. Hansen, H.L. Nielsen, K. Wilsky, M. Alpsten, M. Finger, A. Lindahl, R.A. Naumann and O.B. Nielsen, Nuclear Phys. A148, 249 (1970).
- 3) M. Finger, R. Foucher, J.P. Husson, J. Jastrzebski, A. Johnson, G. Astner, B.R. Erdal, A. Kjelberg, P. Patselt, Å. Höglund, S.G. Malmkog and R. Henk, Nuclear Phys. A188, 369 (1972).
- 4) A. Kjelberg, private communication, and The ISOLDE collaboration, Phys. Letters 28B, 415 (1969).
- 5) A. Luuko, A. Kerek, I. Rezanka and C.J. Herrlander, Nuclear Phys. A135, 49 (1969).
- 6) E. Nolte, W. Kutschera, Y. Shida, and H. Morinaga, Proc. Int. Conf. on the Properties of Nuclei far from the Region of Beta-Stability, Leysin 1970, CERN 70-30 (1970), Vol. II, p. 911.
- 7) I. Bacso, D.D. Bogdanov, Sh. Darotsi, V.A. Karnaukhov and L.A. Petrov, Soviet J. Phys. 7, 689 (1968).
- 8) J.W. Sunier, M. Singh, R.M. DeVries and G.E. Thompson, Proc. Int. Conf. on the Properties of Nuclei far from the Region of Beta-Stability, Leysin 1970, CERN 70-30 (1970), Vol. II, p. 1015.
- 9) E.J. Konopinski and M.E. Rose, Alpha-, Beta-, and Gamma-ray spectroscopy (ed. K. Siegbahn), (North Holland, Amsterdam, 1965), p. 1327.
- 10) L.N. Zyryanova, Once-forbidden beta transitions (Eng. trans. Pergamon Press, London, 1963), p. 36.
- 11) W.D. Myers and W.J. Swiatecki, UCRL-11980 (1965).
- 12) N. Zeldes, A. Grill and A. Simievic, K. Danske Vidensk. Selsk. Mat.-Fys. Skr. 3, No. 5 (1967).
- 13) G.T. Garvey, W.J. Gerace, R.L. Jaffe, I. Talmi and I. Kelson, Rev. Mod. Phys. 41, No. 4, 51 (1969).
- 14) J.W. Truran, A.G.W. Cameron and E. Hilf, Proc. Int. Conf. on the Properties of Nuclei far from the Region of Beta-Stability, Leysin 1970, CERN 70-30 (1970), Vol. I, p. 275.
- 15) P.A. Seeger, and R.C. Perisho, LA 3751 (1967).
- 16) L. Westgaard, J. Żylicz and O.B. Nielsen, in Proc. 4th Int. Conf. on Atomic Masses and Fundamental Constants, NPS, Teddington, 1971.

CHAPTER IV

CALCULATIONS OF PROTON BRANCHING RATIOS AND SPECTRAL SHAPES IN A COMPOUND NUCLEUS MODEL

1. INTRODUCTION

Previously, the two nuclides $^{109,111}\text{Te}^{1)}$ were the only known beta-delayed proton emitters among the elements in the medium- and heavy-weight regions. The shapes of the energy spectra and a determination²⁾ of the quantity $Q - B_p$ for ^{111}Te were the most important experimental results. Attempts³⁾ at calculating the spectral shape for ^{111}Te in a statistical model were performed. It was found that a good fit to the experimental data could be obtained under the assumption of a constant beta strength function. For delayed neutrons, where much more experimental information is available, similar calculations⁴⁻⁷⁾ have been performed. All these calculations have incorporated the same main ingredients: some assumption about the beta strength and a statistical treatment of the competition between particle emission and gamma-ray emission.

In this chapter a model for beta-delayed proton emission, based on similar assumptions as mentioned above, will be examined.

2. OUTLINE OF THE CALCULATION

Calculations on beta-delayed proton emission involve a treatment of two processes:

- i) the beta decay;
- ii) the proton gamma-ray competition in the decay of levels fed in the beta decay.

The proton emitting states have excitation energies of 4-10 MeV. At such excitations the average level distance is expected to be small for nuclei in the medium- and heavy-weight regions, but it is still large compared to the proton and gamma widths (see Table V.1).

In the treatment presented in the following it is assumed that there are no correlations between the beta matrix elements for the individual

states and the proton widths^{*)} and that there are no correlations between partial proton widths contributing for a given state. For the nuclei considered here it is also permissible to leave out processes where two protons are emitted and processes where a gamma-ray precedes the proton emission (Section 5).

A description of the decay process may be formulated on the basis of the compound nucleus model: the intermediate states have excitation energies that are generally high enough for this model to apply and have lifetimes long enough to make their decay independent of the way of formation.

The model decay scheme shown in Fig. IV.1 illustrates some of the symbols used in the following. The initial nucleus A_Z (with spin and parity I^π) beta decays with a total electron capture energy Q to levels (with spin and parity $I_i^{\pi i}$) in the intermediate nucleus. The levels at the energy E are characterized by their level density $\rho_i(E)$, and their total gamma width, $\Gamma_\gamma^i(E)$. The competing process of proton emission occurs to levels in the final nucleus ${}^{A-1}_{Z-2}$ with energy E_f (spin and parity $I_f^{\pi f}$).

The average beta intensity per unit energy interval to levels $I_i^{\pi i}$ at energy E can be expressed as a product of the total beta intensity $I_\beta(E)$, and a weight factor $\omega(I, I_i)$, denoting the fraction of beta decays leading to levels with spin and parity $I_i^{\pi i}$. The proton intensity from the transition $i \rightarrow f$ can then be obtained from the compound nucleus expression

$$I_p^{if}(E_p) = \omega(I, I_i) \cdot I_\beta(E) \frac{\Gamma_p^{if}(E_p)}{\Gamma_i^i}, \quad (\text{IV.1})$$

where the total width is

$$\Gamma^i = \Gamma_\gamma^i + \sum_{f'} \Gamma_p^{if'}(E_p'), \quad (\text{IV.2})$$

and where one has the relation (see Fig. IV.1)

*) The absence of correlations is a convenient assumption, but it is easy to imagine a situation where it fails. One would then speak of a doorway state for delayed proton emission.

The total proton intensity per beta decay is

$$P_p = \int_0^{E_{p,\max}} I_p(E_p) dE_p, \quad (\text{IV.5})$$

with

$$E_{p,\max} = (Q - B_p)(A - 1)/A. \quad (\text{IV.6})$$

The expressions and constants necessary for the numerical evaluation of Eqs. (IV.4) and (IV.5) are considered in the following.

2.1 Masses, spins, and parities

In the calculations, the two parameters Q and B_p have to be known. No experimental information on their individual values is available but their difference, $Q - B_p$, has been determined experimentally in a few cases (see Ref. (2) and Table III.5). The numerical values of Q and B_p were taken from the tables by Myers and Swiatecki. These tables are generally in good agreement with the measured $Q - B_p$ values (Table III.5) and also give good estimates of the total beta-decay energies in the mercury region⁹⁾.

^{183}Hg is the only one of the heavy delayed-proton precursors for which the spin has been measured. A value of $\frac{1}{2}$ has been obtained¹⁰⁾ by optical pumping techniques. In the preliminary calculations for the odd mass nuclei the values on the spin and parity has been chosen according to likely shell-model states (Table IV.1). For the even Cs isotopes, calculations under the assumption of $I^\pi = 1^+$ and $I^\pi = 3^+$ were performed.

Table IV.1

Likely shell model states for the odd neutron
in mercury, xenon, and krypton

Hg	$f_{5/2}, p_{3/2}, p_{1/2}, i_{13/2}$
Xe	$g_{7/2}, d_{5/2}, d_{3/2}$
Kr	$p_{3/2}, f_{5/2}, p_{1/2}$

2.2 The beta strength function and the beta-decay intensity

The beta decay of neutron deficient, heavy nuclides proceeds to excited states in regions where the level density is very high. It thus becomes necessary, both for theoretical and experimental reasons, to treat the beta decay in terms of a beta strength function. For the beta decay to an excitation energy E in the daughter nucleus, the strength is proportional to the product of the average squared matrix element and the level density. An experimental definition is given by Duke et al.¹¹⁾ as

$$S_{\beta}(E) = I_{\beta}(E) \{f(Z, Q - E) \cdot T_{1/2}\}^{-1} \text{ MeV}^{-1} \text{ s}^{-1}, \quad (\text{IV.7})$$

where $I_{\beta}(E)$ is the beta decay intensity per MeV to levels at the energy E , $f(Z, Q - E)$ the usual statistical rate function, Q the total energy available (here $\equiv Q_{\text{EC}}$) and $T_{1/2}$ the half-life.

An approximate picture of the origin of the beta strength can be obtained from the shell-model states shown in Figs. IV.2a,b,c. The single particle transitions indicated in the diagrams suggest that the beta strength for Cs, Xe, and Kr isotopes predominantly comes from allowed Gamow-Teller transitions. Isospin conservation makes any contribution of Fermi-type very weak. For the mercury isotopes (Fig. IV.2c) there are indications¹¹⁾ that the allowed GT transition $(h_{1/2})_p \rightarrow (h_{9/2})_n$ plays a role at lower energies while first forbidden transitions dominate at high energies. The forbidden transitions are assumed to obey the ξ -approximation^{12a)} so that the transition probability has the same energy dependence as for allowed transitions.

With the strength-function picture of the beta decay the total beta intensity per MeV of final states at energy E can be written

$$I_{\beta}(E) = S_{\beta}(E)f(Z, Q - E) / \int_0^Q S_{\beta}(E)f(Z, Q - E) dE, \quad (\text{IV.8})$$

where the f function is the sum of the statistical rate functions for electron capture and positron decay^{13,14)}.

A series of measurements on beta strength functions for short-lived mercury and xenon isotopes has recently been performed¹⁵⁾. Data are available for the two delayed proton precursors ^{117}Xe and ^{183}Hg . These results

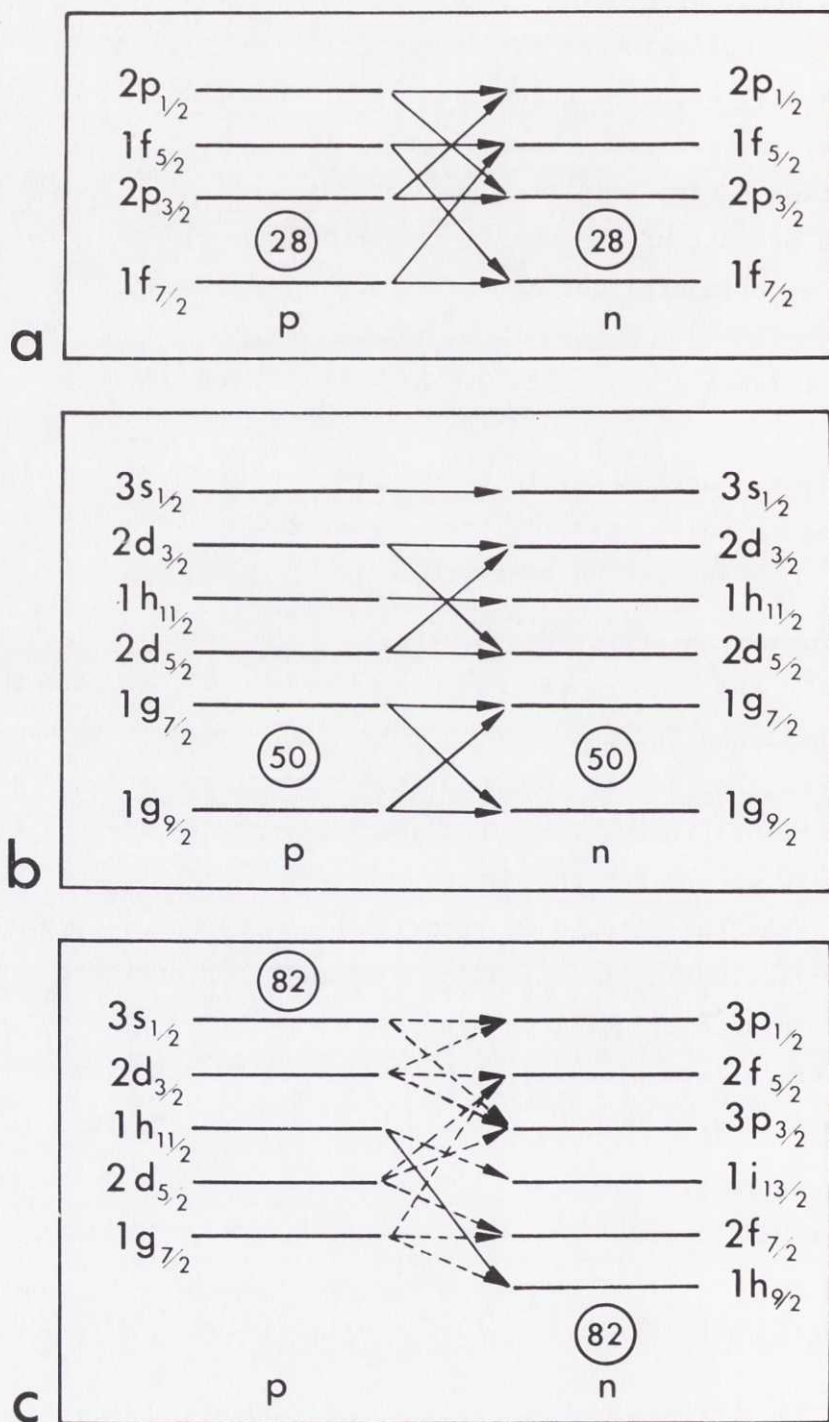


Fig. IV.2 Possible beta transitions in a) the krypton region; b) the xenon region; c) the mercury region. Allowed (GT) transitions are shown as solid arrows and first forbidden transitions as dashed arrows.

will be discussed in Section 4.5. As a first approximation of the beta-strength function, a schematic model has been used in the calculations. The model is the one suggested in Ref.(11), where the strength is assumed to be constant above and zero below a cut-off energy C. This energy is chosen in the following way:

$$\left. \begin{array}{l} \text{i) zero for odd-odd daughter nuclide} \\ \text{ii) } 0.6 \times 2\Delta \text{ for odd-mass daughter nuclide} \\ \text{iii) } 0.6 \times 4\Delta \text{ for even-even daughter nuclide} \end{array} \right\} \quad (\text{IV.9})$$

A good approximation of the gap parameter Δ is $\Delta = 12/\sqrt{A}$ MeV ^{12b)}.

With this treatment one takes into account that most of the transition probability will come from nucleons that initially are in the paired system of the nucleus. This means that the beta strength should have the (approximate) selection rule $\Delta v = +2$ for the seniority v . The filling diagrams in Fig. IV.3, taken from Hansen ¹⁶⁾, give a further illustration of this model. The numerical factor 0.6 in Eq. (IV.9) has been included to correct (in a very rough way) for contributions to the strength from transitions with $\Delta v = 0$ and $\Delta v = -2$.

The statistical weight factor $\omega(I, I_i)$ gives the fraction of intermediate states with spin $I_i^{\pi_i}$. This factor poses a greater problem from the experimental point of view as it is hardly within present experimental possibilities to determine the beta branching ratios to different daughter spins and parities. The following standard approximation was used:

$$\omega(I, I_i) = \frac{2I_i + 1}{3(2I + 1)} \quad , \quad (\text{IV.10})$$

with I_i taking the values $I, I \pm 1$. This relation holds if the beta decay proceeds only via excitations of the paired system and only via transitions of tensor rank one. The assumption of tensor rank one is well justified for the allowed transitions (Gamow-Teller type). For the case of mercury isotopes the beta strength has been assumed only to involve forbidden transitions. A measurement ¹⁷⁾ for ¹⁹⁷Hg shows the 0^- contribution to the $p_{1/2} \rightarrow s_{1/2}$ transition to be small. This is also the result of a theoretical analysis quoted by Bohr and Mottelson ^{12c)}.

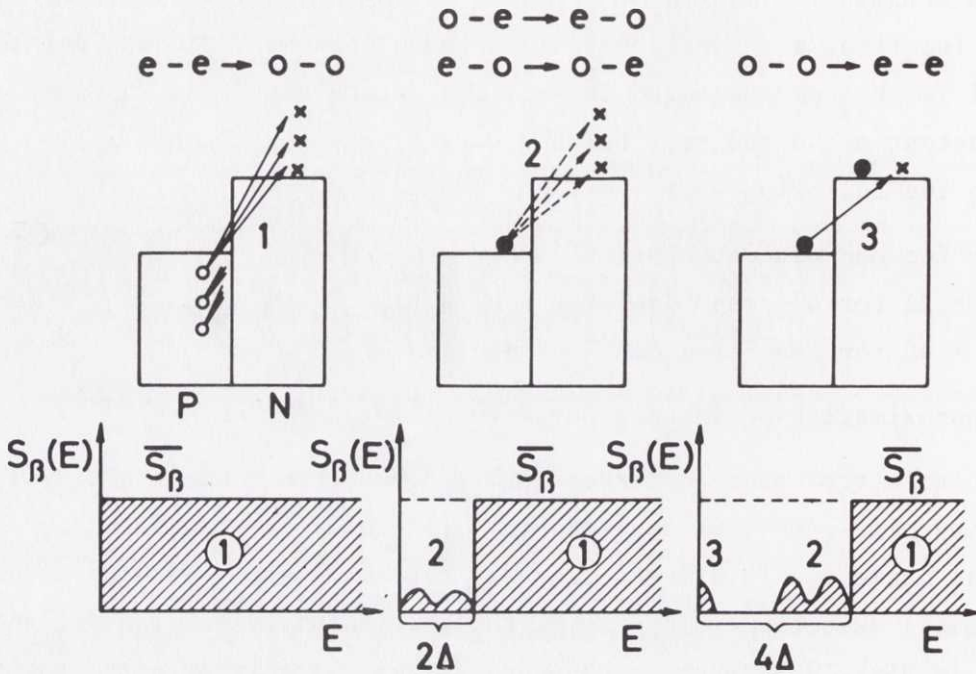


Fig. IV.3 Schematic filling diagrams and model strength functions. The main part of the beta strength originates from $\Delta v = 2$ transitions that create a proton hole and a neutron. These transitions, indicated only in the left diagram, are labelled 1. The odd-mass and odd-odd nuclei in addition have smaller contributions from $\Delta v = 0$ transitions (labelled 2) involving the unpaired nucleon and the odd-odd nuclei, finally, also from a $\Delta v = -2$ transition (labelled 3). This figure is taken from Hansen¹⁶).

2.3 The partial proton width

The partial proton width $\Gamma_p^{if}(E_p)$ [Eqs. (IV.1), (IV.2) and (IV.4)] was calculated from the expression¹⁸⁾

$$\Gamma_p^{if}(E_p) = \left[\sum_{j, \pi_i \pi_f} T_{lj}(E_p) \right] / 2\pi \rho_i(E), \quad (\text{IV.11})$$

where $T_{lj}(E_p)$ are transmission coefficients obtained in an optical model calculation and where the sum extends over the partial waves permitted by the selection rules in spin and parity. The function $\rho_i(E)$ is the density of levels (Section 2.5) with spin and parity $I_i^{\pi_i}$. The excitation energy of the proton emitting state is E .

The calculation of the T_{lj} values was performed on the basis of an optical model calculation^{12d,19)}, including a surface absorption term and an isospin dependent term

$$V_{opt} = -52f(r) + i40 \frac{df(r)}{dr} + \frac{104}{A} T \cdot t + \frac{17}{r} \cdot \frac{df(r)}{dr} l \cdot s \text{ MeV}, \quad (IV.12)$$

with the Woods-Saxon shape of the radial function

$$f(r) = 1/(1 + \exp [(r - R)/a]) \quad (IV.13)$$

and with $R = 1.25 A^{1/3}$ fm, $a = 0.65$ fm. For the cases of interest, the numerical calculations did not give sufficient precision at low energies (below 5 MeV in the mercury region and below 3.5 MeV in the xenon region). Values on T_{lj} , valid at low proton energies, have been obtained by an extrapolation method. The WKB-penetrability $P_l(E_p)$, as given by Morrison²⁰⁾, was used for extrapolating the slowly varying coefficient $\gamma_{lj}(E_p)$ in the equation

$$T_{lj}(E_p) = \gamma_{lj}(E_p) P_l(E_p). \quad (IV.14)$$

The calculations in the krypton region were performed with T_{lj} values taken from the tables by Mani et al.²¹⁾. It has been found that these values have only a slight deviation from the values by Bondorf in the xenon and mercury regions (Section 4.1).

2.4 The total gamma width

Cameron²²⁾ has given an expression for the total gamma width which is normalized to experimental data. He essentially assumes that the transition density is a product of the density of levels and the energy-dependent factor E_Y^3 . This assumption is equivalent to that of pure dipole radiation and a constant gamma-strength function²³⁾. The expression for the total gamma width, obtained with the use of Newton's level density formula²⁴⁾ was then

$$\Gamma_Y \approx 5.2 A^{2/3} b^4 [1 + 2b/U^{1/2}] \times \left[U^2 - \frac{10}{3} bU^{3/2} + 5b^2U - \frac{35}{9} b^3U^{1/2} + \frac{35}{27} b^4 \right] \text{ meV}. \quad (IV.15)$$

The constant A is the mass number, and b is defined as

$$b = 5.97 / (\overline{j_N} + \overline{j_Z} + 1)^{1/2} A^{1/3} . \quad (\text{IV.16})$$

The effective j-values $\overline{j_N}$ and $\overline{j_Z}$, which represent appropriate averages of the total angular momenta of the single-particle states lying near the Fermi level of the nucleon gas, are tabulated in Ref. (22).

Expression (IV.15) is valid for $U > 2$ MeV, where U is the effective excitation energy related to the actual value E, as

$$U = E - \delta \quad (\text{IV.17})$$

with

$$\delta(A > 40) = \begin{cases} 0 & \text{for odd-odd compound nuclei} \\ 1.68 - 0.0042 A & \text{for odd mass compound nuclei} \\ 3.36 - 0.0042 A & \text{for even-even compound nuclei} \end{cases} \quad (\text{IV.18})$$

2.5 The level density

The level density $\rho_i(E, I_i)$ is calculated from the formulas according to Gilbert and Cameron²⁵⁾. They have given the expression for the level density (for the spin I_i and one parity) at the excitation energy E in the form

$$\rho_{i1}(E) = \frac{\sqrt{\pi}}{24} \frac{\exp(2\sqrt{aU})}{a^{1/4} \cdot U^{5/4}} (2I_i + 1) \frac{\exp[-(I_i + 1/2)^2 / 2\sigma^2]}{2\sqrt{2\pi} \sigma^3} \text{MeV}^{-1} , \quad (\text{IV.19})$$

where

$$\sigma^2 = 0.0888 (aU)^{1/2} A^{2/3} \quad (\text{IV.20})$$

and

$$a = A[0.139 + 0.0102 (S - 0.33D)] . \quad (\text{IV.21})$$

The parameter D is the distance (the number of neutrons or protons) to the nearest closed nucleon shell and $S = S(Z) + S(N)$ the total shell energy²⁶⁾.

The effective excitation U is expressed in terms of the pairing corrections $P(Z)$ and $P(N)$ ²⁶⁾ as

$$U = E - P(Z) - P(N) . \quad (\text{IV.22})$$

The relation (IV.19) is valid above excitation energies

$$E_x = 2.5 + 150/A + P(Z) + P(N) . \quad (\text{IV.23})$$

Below this energy the level density was assumed to follow an exponential behaviour

$$\rho_{i2}(E) = \frac{1}{T} \exp \left[\frac{E - E_0}{T} \right] \text{ MeV}^{-1} , \quad (\text{IV.24})$$

where the constants T and E_0 are determined by smoothly fitting ρ_1 and ρ_2 at the excitation energy $E = E_x$.

3. COMPARISON WITH EXPERIMENT

The results of the calculations performed with the assumption of a constant strength function, using $Q - B_p$ values from experiments or from Ref. (8) and a reasonable value on the spin and parity of the proton precursor are given Table IV.2 for Hg, Cs, Xe, and Kr. The experimental proton branching ratio (protons/beta decay) is also given in the table. The deviations between calculated and measured values are in most cases small (less than a factor of 10, except in the ^{120}Cs case).

An investigation of the sensitivity to changes in the parameters and to different assumptions about the beta strength function and the level density will be performed in the following sections.

The energy requirement of beta-delayed proton emission is fulfilled for some of the daughter products of the observed proton emitters and also for some neighbouring activities. Table IV.3 gives the calculated proton branches for some of these nuclides. The results for the gold and platinum isotopes, produced after the alpha or beta decay of $^{179,181,183}\text{Hg}$, have been used to obtain the estimates given in Table II.3.

Search for delayed protons has been performed both for ^{116}Xe (telescope detector) and ^{114}Xe (emulsion) but no events were observed in either cases, which gave upper limits of 10^{-6} p/dis and 10^{-4} p/dis, respectively.

Table IV.2

Calculated proton branching ratios for the
delayed proton precursors given in Table II.6

Nuclide	Assumed I^π	Q a) MeV	B _p a) MeV	P _p (protons/beta decay)	
				Theoretical	Experimental
¹⁸³ Hg ¹⁸³ Hg b)	$\frac{1}{2}^-$	6.40	1.85	5.7×10^{-7}	$(3.1 \pm 0.7) \times 10^{-6}$
	$\frac{1}{2}^-$	6.85 c)	1.85	1.5×10^{-6}	
¹⁸² Hg	0^+	5.22	1.58	1.8×10^{-8}	$\leq 10^{-7}$
¹⁸¹ Hg ¹⁸¹ Hg	$\frac{1}{2}^-$	7.30	1.31	2.9×10^{-5}	$(1.8 \pm 0.5) \times 10^{-4}$
	$\frac{1}{2}^-$	7.46 c)	1.31	3.4×10^{-5}	
¹⁷⁹ Hg ¹⁷⁹ Hg	$\frac{1}{2}^-$	8.21	0.77	3.3×10^{-4}	$\sim 2.8 \times 10^{-3}$
	$\frac{3}{2}^-$	8.21	0.77	2.6×10^{-4}	
¹²⁰ Cs ¹²⁰ Cs d)	1^+	8.31	5.05	2.5×10^{-6}	$\leq 5 \times 10^{-8}$
	3^+	8.31	5.05	1.4×10^{-6}	
¹¹⁸ Cs ¹¹⁸ Cs	1^+	8.99 e)	4.29	5.0×10^{-4}	$(4.2 \pm 0.6) \times 10^{-4}$
	3^+	8.99 e)	4.29	3.0×10^{-4}	

Table IV.2 (cont'd)

^{116}Cs	1^+	11.10	3.49	2.0×10^{-2}	not measured
^{116}Cs	3^+	11.10	3.49	1.5×10^{-2}	
^{117}Xe f)	$5/2^+$	6.87 e)	2.77	2.4×10^{-5}	$(2.9 \pm 0.6) \times 10^{-5}$
^{115}Xe	$5/2^+$	8.14 e)	1.94	2.8×10^{-3}	$(3.4 \pm 0.6) \times 10^{-3}$
^{113}Xe	$5/2^+$	9.58	1.03	6.1×10^{-2}	not measured
^{73}Kr	$1/2^-$	8.13 e)	3.28	6.4×10^{-3}	
^{73}Kr	$3/2^-$	8.13 e)	3.28	3.5×10^{-3}	$(6.8 \pm 1.2) \times 10^{-3}$
^{73}Kr	$5/2^-$	8.13 e)	3.28	1.7×10^{-3}	

- a) The Q and B_p values are taken from Ref. (8) if nothing else is indicated.
- b) For the mercury isotopes the beta strength was assumed to be forbidden. Excited levels in $^{178,180,182}\text{Pt}$ were assumed²⁷⁾ at 0.16 (2^+), 0.5 (4^+), and 1.2 (2^+) MeV. For ^{181}Pt levels were arbitrarily assumed at 0.0 ($1/2^+$), 0.2 ($3/2^+$), 0.4 ($5/2^+$), 0.8 ($7/2^+$), and 0.9 ($1/2^-$) MeV.
- c) Assumed value.
- d) The beta strength was assumed to be allowed. Levels in $^{119,117,115}\text{I}$ were assumed at $0.0(5/2^+)$, $0.12(1/2^+)$, $0.16(7/2^+)$, $0.22(3/2^+)$, and $0.31(3/2^+)$ MeV.
- e) Experimental $Q - B_p$ value. The proton separation energy was taken from Ref. (8) and Q was adjusted to fit the experimental $Q - B_p$ value.
- f) The beta strength was assumed to be allowed. Levels in $^{116,114,112}\text{Te}$ were assumed²⁸⁾ at 0.68, 0.71, 0.8 MeV (2^+); 1.36, 1.48, 1.6 MeV (4^+); 2.00, 2.22, 2.50 MeV (6^+); 2.79, 3.09, 3.50 MeV (8^+).
- g) The beta strength was assumed to be allowed. Levels in ^{72}Se were assumed²⁹⁾ at 0.86 (2^+), 1.32 (2^+), 1.64 (4^+), 2.47 (6^+) MeV.

Table IV.3

Calculated proton branching ratios of delayed proton emission
in the mercury, cesium, xenon, and krypton regions

Nuclide	Assumed I^π	Q (MeV) a)	B_p (MeV) a)	P_p (protons/beta decay)
^{179}Pt b)	$\frac{1}{2}^-$	5.83	2.26	1.4×10^{-8}
^{179}Pt	$\frac{3}{2}^-$	5.83	2.26	9.2×10^{-9}
^{175}Os	$\frac{1}{2}^-$	5.24	2.70	4.0×10^{-11}
^{175}Os	$\frac{3}{2}^-$	5.24	2.70	2.4×10^{-11}
^{181}Au	$\frac{1}{2}^+$	6.12	3.69	1.3×10^{-13}
^{177}Pt	$\frac{1}{2}^-$	6.75	1.72	3.3×10^{-6}
^{177}Pt	$\frac{3}{2}^-$	6.75	1.72	2.5×10^{-6}
^{173}Os	$\frac{1}{2}^-$	6.17	2.14	3.9×10^{-7}
^{173}Os	$\frac{3}{2}^-$	6.17	2.14	2.7×10^{-7}
^{180}Hg	0^+	6.12	1.04	2.5×10^{-6}
^{179}Au	$\frac{1}{2}^+$	7.03	3.16	3.7×10^{-9}

Table IV.3 (cont'd)

^{175}Pt ^{175}Pt	$\frac{1}{2}^-$ $\frac{3}{2}^-$	7.69 7.69	1.17 1.17	1.0×10^{-4} 7.9×10^{-5}
^{171}Os ^{171}Os	$\frac{1}{2}^-$ $\frac{3}{2}^-$	7.12 7.12	1.58 1.58	3.0×10^{-5} 2.2×10^{-5}
^{119}Cs	$\frac{5}{2}^+$	6.97	4.68	5.2×10^{-10}
^{117}Cs	$\frac{5}{2}^+$	8.35	3.90	2.1×10^{-5}
^{116}Xe	0^+	5.36	2.36	1.3×10^{-5}
^{113}I	$\frac{5}{2}^+$	7.92	3.91	3.2×10^{-5}
^{114}Xe	0^+	6.77	1.50	5.0×10^{-3}
^{72}Kr ^{72}Kr	0^+ 3^+	6.53 9.26	2.68 6.66	8.8×10^{-4} 1.2×10^{-5}

- a) Values taken from the tables by Myers and Swiatecki⁸⁾.
b) The beta strength has been assumed to be forbidden in the mercury region and allowed in the xenon, cesium, and krypton regions. The final nucleus after proton decay has been assumed to have excited levels with excitation energies and spins chosen from an extrapolation of known level schemes in the corresponding regions³⁰⁾.

The spectral shape is determined by the shape of the beta strength function as well as by the energy dependence of the proton widths. Figures IV.4-6 show some examples of the calculated spectral shape under the assumption of a constant beta strength function. This assumption, which seems to work well in these cases, is not a good approximation for the xenon isotopes as will be shown in Section 4.5. Figure IV.7 shows a calculation for ^{73}Kr . The high beta-background distorts the spectrum heavily at the low-energy end and the figure has only been included here to show the expected low-energy shape of this spectrum.

The feeding of the final states after proton decay is dependent on the spin and parity of the delayed proton precursor. The populations of levels in platinum, tellurium, and selenium isotopes for different assumptions on I^π are given in Tables IV.4-7.

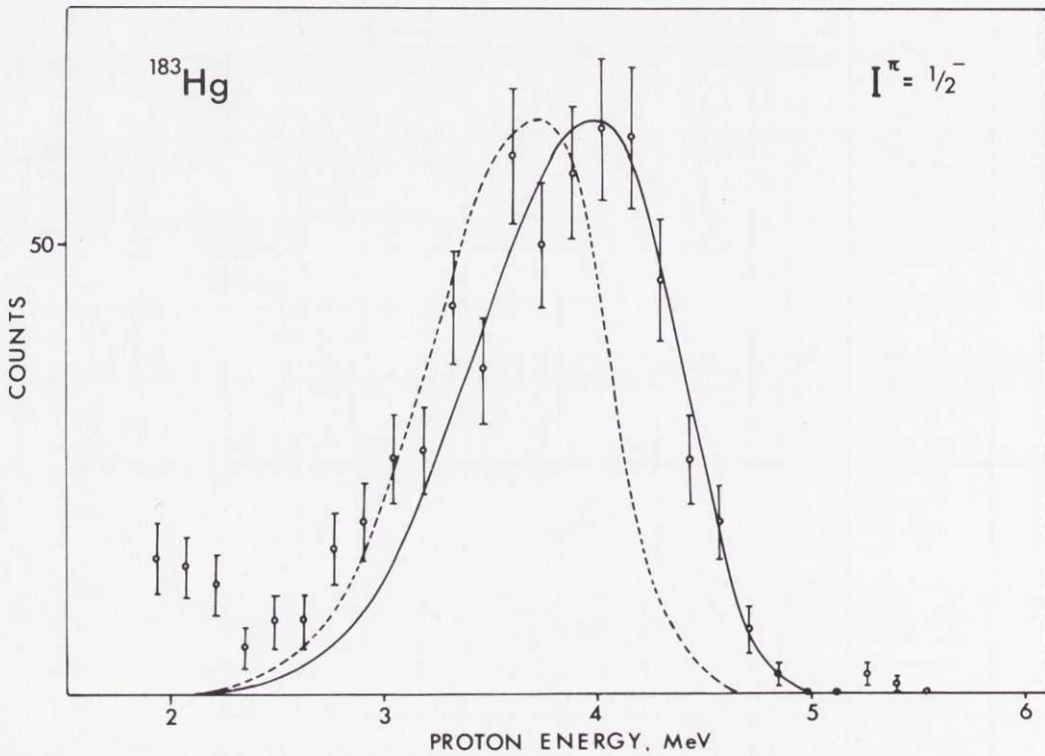


Fig. IV.4 The measured delayed proton spectrum from ^{183}Hg (exp. points) compared with calculations assuming $I^\pi = \frac{1}{2}^-$ and a constant beta strength function. Calculations with two sets of mass parameters are shown (i) $Q = 6.40$ MeV, $B_p = 1.85$ MeV (dashed curve), and (ii) $Q = 6.85$ MeV, $B_p = 1.85$ MeV (solid curve). An arbitrary scale is used for the calculated intensity.

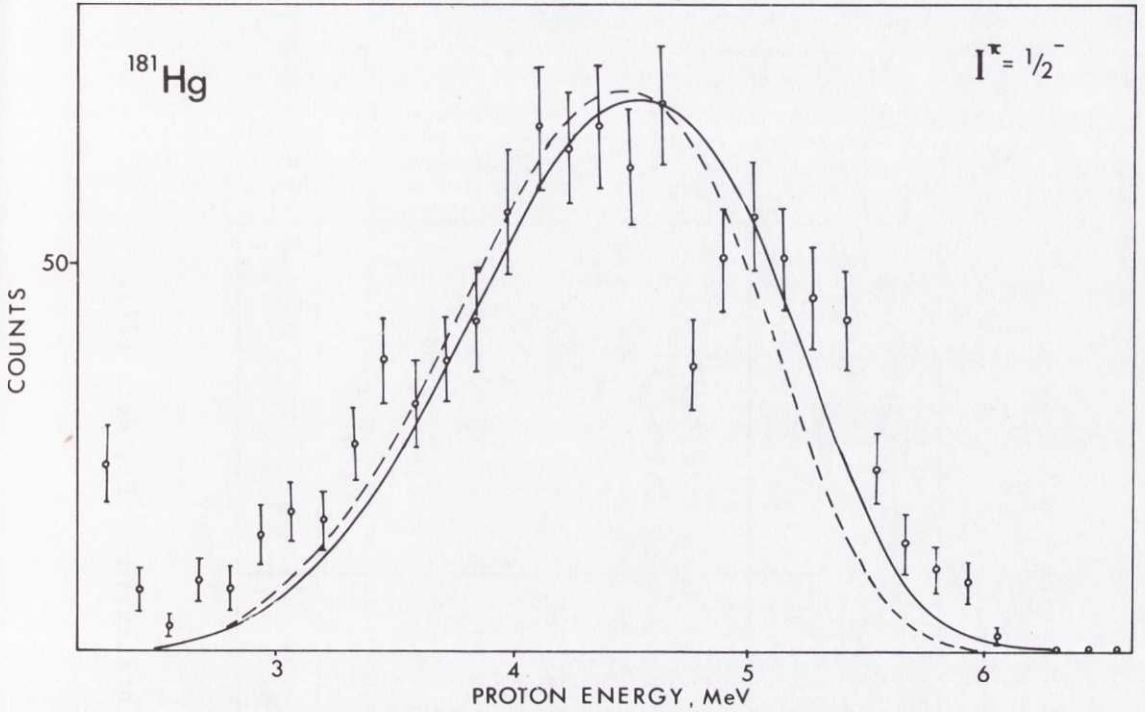


Fig. IV.5 The measured delayed proton spectrum from ^{181}Hg (exp. points) compared with calculations assuming $I^\pi = \frac{1}{2}^-$ and a constant beta strength function. Calculations with two sets of mass parameters are shown (i) $Q = 7.30$ MeV, $B_p = 1.31$ MeV (dashed curve), and (ii) $Q = 7.46$ MeV, $B_p = 1.31$ MeV (solid curve). An arbitrary scale is used for the calculated intensity.

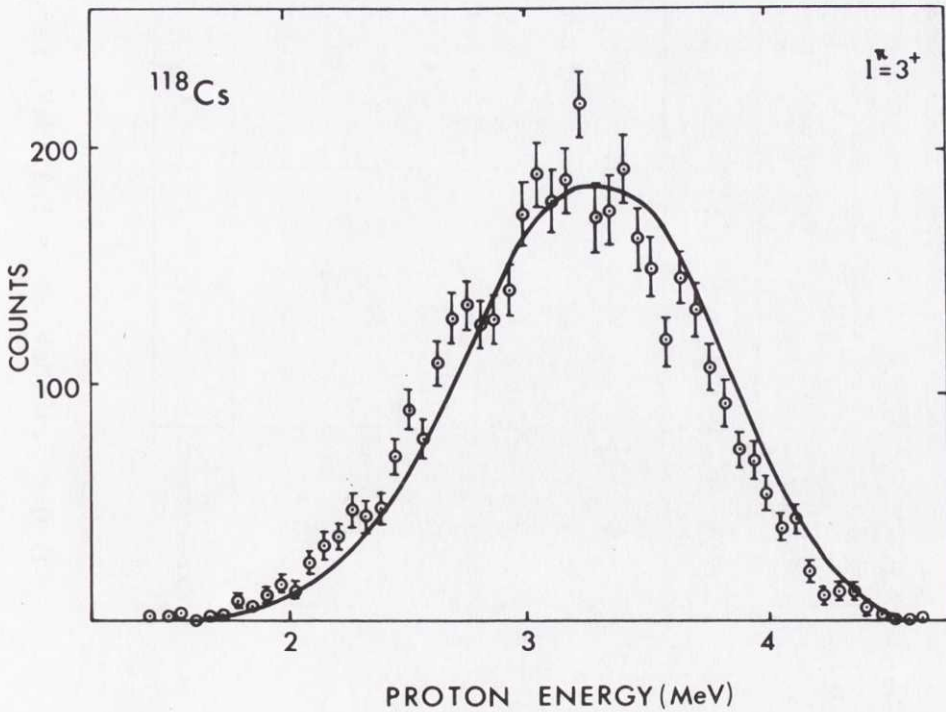


Fig. IV.6 The measured delayed proton spectrum from ^{118}Cs (exp. points) compared with a calculation assuming a constant beta strength function and $I^\pi = 3^+$. The B_p value was taken from Ref. (8) and Q was adjusted to fit the experimental $Q - B_p$ value. An arbitrary scale is used for the calculated intensity.

Table IV.4

Calculated^{a)} proton branches and feeding to final states
for ^{181}Hg with various values of the initial spin and parity

Assumed I^π	Relative intensity (%) b)			Proton branching ratio P_p (p/beta decay)
	0.0 MeV (0^+)	0.16 MeV (2^+)	0.5 MeV (4^+)	
$\frac{1}{2}^-$	53.2	45.1	1.3	2.9×10^{-5}
$\frac{3}{2}^-$	42.3	54.5	2.7	2.2×10^{-5}
$\frac{5}{2}^-$	17.3	70.2	11.8	1.2×10^{-5}
$\frac{7}{2}^-$	11.8	61.3	26.4	6.9×10^{-6}
$\frac{1}{2}^+$	51.1	47.3	1.1	4.1×10^{-5}
$\frac{3}{2}^+$	38.5	56.8	4.2	2.9×10^{-5}
$\frac{5}{2}^+$	26.6	62.4	10.4	1.9×10^{-5}
$\frac{7}{2}^+$	7.8	65.7	26.0	9.5×10^{-6}
Experiment	~ 45	50 ± 10	< 6	$(1.8 \pm 0.5) \times 10^{-4}$

a) $Q = 7.30$ MeV, $B_p = 1.31$ MeV, Ref. (8). b) To states in ^{180}Pt , Ref. (27).

Table IV.5

Calculated^{a)} proton branches and feeding to final states
for ^{117}Xe with various values of the initial spin and parity

Assumed I^π	Relative intensity (%) b)			Proton branching ratio P_p (p/beta decay)
	0.0 MeV (0^+)	0.68 MeV (2^+)	1.36 MeV (4^+)	
$\frac{1}{2}^+$	95.3	4.7	0.0	3.4×10^{-4}
$\frac{3}{2}^+$	90.9	9.1	0.0	1.9×10^{-4}
$\frac{5}{2}^+$	51.9	47.8	0.3	2.4×10^{-5}
$\frac{7}{2}^+$	48.2	50.3	1.5	9.8×10^{-6}
$\frac{1}{2}^-$	95.8	4.2	0.0	2.5×10^{-4}
$\frac{3}{2}^-$	92.2	7.8	0.0	1.3×10^{-4}
$\frac{5}{2}^-$	84.7	15.2	0.1	5.0×10^{-5}
$\frac{7}{2}^-$	2.9	94.8	2.3	4.1×10^{-6}
Experiment	~ 85	(14 ± 3)	not determined	$(2.9 \pm 0.6) \times 10^{-5}$

a) $Q = 6.87$ MeV, $B_p = 2.77$ MeV. b) To states in ^{116}Te , Ref. (28).

Table IV.6

Calculated^{a)} proton branches and feeding to final states for ¹¹⁵Xe with various values of the initial spin and parity

Assumed I^π	Relative intensity (%) b)			Proton branching ratio P_p (p/beta decay)
	0.0 MeV (0^+)	0.71 MeV (2^+)	1.48 MeV (4^+)	
$\frac{1}{2}^+$	83.5	16.5	0.0	1.1×10^{-2}
$\frac{3}{2}^+$	72.4	27.5	0.1	7.6×10^{-3}
$\frac{5}{2}^+$	42.4	54.0	3.6	2.8×10^{-3}
$\frac{7}{2}^+$	33.2	54.4	12.4	1.4×10^{-3}
$\frac{1}{2}^-$	92.8	7.2	0.0	1.1×10^{-2}
$\frac{3}{2}^-$	79.1	20.6	0.3	6.6×10^{-3}
$\frac{5}{2}^-$	60.2	38.1	1.7	3.5×10^{-3}
$\frac{7}{2}^-$	2.2	86.4	11.3	9.8×10^{-4}
Experiment	~ 40	(58 \pm 7)	< 2	(3.4 \pm 0.6) $\times 10^{-3}$

a) $Q = 8.14$ MeV, $B_p = 1.94$ MeV. b) To states in ¹¹⁴Te, Ref. (28).

Table IV.7

Calculated^{a)} proton branches and feeding to final states for ^{73}Kr with various values of the initial spin and parity

Assumed I^π	Relative Intensity (%) b)					Proton branching ratio P_p (p/beta decay)
	0.0 MeV (0 ⁺)	0.86 MeV (2 ⁺)	1.32 MeV (2 ⁺)	1.64 MeV (4 ⁺)	2.47 MeV (6 ⁺)	
$1/2^-$	98.9	0.9	0.1	0.0	0.0	6.4×10^{-3}
$3/2^-$	91.1	8.2	0.6	0.0	0.0	3.5×10^{-3}
$5/2^-$	78.8	19.4	1.6	0.2	0.0	1.7×10^{-3}
$7/2^-$	13.0	73.9	6.0	7.1	0.0	3.2×10^{-4}
$9/2^-$	13.5	61.4	5.5	19.4	0.2	1.4×10^{-4}
$1/2^+$	93.8	6.0	0.2	0.0	0.0	6.4×10^{-3}
$3/2^+$	89.4	10.1	0.5	0.0	0.0	4.5×10^{-3}
$5/2^+$	74.0	23.6	1.3	0.1	0.0	1.7×10^{-3}
$7/2^+$	63.6	30.6	2.0	3.8	0.0	8.0×10^{-4}
$9/2^+$	2.5	69.3	5.9	21.9	0.4	1.3×10^{-4}
Exp.	~ 65	35 ± 9	not determined			$(6.8 \pm 1.2) 10^{-3}$

a) $Q = 8.13$ MeV, $B_p = 3.28$ MeV. b) To states in ^{72}Se , Ref. (29).

The spin values suggested from these calculations are $\frac{3}{2}$ or $\frac{1}{2}$ for ^{181}Hg , $\frac{5}{2}$ for ^{115}Xe , and $\frac{1}{2}$, $\frac{3}{2}$, or $\frac{5}{2}$ for ^{117}Xe . The best fit for ^{73}Kr is obtained with the value $\frac{7}{2}^+$ as the initial spin and parity. This assignment is not in agreement with the likely shell model states (Table IV.1) and could indicate that the nucleus ^{73}Kr is deformed³¹⁾.

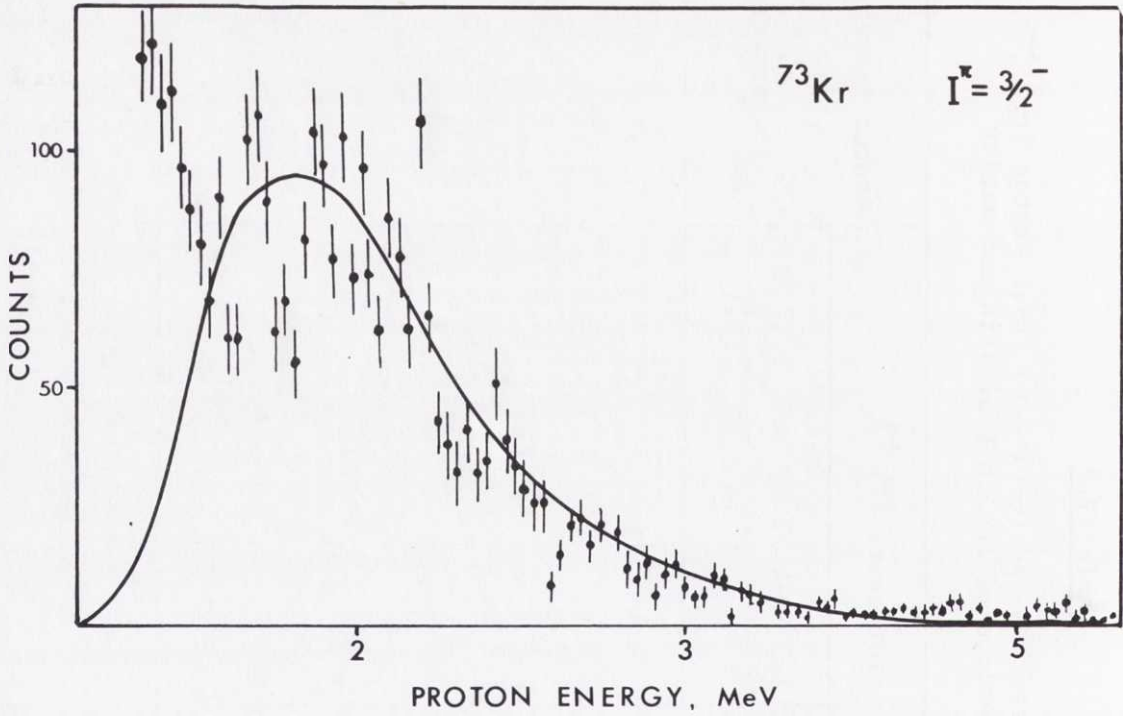


Fig. IV.7 The calculated shape of the ^{73}Kr delayed proton spectrum (with a constant beta strength function and $I^\pi = \frac{3}{2}^-$) together with the measured spectrum (Fig. II.15b).

4. CHANGES IN THE PARAMETERS

The calculations in Section 3 were performed with a "reasonable" set of parameters. The results are sufficiently promising to justify the question of the sensitivity with respect to the choice of the parameters.

4.1 The spin and parity

The spin and parity I^π assumed for the initial state do not only affect the relative feeding of final states but also the proton branching ratios P_p . The last columns in Tables IV.3-7 show that a variation in the spin from $\frac{1}{2}^\pm - \frac{7}{2}^\pm$ ($\frac{9}{2}^\pm$) may change P_p by one or two orders of magnitude. This is due to the effect of the centrifugal barrier on the transmission coefficients. The intermediate and final spins and parities I_i^π and I_f^π determine which partial waves are allowed by the selection rules. Consider ^{115}Xe as an example: A calculation performed with the assumption of $I^\pi = \frac{5}{2}^+$ and allowed decay ($I_i^\pi = \frac{3}{2}^+, \frac{5}{2}^+, \frac{7}{2}^+$) gives the partial waves to the ground state of ^{114}Te (0^+) as $d_{3/2}$, $d_{5/2}$, and $g_{7/2}$, of $I^\pi = \frac{3}{2}^+$ and allowed transitions ($I_i^\pi = \frac{1}{2}^+, \frac{3}{2}^+, \frac{5}{2}^+$) gives the waves $s_{1/2}$, $d_{3/2}$, and $d_{5/2}$ to the ground state. The transmission coefficients calculated for s and d waves are shown in Fig. IV.8, which illustrates that these are about a factor of 10 higher for s waves than for d waves. The partial proton width for decay to the ground state is, therefore, higher in the second case with an increased proton branching ratio as the result.

The feedings of the final states are also dependent on their excitation energy E_f . The energy available for proton decay to a final state (E_f) is $Q - B_p - E_f$, which gives a decreasing proton branch to a state with increasing excitation energy E_f . An investigation of how fast the decrease of the feed is as a function of energy has been performed for two sets of final levels. In order to get the same partial waves participating in the feeding, spin and parity have been chosen as 0^+ for all the states. The results with ^{115}Xe as the proton precursor ($Q = 8.14$ MeV and $B_p = 1.94$ MeV) are given in Table IV.8

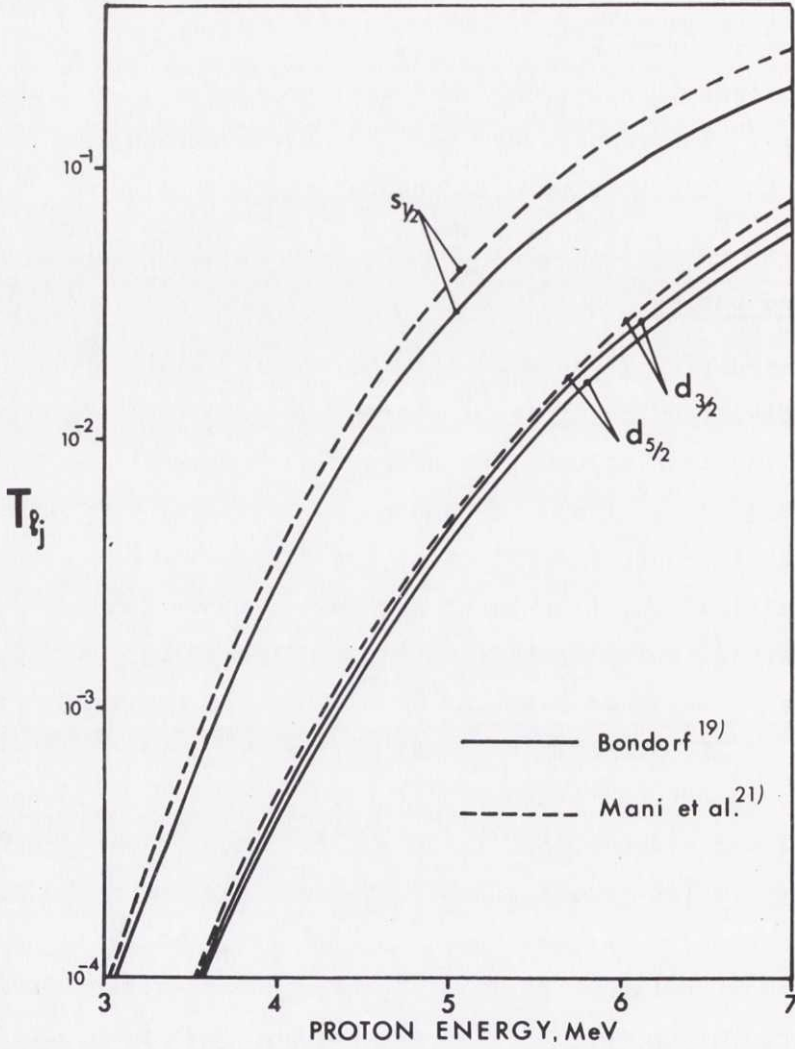


Fig. IV.8 The transmission coefficients for protons on tellurium. The values have been calculated with the target mass 114 [Bondorf (19)] and 120 [Mani et al. (21)]. The proton energy is given in the laboratory system.

The sensitivity to the choice of $\omega(I, I_1)$ on P_p is examined in Table IV.9. Calculations, under the assumption that only one spin in the intermediate nucleus is populated, have been performed. The dominating contributions come from the low spin states which, in analogy with the discussion given earlier, may be understood as an effect of the centrifugal barrier on the transmission coefficients.

Table IV.8

The relative feeding of assumed final states
(with $I_f^{\pi f} = 0^+$) from ^{115}Xe

E_f MeV	Feeding (%)	E_f MeV	Feeding (%)
0.00	87.0	0.00	65.1
0.50	11.4	0.25	23.0
1.00	1.5	0.50	8.1
1.50	0.1	0.75	2.8
2.00	0.0	1.00	1.0

Table IV.9

Calculated intensities of the proton branches from xenon isotopes
in assumed cases where only one intermediate spin is populated

Nuclide	I^{π}	Proton branching ratio P_p (p/beta decay)			
		$\omega(I, \frac{1}{2})$	$\omega(I, \frac{3}{2})$	$\omega(I, \frac{5}{2})$	$\omega(I, \frac{7}{2})$
^{117}Xe a)	$\frac{5}{2}^-$	-	2.0×10^{-4}	1.0×10^{-5}	4.7×10^{-6}
^{117}Xe a)	$\frac{5}{2}^+$	-	5.1×10^{-5}	3.7×10^{-5}	1.0×10^{-6}
^{117}Xe a)	$\frac{3}{2}^+$	9.1×10^{-4}	5.1×10^{-5}	3.7×10^{-5}	-
^{115}Xe b)	$\frac{5}{2}^+$	-	5.2×10^{-3}	4.3×10^{-3}	5.8×10^{-4}
^{113}Xe c)	$\frac{5}{2}^+$	-	9.9×10^{-2}	9.0×10^{-2}	2.0×10^{-2}

a) $Q - B_p = 4.10$ MeV. b) $Q - B_p = 6.20$ MeV. c) $Q - B_p = 8.55$ MeV.

4.2 Q and B_p

The different mass formulas examined in Table III.5 revealed only relatively small differences in the predicted $Q - B_p$ values. The importance of changes in Q and B_p to the calculated intensity is, with ^{115}Xe as the example, examined in Fig. IV.9. The proton branching ratio is very sensitive to the value chosen for the proton separation energy (for fixed Q) but not so much to Q for fixed B_p .

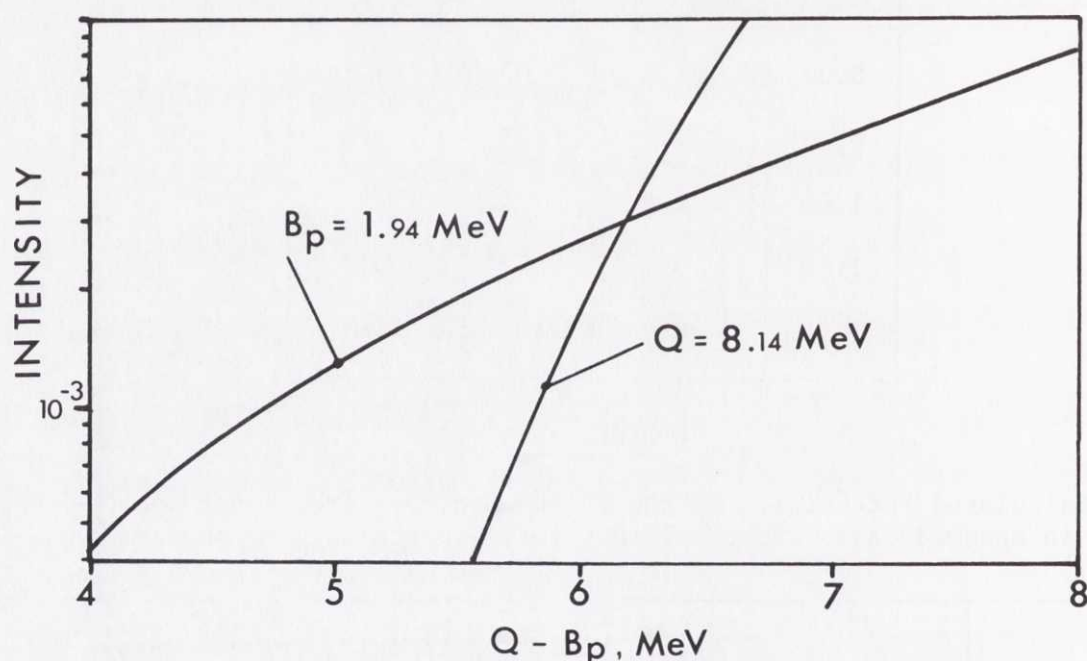


Fig. IV.9 Calculated intensity of delayed protons from ^{115}Xe assuming $I^\pi = 5/2^+$ and a constant beta strength function. The two curves show how the calculated intensity varies as a function of $Q - B_p$ when Q and B_p , respectively, are kept fixed.

The sensitivity to changes in Q and B_p is much more dominating in cases where the $Q - B_p$ value is expected to be low. This is seen in Fig. IV.9, where the decrease in the calculated proton intensity is steeper towards lower energies. A further illustration is given in Fig. IV.10, where the sensitivity to the choice of Q and B_p is examined for ^{120}Cs . The rate of change in P_p is very high both for fixed Q and for fixed B_p . An explanation of this may be found from Fig. IV.11 (next section). The proton width at low energies is much smaller than the

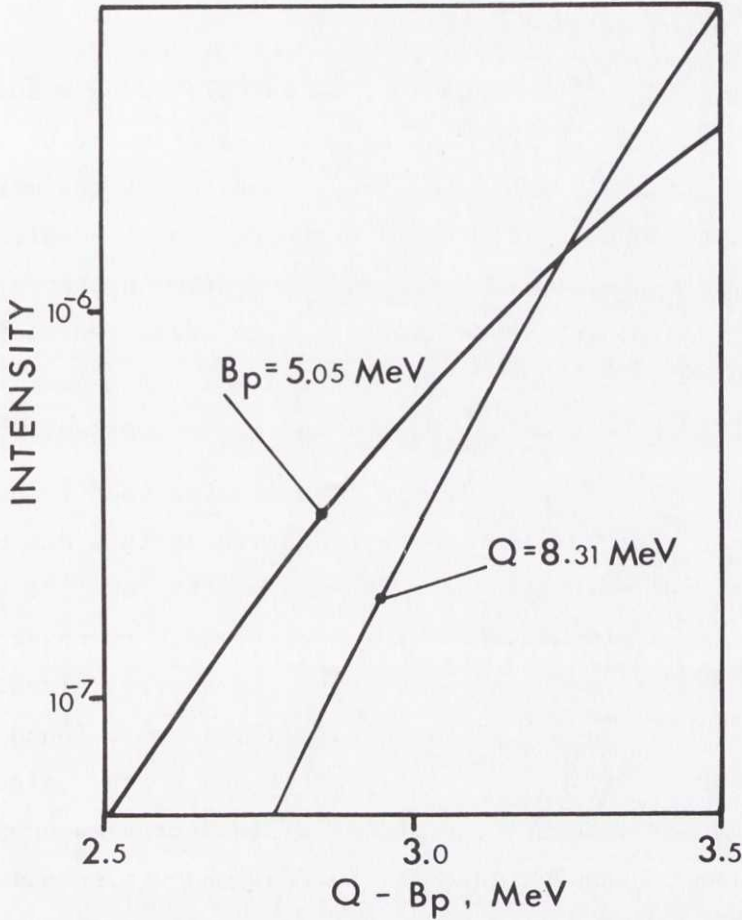


Fig. IV.10 Calculated intensity of delayed protons from ^{120}Cs assuming $I^\pi = 3^+$ and a constant beta strength function. The two curves show how the calculated intensity varies as a function of $Q - B_p$ when Q and B_p respectively, are kept fixed.

corresponding gamma width. With $\Gamma_\gamma \gg \sum_f \Gamma_p^i$, expression (IV.1) can be written

$$I_p^{\text{if}}(E_p) \approx \omega(I, I_i) I_p(E) \frac{\Gamma_p^{\text{if}}}{\Gamma_\gamma} \quad (\text{IV.25})$$

The total gamma width Γ_γ is a slowly varying function of the energy while the partial proton width Γ_p^{if} has a steep decrease towards lower energies, due to the Coulomb barrier. The strong energy dependence of Γ_p^{if} will therefore be reflected in the calculated intensity. The discrepancy between the calculated and measured values of the ^{120}Cs proton branch could then, at least partly, be due to a too high $Q - B_p$ value chosen in the calculation. The estimate from Ref. (8) was also found to be too high for ^{118}Cs (Table III.5). Another explanation can be found in the approximation of the beta strength function: The beta decay of ^{120}Cs could proceed via strong branches to the ground state and first excited states of ^{120}Xe . This would be analogous to the decays of ^{128}Cs and $^{126}\text{Cs}^{30}$ if the ground state has $I^\pi = 1^+$.

4.3 The transmission coefficients

The transmission coefficients $T_{\ell j}$, as calculated by Bondorf¹⁹⁾, were compared to those calculated by Mani et al.²¹⁾ in Fig. IV.8. There is a slight numerical discrepancy between their results but the main behaviour is the same in both cases. (It should be noted that the calculations were performed for different masses.) A comparison between the calculated proton branching ratios for xenon isotopes with these two choices of $T_{\ell j}$ is given in Table IV.10. The last column in the table gives the results obtained with the WKB penetrability $P_{\ell}(E_p)$ and $\gamma_{\ell j} = \text{constant}$.

The sensitivity to changes in the transmission coefficients is low according to these calculations. An explanation of this can be found in Fig. IV.11, where the total proton and gamma widths for ^{115}I are plotted as functions of the proton energy. The proton width increases steeply with energy and begins to dominate over the gamma width already at low proton energies. With $\sum_f \Gamma_p^{if} \gg \Gamma_{\gamma}$ in Eq. (IV.1) it is found that a change in the function $\gamma_{\ell j}$ is of minor importance to the calculated intensity. For heavier elements the proton width decreases compared to the gamma width, owing to the increase in the Coulomb barrier and the increased level density [Eq. (IV.11)]. Figure IV.12 shows the total proton and gamma widths for ^{101}Au , and in this case the gamma width dominates over the whole energy range of interest.

An important consequence of this is that in the cases where the proton decay is the dominating decay mode of the intermediate states (as for xenon) the spectral shape is determined mainly by the shape of the beta strength function. A study of the beta-delayed proton spectra may therefore be a valuable tool for determining the shape of beta strength functions for extremely neutron deficient nuclides. The analysis of ^{115}Xe given in Section 4.5 is an example of this.

In regions where $\Gamma_{\gamma} \gg \sum_f \Gamma_p^{if}$, the spectral shape is determined by both the shape of the beta strength function and the energy dependence of the proton widths. Methods for experimental determination of the energy dependence of the beta strength^{11,15)} and the density of levels (Chapter V) are available. Information about the transmission coefficients for sub-barrier protons may, therefore, be obtained in some cases. Such data will be of importance in the study of the optical potential at low proton energies.

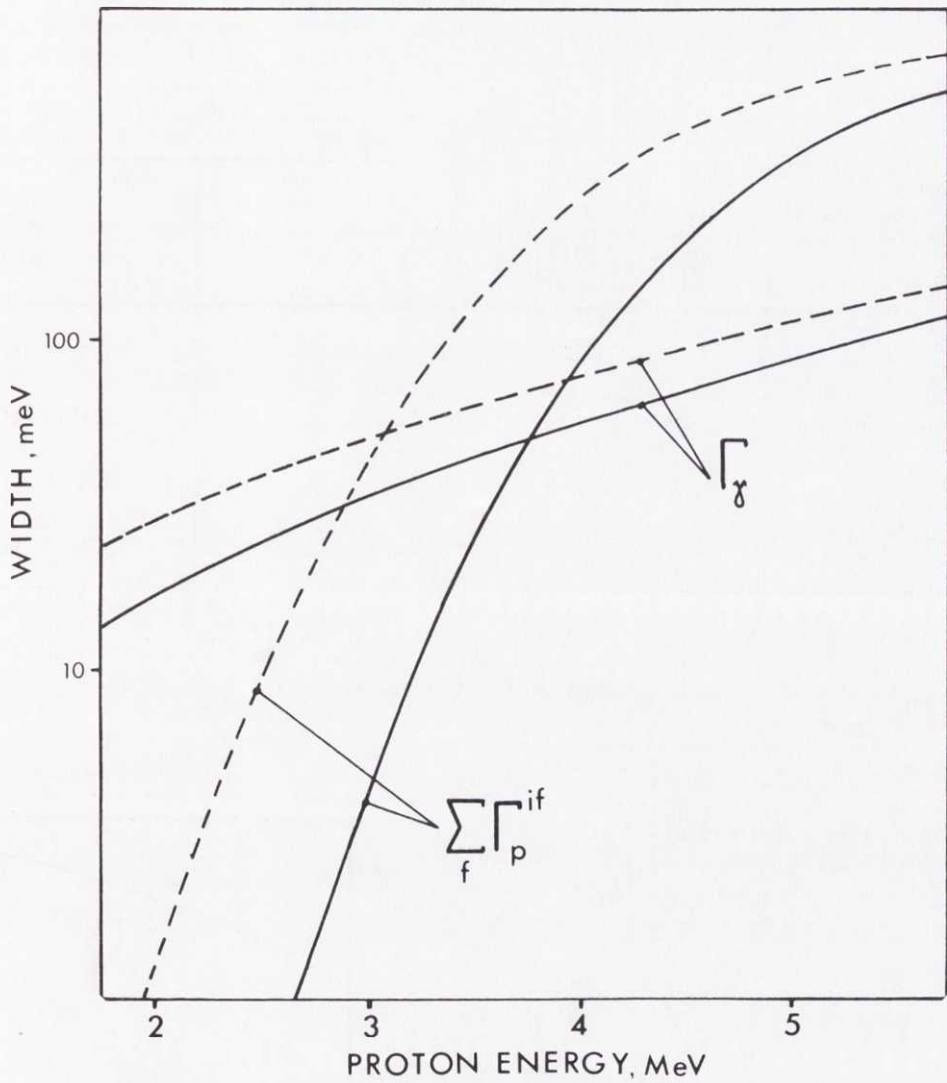


Fig. IV.11 The calculated total proton and gamma widths of excited states in ^{115}I . The solid curve shows the values for protons feeding the ground state of ^{114}Te (0^+) [corresponding to excitation energies in ^{115}I of $B_p + E_p A/(A - 1)$ MeV] and the dashed curve shows the values for feeding of the first excited state at 709 keV (2^+) [corresponding to excitation energies $B_p + E_p A/(A - 1) + 0.709$ MeV]. The calculations were performed with $I^\pi = 5/2^+$ and with $B_p = 1.94$ MeV.

Table IV.10

Calculated delayed proton branching ratios for xenon with different choices of T_{lj}

Nuclide	Assumed I^π	P_p [Bondorf ¹⁹⁾]	P_p [Mani et al. ²¹⁾]	P_p $\gamma_{lj} = \text{constant a)}$
^{117}Xe b)	$5/2^+$	2.4×10^{-5}	2.6×10^{-5}	3.1×10^{-5}
^{117}Xe b)	$3/2^+$	1.9×10^{-4}	2.1×10^{-4}	2.0×10^{-4}
^{115}Xe c)	$5/2^+$	2.8×10^{-3}	3.0×10^{-3}	3.1×10^{-3}
^{113}Xe d)	$5/2^+$	6.1×10^{-2}	6.3×10^{-2}	5.6×10^{-2}

a) γ_{lj} in Eq. (IV.14) was chosen constant and equal to $\gamma_{lj}(E_p)$, as calculated from Ref. (19), at 3 MeV

b) $Q = 6.87$ MeV, $B_p = 2.77$ MeV

c) $Q = 8.14$ MeV, $B_p = 1.94$ MeV

d) $Q = 9.58$ MeV, $B_p = 1.03$ MeV

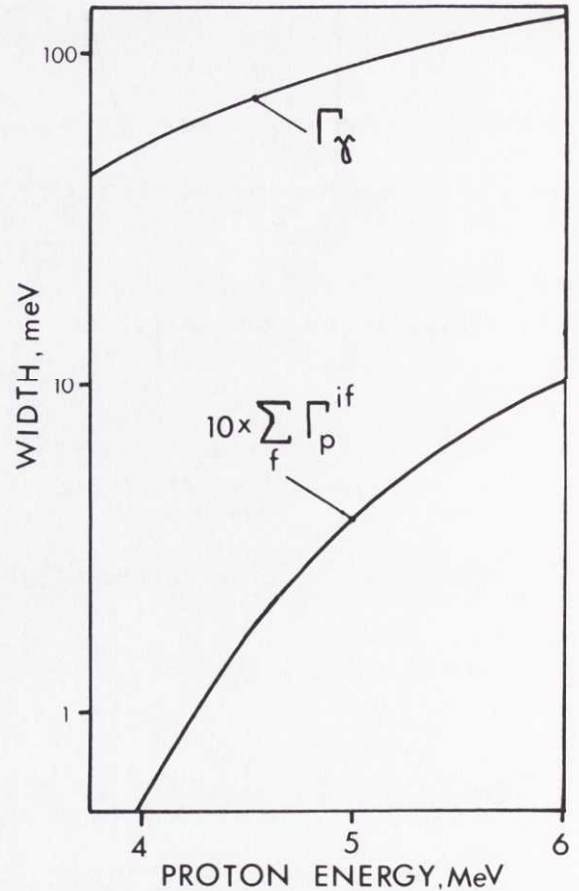


Fig. IV.12

The calculated total proton and gamma widths of excited states in ^{181}Au . The calculations are valid for protons feeding the ground state of ^{180}Pt (0^+) [corresponding to excitation energies in ^{181}Au of $B_p + E_p A/(A-1)$ MeV]. The calculations were performed with $I^\pi = 1/2^-$ and with $B_p = 1.31$ MeV.

4.4 Choice of the level density formula

The proton width, calculated from Eq. (IV.11), is dependent on the transmission coefficients T_{lj} and the level density $\rho_i(E)$. In this section two level density formulas, besides the one by Gilbert and Cameron²⁵⁾, will be examined.

With a Fermi gas treatment of the nucleus^{12e)} the expression for the level density (valid for spin I_i and one parity) is

$$\rho_i(E) = \frac{2I_i + 1}{24} \left(\frac{\pi^2}{6} g_0 \right)^{\frac{1}{2}} \left(\frac{\hbar^2}{2J_{\text{rig}}} \right)^{\frac{3}{2}} \left[U - \frac{\hbar^2}{2J_{\text{rig}}} I_i(I_i + 1) \right]^{-2} \times \exp \left\{ 2 \left[\frac{\pi^2}{6} g_0 \left(U - \frac{\hbar^2}{2J_{\text{rig}}} I_i(I_i + 1) \right) \right]^{\frac{1}{2}} \right\} \text{MeV}^{-1}, \quad (\text{IV.26})$$

where $\frac{\pi^2}{6} g_0 = A/8 \text{ MeV}^{-1}$,

$$\frac{\hbar^2}{2J_{\text{rig}}} = 0.015 \text{ MeV},$$

and where the effective excitation was chosen according to Eq. (IV.17). Newton²⁴⁾ has given the level density as

$$\rho_i(E) = (2I_i + 1) A^{-5/3} (2\bar{J}_N + 1)^{-\frac{1}{2}} (2\bar{J}_Z + 1)^{-\frac{1}{2}} \times (U + bU^{\frac{1}{2}})^{-2} \exp [3U^{\frac{1}{2}}/b - 10.258] \text{ eV}^{-1}. \quad (\text{IV.27})$$

The parameters in this formula are the same as were used in Eq. (IV.15). Figure IV.13 shows the predictions of $\rho_i(E)$ in the different treatments. The formula by Newton²⁴⁾ differs from the other two by a factor of 10 in the case of gold. Owing to the dominating gamma widths for mercury (Fig. IV.12) the discrepancy in the prediction of the level density is strongly reflected in the calculated proton branching ratios (Table IV.11).

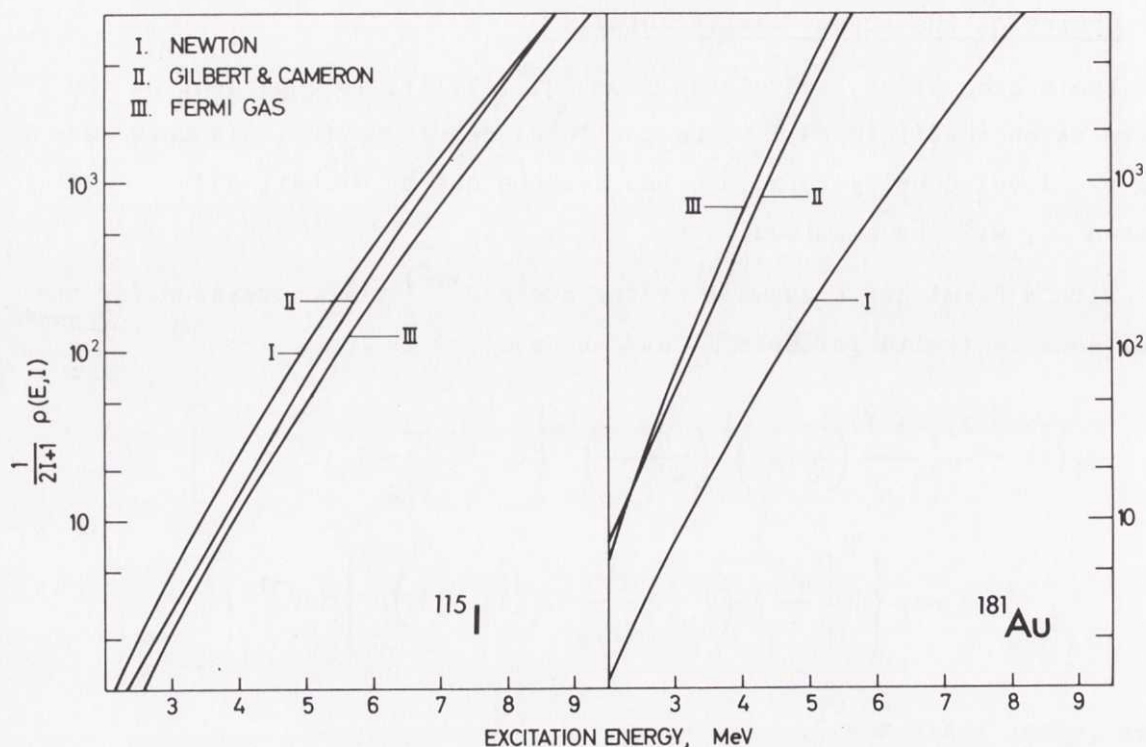


Fig. IV.13 Level densities (in MeV^{-1}) for spin "zero" in ^{115}I and ^{181}Au according to various semi-empirical formulas [Refs. (24), (25), (26) and (12e)].

Table IV.11

Proton branching ratios P_p calculated with different level density formulas^{a)}.

Nuclide	I^π	Gilbert and Cameron ^{25,26)}	Newton ²⁴⁾	Fermi gas ^{12e)}
^{117}Xe	$5/2^+$	2.4×10^{-5}	2.8×10^{-5}	5.0×10^{-5}
^{115}Xe	$5/2^+$	2.8×10^{-3}	2.3×10^{-3}	3.5×10^{-3}
^{183}Hg	$1/2^-$	1.5×10^{-6}	3.8×10^{-5}	9.1×10^{-7}
^{181}Hg	$1/2^-$	3.4×10^{-5}	8.7×10^{-4}	2.3×10^{-5}
^{179}Hg	$1/2^-$	3.3×10^{-4}	7.8×10^{-3}	2.8×10^{-4}

a) Mass parameters as in Table IV.2

4.5 The beta strength function

The model strength function¹¹⁾ used up to this point clearly represents an over-simplification. However, it brings out two important features of the experimental distribution:

- i) the main part of the strength is associated with transitions that excite protons which are initially in paired orbits; consequently the schematic model has no strength below a certain energy for odd mass and odd-odd-nuclei [Fig. IV.3 and Eq. (IV.9)];
- ii) the beta strength varies slowly with energy; this feature is represented by the use of a constant value \bar{S}_β .

The experimental beta strength functions in the mercury region^{11,15)} show only relatively small fluctuations around the average value. The assumption of a constant beta strength function is therefore a sufficiently good approximation in these cases.

In the xenon region the beta strength function determines the high-energy shape of the proton spectrum according to the analysis given in Section 4.3. The experimental spectra may consequently give information about the energy distribution of the strength. The dashed curve in Fig. IV.14 shows the spectral shape of ^{115}Xe calculated under the assumption of a constant beta strength function. An improved fit to the experimental points can be obtained if the strength is assumed to have a broad peak at 5 MeV excitation energy in ^{115}I (the solid curve).

The beta strength function for ^{117}Xe has been determined experimentally¹⁵⁾. The result is shown in Fig. IV.15. This strength function was obtained after an unfolding³²⁾ of a gamma spectrum from ^{117}Xe measured with a total absorption spectrometer¹¹⁾. The unfolded spectrum, which represents the beta intensity as a function of energy, was then divided by $f(Z, Q - E) \cdot T_{1/2}$ [Eq. (IV.17)] to give $S_\beta(E)$. The result indicates a broad peak in the strength at about 4 MeV excitation energy in ^{117}I . According to the estimated proton separation energy for ^{117}I [2.77 MeV⁸⁾] the proton emission will take place from levels above 4.5 MeV. The peak in the strength will, therefore, be of no importance for the spectral shape in this case. A calculation with the experimental strength function, and the assumption that the strength is constant

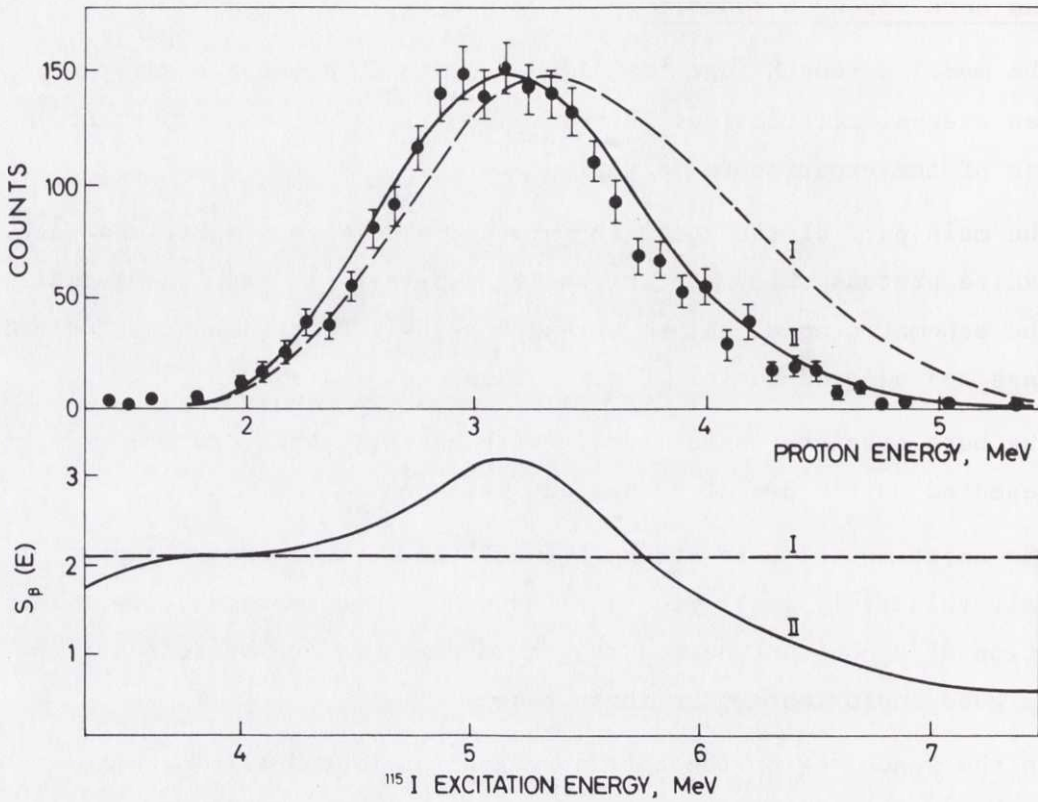


Fig. IV.14 The measured delayed proton spectrum (upper graph) from ^{115}Xe (exp. points) compared with two calculations, both assuming $I^\pi = \frac{5}{2}^+$. In one calculation the beta strength function is assumed to be constant (I), and in the other it has been assumed to have the shape shown by the solid curve in the lower graph (II). An arbitrary scale is used for the calculated intensity.

above 5.5 MeV, was performed. The result is shown in Fig. IV.16. The decline of the spectrum calculated under this assumption is identical to the one obtained from a constant strength function. A somewhat improved fit to the experimental points was obtained in Ref. (C), where the strength was assumed to decrease towards higher energies. However, no detailed conclusions can be drawn with the present statistics of the ^{117}Xe delayed proton spectrum.

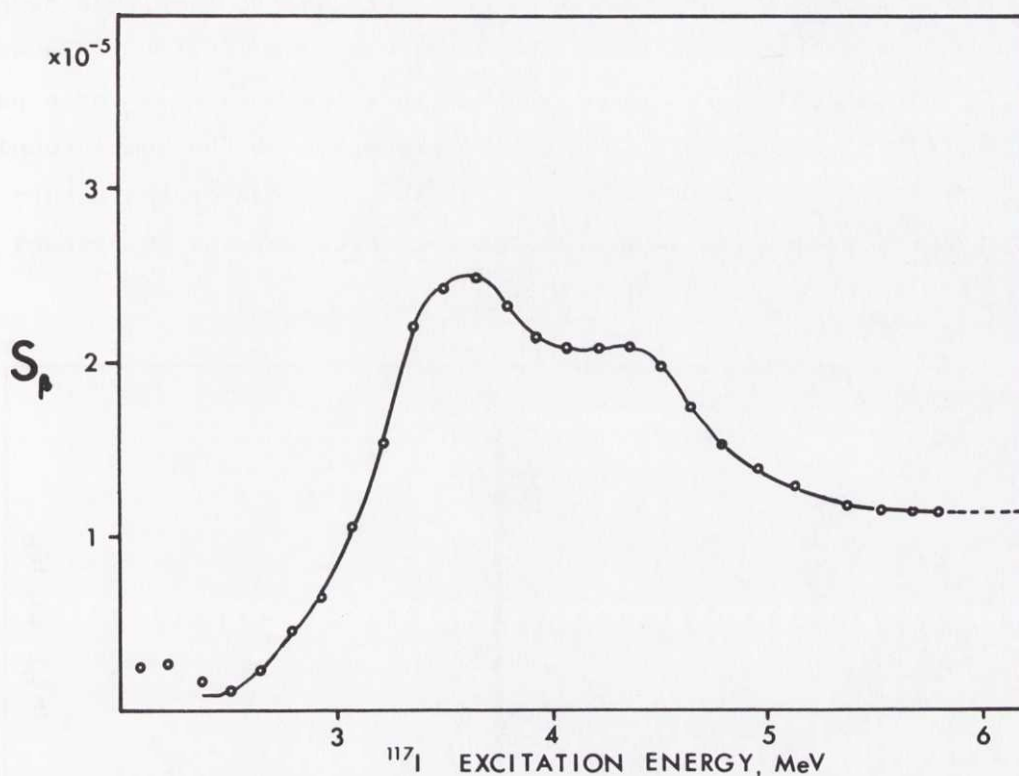


Fig. IV.15 The beta strength function for ^{117}Xe measured¹⁵⁾ with a total absorption spectrometer.

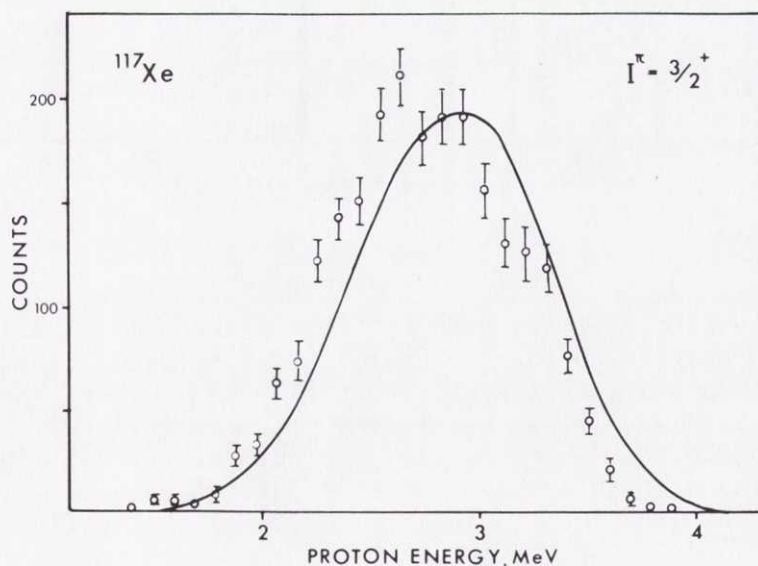


Fig. IV.16 The measured delayed proton spectrum from ^{117}Xe (exp. points) compared with a calculation assuming $I^\pi = 3/2^+$ and with the beta strength function shown in Fig. IV.15. The B_p value was taken from Ref. (8) and Q was chosen to fit the experimental value on $Q - B_p$.

The possible peak in the beta strength functions for the light xenon isotopes may be explained from shell model calculations³³⁾ (for ^{115}Xe see Fig. IV.17) which suggest that it originates in a $(g_{9/2})_p^{-1} (g_{7/2})_n$ hole particle excitation. In analogy with the interpretation of the humps found in gamma spectra by various methods^{23, 34-37)} the peak can be characterized as a pygmy resonance arising from the beta decay of the 10 protons in the $g_{9/2}$ shell to the $g_{7/2}$ neutron shell.

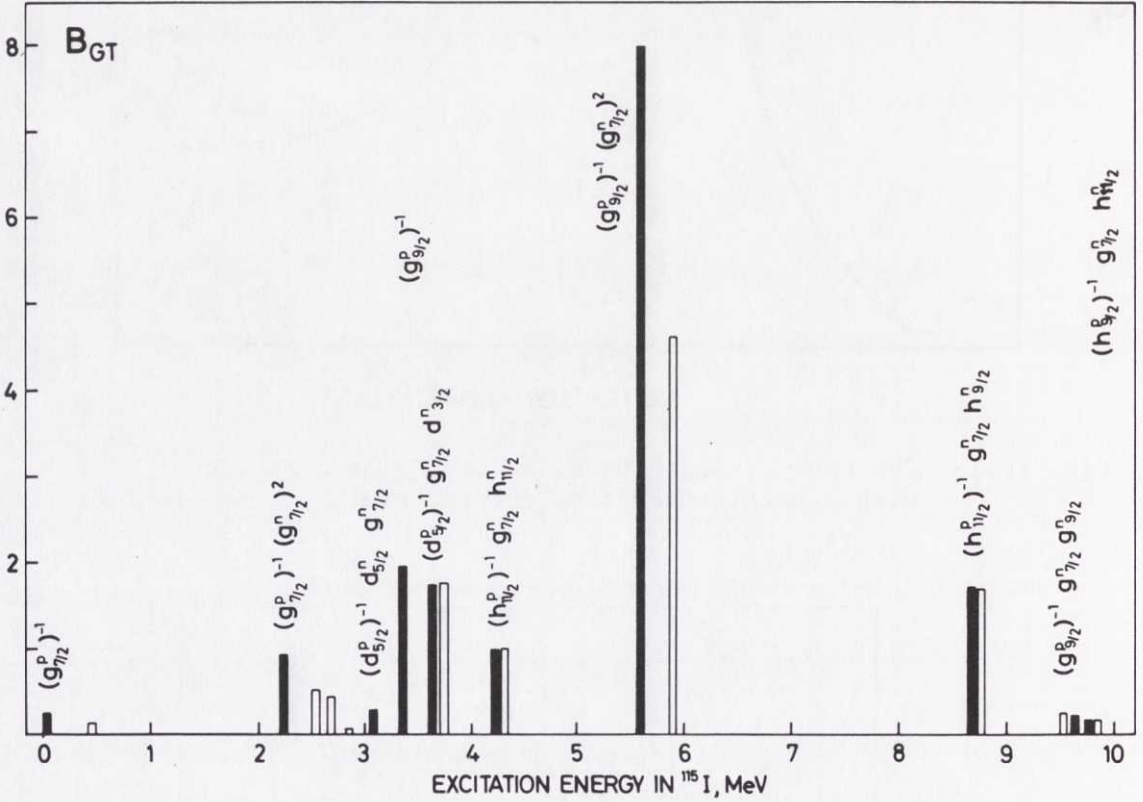


Fig. IV.17 Reduced beta transition probabilities for ^{115}Xe calculated by Martinsen and Randrup³³⁾ from the simple shell model with pairing ($\Delta_n = \Delta_p = 1.1$ MeV) included. The full lines assume a set of single-particle levels where the $d_{5/2}$ neutron level fills before the $g_{7/2}$ neutron level. If these two levels are inverted, one obtains the distribution shown in thin lines, which predict a spin of $5/2$ in agreement with the feedings to the final states (Table IV.6).

5. OTHER MECHANISMS THAT COULD CONTRIBUTE TO THE DELAYED PROTON SPECTRA

Three processes that in principle could give contributions to the delayed proton spectra should be mentioned:

- i) the emission of two successive protons after beta decay;
- ii) the emission of a proton pair after beta decay;
- iii) the $\beta\gamma p$ process.

The two first mentioned processes are energetically forbidden in the cases of interest.

Proton emission from states fed by gamma decay of states populated in beta decay ($\beta\gamma p$) should, in principle, be possible. An analogous $n\gamma\alpha$ process has been observed experimentally³⁸⁾ in alpha spectra following thermal neutron capture. A theoretical estimate of the contribution from the $\beta\gamma p$ mechanism to the proton spectra from the xenon delayed proton emitters has been made. The calculation was carried out under the assumption of a constant gamma strength function and pure dipole radiation. An integration over all intermediate levels was performed. The contribution from this process is 1-3% of the βp intensity for the odd xenon isotopes, according to such an estimate.

6. SUMMARY

The statistical model for beta-delayed proton emission, from elements in the medium- and heavy-weight regions, is seen to work well. The proton branching ratios, the feeding of final states, and the gross shapes of the spectra could be reproduced satisfactorily in almost all cases. The model is, however, based on very simple assumptions and has therefore to be considered only as a convenient starting point for further studies of beta-delayed proton emission. The present calculations have mainly served to get a better understanding of the decay process under study; which quantities that are involved and their importance in different energy regions and mass regions. It has also been shown that the calculations in combination with the experimental data may give information about some parameters of interest to nuclear physics:

- i) The beta strength function. The energy dependence of the beta strength may be extracted from the delayed proton spectra if proton emission is the dominating decay mode of the intermediate states. Beta strength functions for nuclides so far from the region of beta stability are only in a few cases obtainable with the conventional technique^{11,15}).
- ii) The energy dependence of the partial proton widths. From the partial widths the transmission coefficients for sub-barrier protons may be determined. Such data would give a valuable contribution to the study of the optical model parameters at low kinetic energies, and for cases where the protons have extremely low binding energies.
- iii) The spins involved in the process. Spin determinations from atomic beam experiments, optical pumping experiments, and decay scheme work will, in the extremely neutron deficient regions, meet severe intensity problems. The study of proton branches to final states may therefore become a valuable complementary method. The possibility of determining the spin weight factors is, however, more interesting since it is hardly within present experimental possibilities to determine the beta branching ratios to states with different spins and parities in the daughter nucleus.

This treatment of beta-delayed proton emission has dealt only with the average properties of the nuclear levels. A gross structure in the beta strength ("pygmy resonance") as well as the gross structure associated with the optical model have been incorporated. The observable fine structure which shall be interpreted as fluctuations around the average intensity will be discussed in the next chapter.

REFERENCES TO CHAPTER IV

- 1) A. Siivola, Phys. Rev. Letters 14, 142 (1965).
R.D. Macfarlane, Arkiv för Fysik 36, 431 (1967).
V.A. Karnaukhov, G.M. Ter-Akopyan, L.A. Petrov and V.G. Subbotin,
Soviet J. Nuclear Phys. 1, 581 (1965).
- 2) I. Bacso, D. D. Bogdanov, Sh. Darotsi, V.A. Karnaukhov and L.A. Petrov,
Soviet J. Nuclear Phys. 7, 689 (1968).
- 3) D.D. Bogdanov, Sh. Darotsi, V.A. Karnaukhov, L.A. Petrov,
G.M. Ter-Akopyan, Soviet J. Nuclear Phys. 6, 650 (1968).
V.A. Karnaukhov, Soviet J. Nuclear Phys. 10, 257 (1970).
- 4) A.C. Pappas and T. Tunaal, Arkiv för Fysik 36, 475 (1967).
- 5) H. Gauvin and R. de Turreil, 2nd Symposium on the Physics and
Chemistry of Fission, Vienna (1969) (IAEA, Vienna, 1969), p. 621.
- 6) K. Takahashi, Progress Theoretical Physics (Kyoto) 47, 1500 (1972).
- 7) T. Sverdrup and A.C. Pappas, Nuclear Phys. A188, 48 (1972).
- 8) W.D. Myers and W.I. Swiatecki, UCRL-11980 (1965).
- 9) L. Westgaard, J. Żylicz and O.B. Nielsen, in Proc. 4th Int. Conf. on
Atomic Masses and Fundamental Constants, NPS, Teddington, 1971.
- 10) J. Bonn, G. Huber, H.J. Kluge and E.W. Otten, Phys. Letters 38 B, 308
(1972).
- 11) C.L. Duke, P.G. Hansen, O.B. Nielsen and G. Rudstam, Nuclear Phys. A151,
609 (1970).
- 12) A. Bohr and B.R. Mottelson, Nuclear Structure (Benjamin, New York,
1969), Vol. I a) p. 413, b) p. 169, c) p. 352, d) p. 236, and
e) p. 155.
- 13) E.J. Konopinski and M.E. Rose, Alpha, Beta, and Gamma Ray Spectro-
scopy (ed. K. Siegbalm) (North Holland Publ. Co., Amsterdam,
1965), p. 1327.
- 14) L.N. Zyryanova, Once-forbidden Beta Transitions (English trans.
Pergamon Press, London, 1963), p. 36.
- 15) P. Hornshøj, B.R. Erdal, P.G. Hansen, B. Jonson, J. Żylicz, K. Johansson,
and G. Nyman, to be published.
- 16) P.G. Hansen, Proc. Int. Conf. on Properties of Nucleon States, Montreal,
1969 (Presses de l'Université de Montreal, 1969), p. 189.
- 17) G.J. Ehnholm, T.E. Kattila, O.V. Lounasmaa, P. Reivari and G.M. Kalvius,
Phys. Rev. C1, 2109 (1970).
- 18) J.M. Blatt and V.F. Weisskopf, "Theoretical Nuclear Physics" (Wiley,
New York, 1952), p. 386.

- 19) J. Bondorf, private communication.
- 20) P. Morrison, *in* Experimental Nuclear Physics (ed. E. Segré) (Wiley, New York, 1953) Vol. II, p. 50.
- 21) G.S. Mani, M.A. Melankoff and I. Iori, CEA-2379 (1963).
- 22) A.G.W. Cameron, Can. J. Phys. 34, 666 (1956).
- 23) I. Bergqvist and N. Starfelt, Progr. Nuclear Phys. 11, 1 (1970).
- 24) T.D. Newton, Can. J. Phys. 34, 804 (1956).
- 25) A. Gilbert and A.G.W. Cameron, Can. J. Phys. 43, 1446 (1966).
- 26) J.W. Truran, A.G.W. Cameron and E. Hilf, Proc. Int. Conf. on the Properties of Nuclei far from the Region of Beta Stability, Leysin 1970, CERN 70-30 (1970), Vol. I, p. 275.
- 27) P.G. Hansen, H.L. Nielsen, K. Wilsby, M. Alpsten, M. Finger, A. Lindahl, R.A. Naumann and O.B. Nielsen, Nuclear Phys. A148, 249 (1970).
- 28) A. Luuko, A. Kerek, I. Rezanka and C.J. Herrlander, Nuclear Phys. A135, 49 (1969).
- 29) E. Nolte, W. Kutschera, Y. Shida and H. Morinaga, Proc. Int. Conf. on the Properties of Nuclei far from the Region of Beta Stability, Leysin 1970, CERN 70-30 (1970), Vol. II, p. 911.
- 30) C.M. Lederer, J.M. Hollander and I. Perlman, Table of Isotopes (Wiley, New York, 1967).
- 31) F. Dickmann, V. Metag and R. Repnow, Phys. Letters 38 B, 207 (1972).
- 32) B.R. Erdal and G. Rudstam, to be published in Nuclear Instr. and Methods.
- 33) P.O. Martinsen and J. Randrup, Nuclear Phys. A 195, 26 (1972).
- 34) P. Axel, K. Min, N. Stein and D.C. Sutton, Phys. Rev. Letters 10, 299 (1963).
- 35) G.A. Bartholomew *in* Neutron Capture Gamma Ray Spectroscopy (IAEA, Vienna, 1969), p. 553.
- 36) M.A. Lone, E.D. Earle and G.A. Bartholomew, Nuclear Phys. A143, 457 (1970).
- 37) C. Gaarde, K. Kemp, Y.V. Naumov and P.R. Amudsen, Nuclear Phys. A143, 497 (1970).
- 38) N.S. Oakey and R.D. Macfarlane, Phys. Letters 26 B, 662 (1968).

CHAPTER V

FLUCTUATIONS IN DELAYED-PROTON SPECTRA

1. INTRODUCTION

The statistical model for beta delayed proton emission (examined in the previous chapter) reproduces the gross shape of the spectra well, under the assumption that the main structure varies slowly with energy. The quantities involved in the calculations, as for example, the beta-decay intensity to the intermediate levels and the partial widths of the levels for proton decay to the final states, were taken to represent average values over a great number of states with the same $I_i^{\pi i}$. For a finite sample one will clearly have fluctuations around the average. These can be taken into account in a statistical theory. It has been found¹⁾ that the statistical distributions that may describe the average properties of the quantities involved are broad. For an experiment the finite number of levels participating within the experimental resolution will then give rise to fluctuations in the intensity. Such fluctuations, which have been observed in the cases where the measurements were performed with good resolution and good statistics (see Figs. II.7 and II.10), are a joint effect of the different processes participating. They originate in nuclear structure effects and are experimentally reproducible. The phenomenon is analogous to the fluctuations in slow-neutron average cross-sections discussed by Egelstaff²⁾. A theoretical expression of $\text{Var} (I_p / \bar{I}_p)$ can be derived by considerations akin to those given in Ref. (2).

2. GENERAL CONSIDERATIONS

The emission of delayed protons takes place from levels at 4-10 MeV excitation energy in the intermediate nucleus. In a heavy nuclide the mean level spacing \bar{D}_i at such excitation energies is expected to be small but still much greater than the total width $\bar{\Gamma}^i$. Table V.1 gives some estimated values of \bar{D}_i and $\bar{\Gamma}^i$ in the case of ^{115}I .

The delayed proton spectra reported here were measured with detectors having a full width at half maximum ΔE of typically 15-60 keV. The relation

Table V.1

Mean level spacings and total radiation widths
for ^{115}I ($I_i^{\pi i} = 3/2^+$)

Proton energy MeV	$\bar{D}_{3/2}$ a) keV	$\bar{\Gamma}^i$ b) eV
3.0	3.35	0.04
4.0	0.75	0.14
5.0	0.20	0.45

- a) The values were calculated from Gilbert and Cameron³⁾ and are valid at an excitation energy $B_p + E_p$ ($A/A - 1$) in the intermediate nucleus.
- b) Calculated from the formulas given in Chapter IV; the values are valid at the excitation energy $B_p + E_p$ ($A/A - 1$) in the intermediate nucleus.

$$\Delta E \gg \bar{D}_i \gg \bar{\Gamma}^i \quad (\text{V.1})$$

is then valid over the whole energy range of interest.

These estimates indicate that a delayed proton spectrum from ^{115}Xe consists of proton lines from a great number of individual, closely spaced levels which remain experimentally unresolved. The number of levels participating within the experimental resolution is great but, as mentioned, the broad distributions of the quantities involved will still give observable fluctuations. This is illustrated in Fig. V.1: A number of proton groups from equally spaced levels is assumed to be measured with a detector for which the expression (V.1) is fulfilled. The magnitudes of the intensities were chosen to follow a Porter-Thomas distribution (see next section) and the detector-response function is assumed to have a Gaussian shape. The solid curve in the lower part of the figure shows the expected result from the measurement (with infinite statistics). In

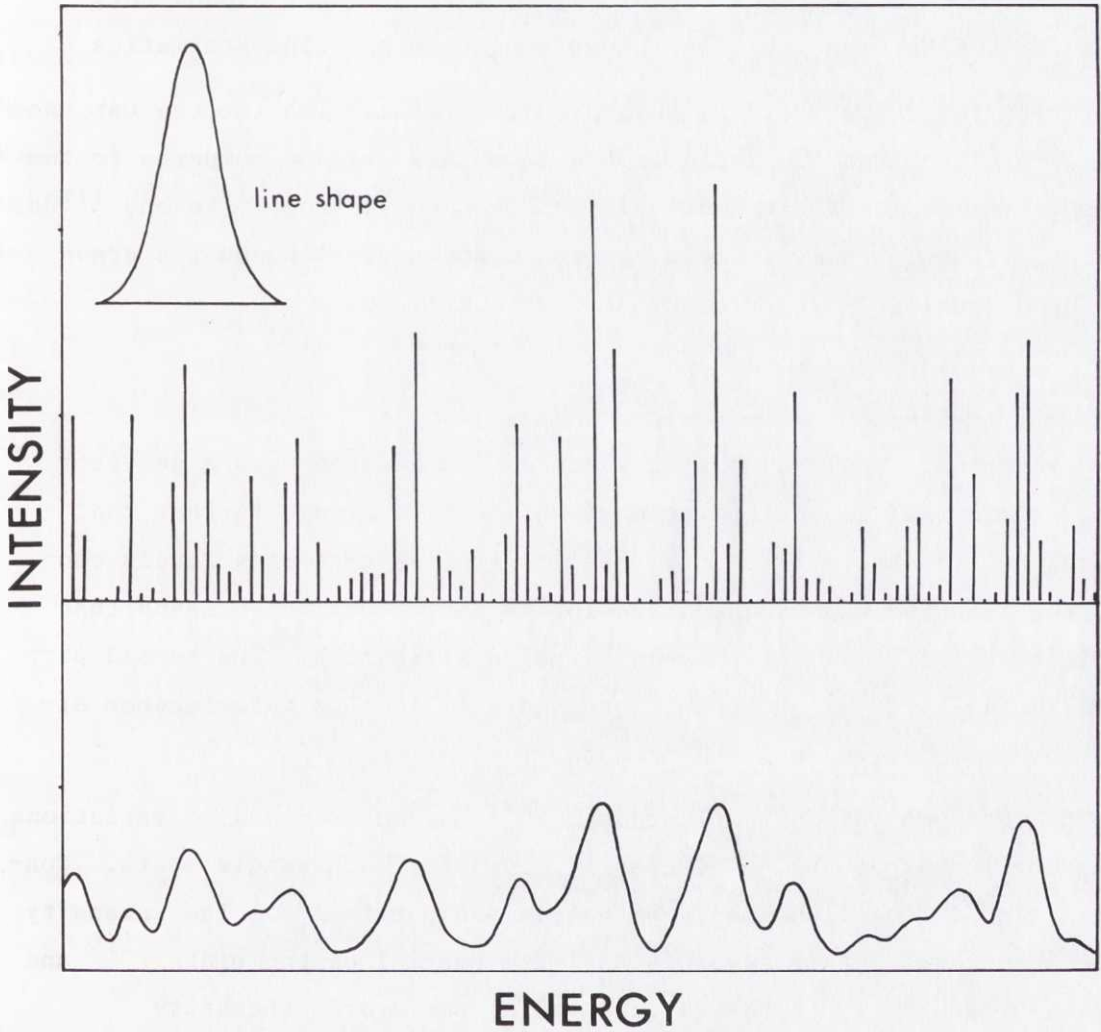


Fig. V.1 The lines in the upper part of the figure represent proton emission from a number of equally spaced resonances. The intensities of the lines have been chosen proportional to random Porter-Thomas distributed numbers for one spin and one parity. A smoothing of the line spectrum with the response function indicated in the figure (Gaussian shape) gives the solid curve.

the realistic case the experimental points would scatter around this curve with the Poisson distribution arising from counting statistics.

In the following sections an approximate expression for the variance in I_p will be derived and the estimate from this will be compared to the observed fluctuations in the delayed proton spectra from ^{115}Xe and ^{118}Cs . Here the discussion aims at delayed-proton spectra, although the arguments hold equally well for other kinds of particles.

THEORETICAL ESTIMATE OF $\text{Var}(I_p/\bar{I}_p)$

Assume that a delayed proton spectrum is measured with a detector having a Gaussian response function ($\text{FWHM} = \Delta E$). Assume further that expression (V.1) is valid. This relation implies that many levels contribute within the experimental resolution ($\Delta E \gg \bar{D}_i$) which means that the fluctuations in I_p will have a normal distribution. The second part of the inequality $\bar{D}_i \gg \bar{\Gamma}_i$ shows that there will be no interference effects which could give rise to Ericson fluctuations^{4)*}.

The observed intensity fluctuations^{**}) may be ascribed to variations in the magnitudes of the quantities involved for each single state. Consider a single level labelled v with spin and parity $I_i^{\pi i}$. The intensity of the beta feed to this level is R_β^{iv} , the partial proton width Γ_p^{ifv} and the gamma width Γ_γ^{iv} . In the calculation of the proton intensity [Eq. (IV.1)] the corresponding quantities were taken to represent average values over many states. One then has the relations

$$\begin{aligned} \omega(I, I_i) \cdot I_\beta &= \bar{R}_\beta^i \cdot \frac{1}{\bar{D}_i} \\ \Gamma_p^{if} &= \bar{\Gamma}_p^{if} \\ \Gamma_\gamma^i &= \bar{\Gamma}_\gamma^i. \end{aligned} \quad (\text{V.2})$$

*) Both criteria were clearly chosen to make the calculations easy. They could be relaxed without changing the physical content of the arguments given in this chapter.

***) Apart from fluctuations due to counting statistics.

The quantities of interest are consequently the beta-decay intensity, the partial proton widths, the total gamma widths, and the level spacing. The fluctuations in the gamma widths are known^{5a)} to be very small and the contribution from them will therefore be omitted. The spacing between neighbouring levels have fluctuations that may be described by a Wigner distribution^{*)5b)} but as long as $\Delta E/\bar{D}_i \gg 1$ the existence of long-range correlations in the spacings^{5c)} will make the contribution from fluctuations in the level spacings negligible. The main source of fluctuations comes from the beta decay intensity and the partial proton widths, which are both assumed to follow the Porter-Thomas distribution^{6)**)}.

If the proton intensity from the state ν is $R_p^{if\nu}$ one has

$$\overline{R_p^{if}} = D_i \cdot \overline{I_p^{if}}. \quad (V.3)$$

Postulate that there are no correlations either between the beta and proton channels or between different proton channels. A rough estimate of the variance in R_p^{if} can be obtained using the expression⁷⁾

$$\text{Var} [f(x_1, x_2, \dots, x_n)] \simeq \sum_{i=1}^N \left(\frac{df}{dx_i} \right)^2 \text{Var } x_i. \quad (V.4)$$

Applying this with

$$\text{Var } R_p^{if} = \text{Var} (D_i \cdot I_p^{if}) \quad (V.5)$$

one gets

*) For a Wigner distributed variable x with mean 1 the probability density is

$$p(x) = \frac{\pi x}{2} \exp [-(\pi x^2/4)].$$

**) For a Porter-Thomas distributed variable x with mean 1 the probability density is

$$p(x) = \frac{1}{\sqrt{2\pi x}} \exp [-(x/2)].$$

$$\begin{aligned}
 \text{Var } R_p^{if} \approx & (I_p^{if})^2 \text{Var } D_i + \left(D_i \frac{\partial I_p^{if}}{\partial I_\beta} \right)^2 \text{Var } I_\beta + \\
 & + \left(D_i \cdot \frac{\partial I_p^{if}}{\partial \Gamma_p^{if}} \right)^2 \text{Var } \Gamma_p^{if} + \left(D_i \cdot \frac{\partial I_p^{if}}{\partial \Gamma_p^{if'}} \right)^2 \text{Var } \Gamma_p^{if'} + \\
 & + \left(D_i \cdot \frac{\partial I_p^{if}}{\partial \Gamma_\gamma^i} \right)^2 \text{Var } \Gamma_\gamma^i .
 \end{aligned} \tag{V.6}$$

Following the discussion given above the variance in the gamma width and the level spacing are equal to zero. The assumed Porter-Thomas distributions for Γ_p^{if} and I_β gives (in terms of the mean values) the variance 2 for these quantities. The result then becomes

$$\left(\overline{R_p^{if}} \right)^{-2} \text{Var } R_p^{if} \equiv \alpha^{if} = 2 + 2 \left[1 - \frac{2\Gamma_p^{if}}{\Gamma_\gamma^i} + \sum_{f'} \left(\frac{\Gamma_p^{if'}}{\Gamma_\gamma^i} \right)^2 \right] . \tag{V.7}$$

The limiting values of Eq. (V.7) are 4 if $\Gamma_\gamma^i \gg \Gamma_p^{if}$ and 2 if the proton channel $i \rightarrow f$ dominates. It can be shown⁹⁾ that this expression gives an underestimate in the limit $\Gamma_\gamma^i \gg \Gamma_p^{if}$ since the product of two Porter-Thomas distributions have the variance 8 instead of the value 4, implied by Eq. (V.7). This is, however, of little consequence here since, for the two cases where fluctuations have been observed (^{115}Xe and ^{118}Cs), the proton channel begins to dominate at low energies.

The variance of the total proton intensity can be obtained by weighting the individual contributions (V.7) according to the response function of the detector and by summing over all intermediate spins and all final states

$$\text{Var } I_p = (2 \ln 2)^{\frac{1}{2}} \pi^{-\frac{1}{2}} \Delta E^{-1} \sum_f \sum_i (I_p^{if})^2 D_i \alpha^{if} . \tag{V.8}$$

$\text{Var } (I_p / \bar{I}_p) = (\bar{I}_p)^{-2} \text{Var } I_p$ as calculated from these expressions will, in the next section, be compared to those obtained experimentally.

4. EXPERIMENTAL RESULTS

In an experimental spectrum the fluctuations discussed until now are encountered with those from counting statistics. A simple method to separate the two sources of fluctuations from the experimental data is given in the Appendix.

The results of calculations based upon the ^{115}Xe (Fig. II.10) and ^{118}Cs (Fig. II.7) spectra are shown in Figs. V.2, and V.3, respectively. The theoretical curves were calculated from Eqs. (V.7) and (V.8). The formulas and parameters were chosen as in Chapter IV. The experimental spectra were divided into sub-intervals and $\text{Var} (I_p / \bar{I}_p)$ was calculated for each interval. An estimate of the errors in the experimentally obtained variance may be found from the following considerations: The experimental points are obtained from finite samples of size n (the number of experimental points in the interval of energy range E_i). The theoretical sampling distribution of the variance of random samples from normal populations is related to the gamma distribution ^{*)8)} (with $\alpha = n/2 - 1$ and $\beta = 2$) which gives a relative sampling error of $\sqrt{2/n}$ if $n \gg 2$. The relevant sample size is, however, not identical to the actual number of points in the interval E_i but may be shown ⁹⁾ to equal an effective number of points n_{eff} which is defined as

$$n_{\text{eff}} = \frac{E_i}{\Delta E} \cdot k, \quad (\text{V.9})$$

where the constant is determined from the response function of the detector (a Gaussian shape gives $k = \sqrt{8 \ln 2 / \pi}$). Following these arguments the experimental error can be estimated as $\text{Var } N \cdot \sqrt{2/n_{\text{eff}}}$. This is valid provided that the fluctuations are normally distributed and that no additional uncertainty comes from the method of separating $\text{Var} (I_p / \bar{I}_p)$ from the experimental data. In Figs. V.2 and V.3 the errors have been increased by a factor of two over this rough estimate.

*) For a gamma distributed variable x with mean 1 the probability density is

$$p(x) = \frac{1}{\beta^{\alpha+1} \Gamma(\alpha + 1)} x^{\alpha} e^{-x/\beta}.$$

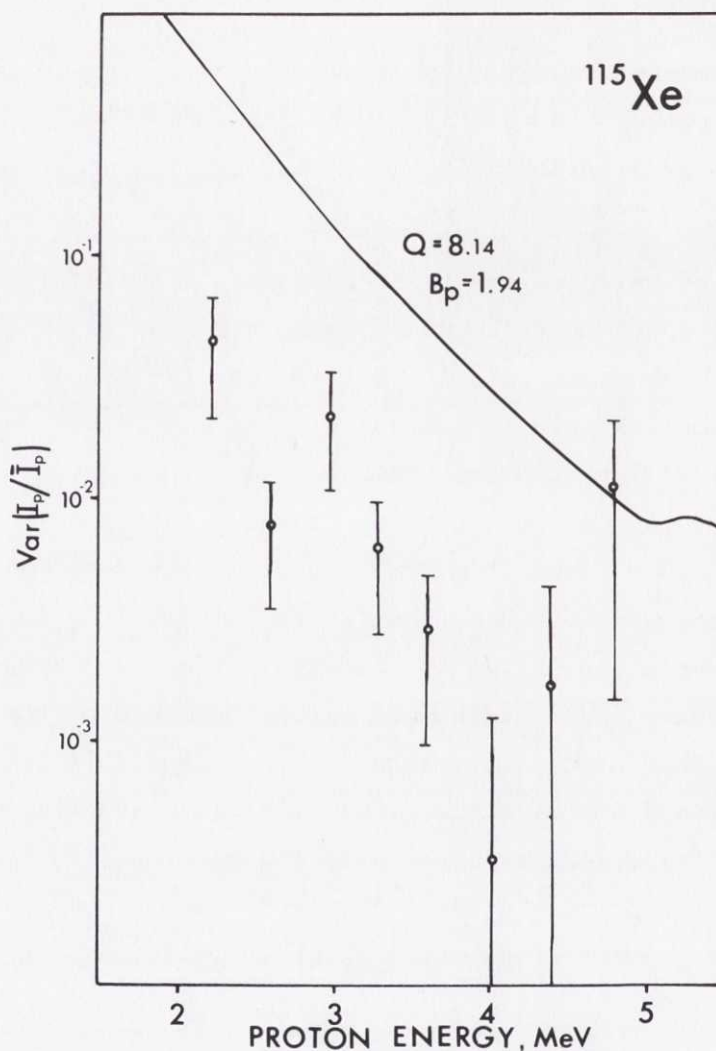


Fig. V.2 The variance of the delayed proton intensity from ^{115}Xe . The curve shows the theoretically predicted energy dependence calculated with $Q = 8.14$ MeV, $B_p = 1.94$ MeV, and $I^\pi = 5/2^+$. The experimental points were obtained with the method given in the Appendix.

The only parameter of importance in the theoretical expression for $\text{Var}(I_p / \bar{I}_p)$ as given in Eq. (V.8) is the level spacing, D_i . The results shown in Figs. V.2 and V.3 therefore indicate that the level spacing calculated from the formulas in Ref. (3) gives an over-estimate for ^{115}I and an underestimate for ^{118}Cs .

SUMMARY

It has been shown that a study of the fluctuations in a beta-delayed proton spectrum provides a method for determining the level density of

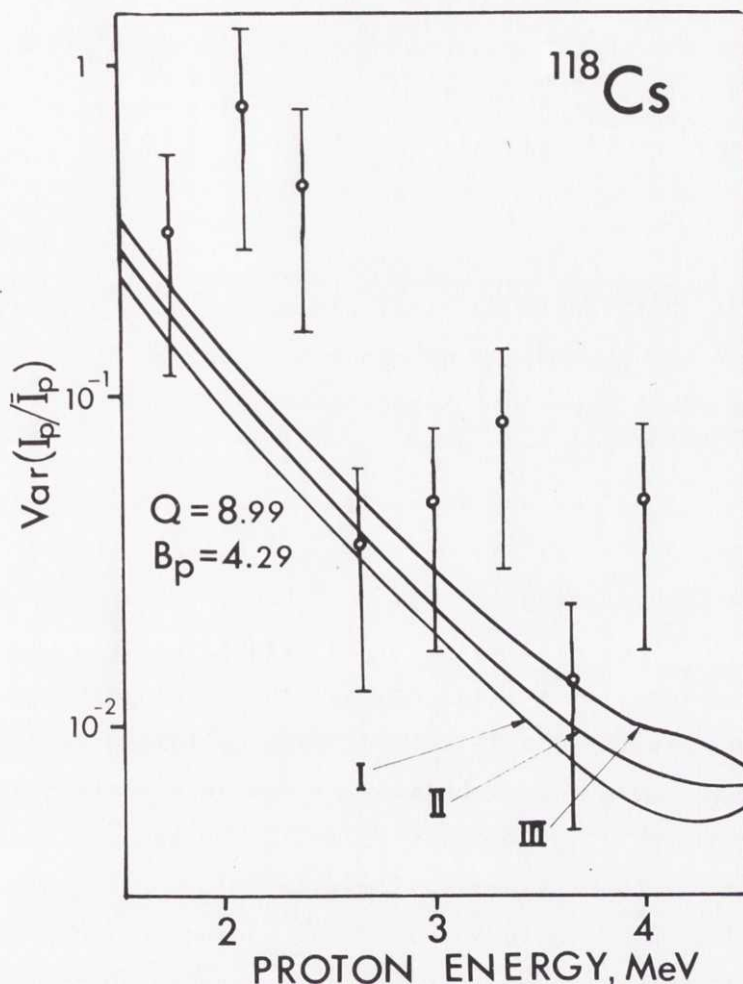


Fig. V.3 The variance of the delayed proton intensity from ^{118}Cs . The curves represent the theoretically predicted variances, calculated with $Q = 8.99$ MeV, $B_p = 4.29$ MeV, and $I^\pi = 3^+$. The final states were chosen as: I) 0.0 MeV ($5/2^+$), 0.12 MeV ($1/2^+$), 0.16 MeV ($7/2^+$), 0.22 MeV ($3/2^+$), and 0.31 MeV ($3/2^+$). II) 0.0 MeV ($5/2^+$), 0.16 MeV ($1/2^+$), 0.22 MeV ($7/2^+$), and 0.31 MeV ($3/2^+$). III) 0.0 MeV ($5/2^+$), 0.22 MeV ($1/2^+$), and 0.31 MeV ($7/2^+$). The experimental points were obtained with the method given in the Appendix.

the intermediate nucleus. The two cases analysed were especially favourable since the conditions $\Delta E/D_1 \gg 1$ and $\Gamma_Y^i \ll \sum_f \Gamma_p^{if}$ are fulfilled. In regions where either or both of these conditions are not valid one has to resort to other methods to find a suitable function to describe the statistical distribution. An example on this (in the case where $\Gamma_Y^i \gg \sum_f \Gamma_p^{if}$) is given in Ref. (9). The physical content of the ideas remain, however, the same.

REFERENCES TO CHAPTER V

- 1) C. Porter, Statistical Theories of Spectra, Academic Press, New York and London (1965).
- 2) P.A. Egelstaff, Proc. Phys. Soc. 71, 910 (1958).
- 3) A. Gilbert and A.G.W. Cameron, Can. J. Phys. 43, 1446 (1965).
- 4) M.G. Braga Marcazzan and L.M. Colli, Progr. Nuclear Phys. 11, 145 (1970).
- 5) J.E. Lynn, The Theory of Neutron Resonance Reactions, Clarendon Press, Oxford (1968); a) p. 319, b) p. 180, c) p.201.
- 6) C.E. Porter and R.G. Thomas, Phys. Rev. 104, 483 (1956).
- 7) W.T. Eadie, D. Drijard, F.E. James, M. Roos, B. Sadolet, Statistical Methods in Experimental Nuclear Physics, North Holland Publishing Company, Amsterdam and London (1971) p. 27.
- 8) L. Maisel, Probability, Statistics and Random Processes, Simon and Schuster, New York (1971) p. 119.
- 9) P. Hornshøj, P.G. Hansen and B. Jonson, to be published.

APPENDIX

Var (I_p / \bar{I}_p) FROM THE EXPERIMENTAL DATA

Assume that the outcome of an experiment is $N_1, N_2, \dots, N_n, \dots$ counts in the channels 1, 2, ..., n, ... (from a great number of contributing resonances). Further assume that there are two sources of fluctuations:

- i) a contribution from the counting statistics which has a Poisson distribution and the variance

$$\text{Var } N_c = \bar{N} ; \quad (\text{A.1})$$

- ii) a contribution from fluctuations with the variance

$$\text{Var } N_{fl} = k\bar{N}^2 . \quad (\text{A.2})$$

If the spectrum is smoothed by a Gaussian function one obtains for the number of counts in channel i

$$N_i^S = \sum_{i'} N_i' \frac{1}{\sqrt{2\pi\sigma^2}} \exp \left[-\frac{(i - i')^2}{2\sigma^2} \right] , \quad (\text{A.3})$$

where the sum extends over all channels. Let the experimental data be smoothed with two different widths σ of the smoothing function σ_1 and σ_2 where $\sigma_2 \gg \sigma_1$. The difference between the counts in corresponding channels in the smoothed spectra is then

$$\begin{aligned} \Delta N_i = N_i^{S_1} - N_i^{S_2} = \sum_{i'} N_i' & \left[\frac{1}{\sqrt{2\pi\sigma_1^2}} \exp \left[-\frac{(i - i')^2}{2\sigma_1^2} \right] - \right. \\ & \left. - \frac{1}{\sqrt{2\pi\sigma_2^2}} \exp \left[-\frac{(i - i')^2}{2\sigma_2^2} \right] \right] . \end{aligned} \quad (\text{A.4})$$

The variance of ΔN is given by

$$\text{Var } \Delta N = \sum_{i'} [\dots]^2 \text{Var } N \quad . \quad (\text{A.5})$$

If one assumes that the number of channels is large and that $1 \ll \sigma_1 \ll \sigma_2$ one may use the approximation

$$\sum_{i'} [\dots]^2 \approx \int_0^\infty [\dots]^2 di' \equiv f(\sigma_1, \sigma_2) \dots \quad (\text{A.6})$$

which gives

$$\begin{aligned} f(\sigma_1, \sigma_2) = & \int_0^\infty \left\{ \frac{1}{2\pi\sigma_1^2} \exp \left[-\frac{(i - i')^2}{\sigma_1^2} \right] + \frac{1}{2\pi\sigma_2^2} \exp \left[-\frac{(i - i')^2}{\sigma_2^2} \right] - \right. \\ & \left. - \frac{1}{\pi\sigma_1\sigma_2} \exp \left[- (i - i')^2 \left\{ \frac{\sigma_1^2 + \sigma_2^2}{2\sigma_1^2\sigma_2^2} \right\} \right] \right\} di' \end{aligned} \quad (\text{A.7})$$

if $i \gg 1$ the integration may be extended from $-\infty$ to $+\infty$ which gives

$$f(\sigma_1, \sigma_2) = \frac{1}{2\sqrt{\pi}} \left(\frac{1}{\sigma_1} + \frac{1}{\sigma_2} - \frac{2\sqrt{2}}{\sqrt{\sigma_1^2 + \sigma_2^2}} \right) \quad (\text{A.8})$$

With the parameter $y = \sigma_2/\sigma_1$, and $B_{1/2,1} = 2\sqrt{2 \ln 2} \sigma_1$ one may write

$$f(\sigma_1, \sigma_2) = \frac{\sqrt{2 \ln 2}}{B_{1/2,1} \cdot \sqrt{\pi}} \left[1 + \frac{1}{y} - \frac{2\sqrt{2}}{\sqrt{1 + y^2}} \right] \quad (\text{A.9})$$

Under the assumption that there are no correlations between the two types of fluctuations one gets

$$\frac{\text{Var } \Delta N_i}{\bar{N}^2} = \left(k + \frac{1}{\bar{N}} \right) \frac{\sqrt{2 \ln 2}}{B_{1/2,1} \cdot \sqrt{\pi}} \cdot \left[1 + \frac{1}{y} - \frac{2\sqrt{2}}{\sqrt{1 + y^2}} \right] \quad (\text{A.10})$$

In this expression $k\sqrt{2 \ln 2} \pi^{-\frac{1}{2}} B_{1/2,1}^{-1}$ corresponds to $\text{Var } (I_p/\bar{I}_p)$ as given in Eq. V.8 and one has to solve

$$\text{Var } \left(\frac{I_p}{\bar{I}_p} \right) = \text{Var } \left(\frac{\Delta N_i}{\bar{N}} \right) \left(1 + \frac{1}{y} - \frac{2\sqrt{2}}{\sqrt{1 + y^2}} \right)^{-1} - \frac{\sqrt{2 \ln 2}}{\bar{N} \cdot B_{1/2,1}} \quad (\text{A.11})$$

to extract the experimental estimate on the variance.

Acknowledgements

This work has been performed in the stimulating atmosphere of the ISOLDE facility at CERN. I am indebted to my colleagues in the ISOLDE collaboration for their help in these investigations. Special thanks are due to: Professor G. Andersson for his continual support ever since I joined his group, and especially for his valuable help and comments during the development of this work; Professor P.G. Hansen for introducing me into this exciting branch of nuclear physics and for innumerable discussions which have been of invaluable importance for me; Dr. P. Hornshøj for a very pleasant and stimulating co-operation both "on-line" and "off-line" and also for his kind interest and comments on this work.

The work has been financially supported by the Swedish Atomic Research Council.

Geneva in November 1972

Björn Jonson

CHALMERS BIBLIOTEK



1203583102